Free and Rydberg electron attachment to molecules

A Thesis

Submitted to the
Tata Institute of Fundamental Research, Mumbai
for the degree of Doctor of Philosophy
in Physics

by

Vaibhav S. Prabhudesai

School of Natural Sciences
Tata Institute of Fundamental Research
Mumbai
July, 2006

DECLARATION

This thesis is the presentation of my original research work. Wherever contributions of others are involved, every effort is made to indicate this clearly, with due reference to the literature, and acknowledgment of collaborative research and discussions.

The work was done under the guidance of Prof. E. Krishnakumar, at the Tata Institute of Fundamental Research, Mumbai.

Vaibhav S. Prabhudesai

In my capacity as supervisor of the candidate's thesis, I certify that the above statements are true to the best of my knowledge.

E. Krishnakumar

Date: 31st July, 2006.

To

Aai and Baba

Acknowledgment

This work would not have been possible within the period of a Ph.D. thesis without the help of many supporting hands. At this place I wish to thank all those who contributed to this work in some way.

Many thanks to *Prof. E. Krishnakumar* for all his efforts and the patience he showed during the entire work. It was never difficult to interest him to see my own work in a new light and to become aware of the physical importance inherent in it. I express my gratitude to him for his smiling demeanor and the learning experience with him in the laboratory. The most important ingredient in this collaboration was his ability to instill confidence in my work and to encourage me to come up with newer ideas. His meticulous corrections and his comments are greatly appreciated.

I would like to thank *Dr. Dhanajay Nandi* for his help, meaningful discussions, and the fun we both had inside and outside the laboratory. He had been an ideal senior lab-mate for me.

All the technical help extended by both, *Mr. Satej Tare* and *Mr. Yogesh Upalekar* is gratefully acknowledged here. The innovative solutions provided by them to the various technical problems, which arose during the doctoral work are highly appreciated. Special thanks to *Mr. Satej* for those informal machine shop tutorials and to *Mr. Yogesh* for excimer laser related help.

It was always a pleasure to discuss various physics problems with *Mr. Aditya H. Kelkar*. It was during one such discussions that the idea of 'functional group dependence of site specific fragmentation', which is one of the salient features of the doctoral work, emerged.

The contribution of *Dr. Rajendra Parajuli* from Kathmandu University, Nepal in the absolute cross section measurement for *DEA* to formic acid is duly acknowledged.

I am thankful to *Dr. Amber Chaterjee* and *Mr. Ramachandran* from B. A. R. C., Mumbai for their help regarding the data acquisition system used for angular distribution measurements. Help from *Mr. T. S. Ananthkrishnan* from B.A.R.C.,

Mumbai and *Prof. S. V. K. Kumar*, towards the data acquisition system used for absolute cross section measurements is also duly acknowledged.

I am grateful to *Dr. Amol Tipnis* from U.I.C.T. Mumbai, for providing me with various chemicals that were used in the studies reported in this thesis. I would also like to thank *Dr. Amarnath Chatterjee* and *Mr. Ashutosh Mishra* for their help in verifying the purity levels of the partially deuterated samples used in the reported studies.

It will be impossible to express in words my gratitude towards *Prof. S. H. Patil* from I.I.T. Mumbai, for the fruitful discussions we had regarding the angular distributions in electron scattering by atoms and molecules and many other such topics in quantum mechanics.

It is highly warranted to acknowledge the support extended by *Mr. G. Aravind* during the course of this thesis work. The stimulating discussions with him on almost any topic under the sun form the memorable part of my stay in this laboratory. Interesting discussions with *Mr. Bhargava Ram* on Physics related topics helped me in deepening my understanding. It was an absolute pleasure to work with them. We had very good time while working in the laboratory.

I would like to thank my colleagues *Dr. Prashant Rawat* and *Dr. V. S. Ashoka* for their help and support in various experiments. Thanks are also due to Dr. M. Krishnamurthy for teaching me quantum chemistry and for many insightful discussions on different issues regarding negative ions. I am thankful to *Dr. Vandana Nanal* and *Dr. Rudrajyoti Palit* for extending their help in various electronics and data acquisition related work. I would also like to thank *Prof. G. Ravindrakumar* for his help in many laser related stuff at various point of time. Thanks to *Mr. Atique-ur-Rehman* for his help in the laboratory related work.

The valuable help extended by *Mr. Sangam Sinha* from central workshop in various design related problems, besides the excellent support provided by the central workshop, especially by *Mr. Chogale*, *Mr. Arora*, *Mr. Satpute*, *Mr. Chowbe*, *Mr. Dilip*, *Mr. More* (for pulsed valve) and *Mr. Vikas* (for electron monochromator) is gratefully acknowledged here. I appreciate the wonderful job done by the glass blowing section in making glass to metal seals and glass bulbs that were used in the DEA experiments. I am also thankful to *Mr. S. P. Pai* and *Mr. Raju Patil* for many suggestions in instrumentation. I would also like to thank all the library and canteen staff of TIFR for their help and excellent services.

I am grateful to *Prof. Sumit Das* and *Prof. Mustansir Barma* for fantastic courses given to us in the first year of my graduate school.

Special thanks to *Mr. Deepankar Misra, Mr. M. Anand, Mr. Suman Bagchi* and *Dr. Ajaykumar* for all their support at different stages of this thesis work. I could seek their help at any hour of the day.

And now is the time to talk about the best part of my stay at TIFR apart from those enjoyable moments in the laboratory. I cannot even imagine my stay in TIFR without Deepankar, Deepshikha, Apoorva, Aditya, Anand, Vishal, Ajaykumar and Seema. The course work days with Deepankar, Deepshikha, Apoorva and Anand are just unforgettable.

I will always cherish the good time spent with *Vinod, Balaji, Tirtho, Alfica, Neel, Umesh, Sarita, Ashok, Yeshpal, Dishant, Amitava, Krishnan, Laxmi, Sulakshana, Amala, Arati, Anindya, Ramkumar, Vishal, Shanta, Amit, Jeet, Ashutosh Mishra, Ashutosh Mahajan, Goutam, Sriram, Rahul Jain, Ajay, Kanchan, Anup, Shamik, Sanjeev, Ayesha, Deepak, Narayan* and many more TIFR-mates in the last six years.

I am thankful to my friend *Sameer* for helping me in passport related work.

I am grateful to all my family members, especially *Tai* and *Sameer* for providing support during the emotional and difficult times. I will never forget the ever smiling face of niece *Kinneri* that made all my tensions vanished in no time. My parents always encouraged me to pursue my interests. I can never forget the struggle that they have gone through to make me see this day in my life. This acknowledgement can never be complete without mentioning them.

Finally, I acknowledge the *TIFR Alumni Association* for the *Carrier Development* scholarship through the *TIFR Endowment fund*. I would also like to thank the *Sarojini Damodaran Trust* for supporting my visits to a few labs in *Germany* through their esteemed Fellowship.

Contents:

List of publications:

1. Dissociative electron attachment to formic acid.
   Vaibhav S. Prabhudesai, Dhananjay Nandi, Aditya H. Kelkar, Rajendra Parajuli, and E. Krishnakumar, *Chem. Phys. Lett.* **405**, 172 (2005).

2. Low energy electron attachment to C_{60}.
   V. S. Prabhudesai, D. Nandi, and E. Krishnakumar, *Eur. Phys. J. D* **35**, 261 (2005).

3. Functional group dependent site selective fragmentation of molecules by low energy electrons.
   Vaibhav S. Prabhudesai, Aditya H. Kelkar, Dhananjay Nandi, and E. Krishnakumar, *Phys. Rev. Lett.* **95**, 143202 (2005).

4. Velocity slice imaging for dissociative electron attachment.
   Dhananjay Nandi, **Vaibhav S. Prabhudesai**, E. Krishnakumar, and A. Chatterjee, *Rev. Sci. Instrum.* **76**, 053107 (2005).

5. Velocity Map Imaging for low energy electron molecule collision.
   D. Nandi, **V. S. Prabhudesai,** and E. Krishnakumar (*accepted in Radiat. Phys. Chem.*).

6. On the presence of $^4\Sigma_u^-$ state in dissociative electron attachment to O_2.
   Vaibhav S. Prabhudesai, Dhananjay Nandi, and E. Krishnakumar *J. Phys. B: At. Mol. Opt. Phys.* **39**, L277.

7. Probing site selective fragmentation of molecules using Velocity Map maging.
   Vaibhav S. Prabhudesai, N. Bhargavaram, G. Aravind, P. Rawat, and E. Krishnakumar, (*under preparation*).

8. Rydberg electron attachment to excited molecules.
   Vaibhav S. Prabhudesai and E. Krishnakumar (*under preparation*).

9. Electron attachment to small carboxylic acids and alcohols.
   Vaibhav S. Prabhudesai, G. Aravind, P. Rawat, Aditya H. Kelkar, and E. Krishnakumar (*under preparation*).

Other publications (Not related to the thesis)

10. Dynamics of the dissociative electron attachment to NO.
    D. Nandi, **Vaibhav S. Prabhudesai**, and E. Krishnakumar (*under preparation*).

11. Resonances in electron attachment to N_2O.
    D. Nandi, **Vaibhav, S. Prabhudesai**, and E. Krishnakumar (*under preparation*).

Presentations in Conferences

1. **Probing site selective fragmentation of molecules using Velocity Map Imaging (VMI) for hydroxyl group containing compounds**
   Vaibhav S. Prabhudesai, N. Bhargavaram, G. Aravind, P. Rawat and E. Krishnakumar
   7th Asian International Seminar on Atomic and Molecular Physics, IIT Chennai, Decembar 2006.

2. **Absolute cross sections for Dissociative Electron Attachment to water and methane**
   P. Rawat, **Vaibhav S. Prabhudesai**, G. Aravind, N. Bhargavram, A. Rahman and E. Krishnakumar
   7th Asian International Seminar on Atomic and Molecular Physics, IIT Chennai, December 2006.

3. **Velocity Map Imaging of H^- ions resulting from Dissociative electron attachment to H_2O**

   N. Bhargavaram, **Vaibhav S. Prabhudesai**, G. Aravind, P. Rawat, and E. Krishnakumar

   7^{th} Asian International Seminar on Atomic and Molecular Physics, IIT Chennai, December 2006.

4. **Probing site selective fragmentation of molecules using Velocity Map Imaging (VMI)**

   Vaibhav S. Prabhudesai, N. Bhargavaram, G. Aravind, P. Rawat and E. Krishnakumar

   Discussion meeting on molecular dynamics and spectroscopy, Goa, April 2006.

5. **Studying Dissociative Electron Attachment (DEA) to H_2O using Velocity Map Imaging (VMI)**

   N. Bhargava Ram, **Vaibhav S. Prabhudesai**, G. Aravind, P. Rawat and E. Krishnakumar

   Discussion meeting on molecular dynamics and spectroscopy, Goa, April 2006

6. **Control of molecular dissociation using low energy electrons**

   Vaibhav S. Prabhudesai, Dhananjay Nandi, Aditya H. Kelkar and E. Krishnakumar,

   National Conference on Mass Spectrometry, Jan. 2006, Munnar, Kerala. (Won the best poster award.)

7. **Velocity map imaging for dissociative electron attachment**

   D. Nandi**, Vaibhav S. Prabhudesai,** A. Chatterjee, and E. Krishnakumar

   National Conference on Mass Spectrometry, Jan. 2006, Munnar, Kerala.

8. **Velocity map imaging of H^- from DEA to hydrogen containing molecules**
   Vaibhav S. Prabhudesai, N. Bhargavram, G. Aravind, P. Rawat and E. Krishnakumar,
   Topical conference on atomic and molecular physics, Dec. 2005, IACS, Kolkata.

9. **Site Selective Fragmentation of Molecules Using Low Energy Electrons.**
   Vaibhav S. Prabhudesai, Dhananjay Nandi, Aditya H. Kelkar, and E. Krishnakumar.
   Discussion Meeting on Advances in Spectroscopy (DMAS), from 21st February to 24th February, 2005, Indian Institute of Sciences, Bangalore, India. (Won the best poster award.)

10. **Site Selective Fragmentation of Molecules Using Low Energy Electrons.**
    Vaibhav S. Prabhudesai (Invited talk)
    XV National Conference on Atomic & Molecular Physics (NCAMP-XV), from 21st December to 24th December, 2004, Physical Research Laboratory, Ahmedabad, India.

11. **Dissociative Electron Attachment to Formic Acid.**
    Vaibhav S. Prabhudesai, Dhananjay Nandi, Aditya H. Kelkar, R. Parajuli and E. Krishnakumar
    XV National Conference on Atomic & Molecular Physics (NCAMP-XV), from 21st December to 24th December, 2004, Physical Research Laboratory, Ahmedabad, India.

12. **Low energy electron attachment to C_{60}**
    Vaibhav S. Prabhudesai, Dhananjay Nandi, and E. Krishnakumar
    XV National Conference on Atomic & Molecular Physics (NCAMP-XV), from 21st December to 24th December, 2004, Physical Research Laboratory, Ahmedabad, India.

13. Velocity Map Imaging for Angular Distribution in DEA

Dhananjay Nandi, **Vaibhav S. Prabhudesai**, Amber Chatterjee and E. Krishnakumar

XV National Conference on Atomic & Molecular Physics (NCAMP-XV), from 21st December to 24th December, 2004, Physical Research Laboratory, Ahmedabad, India. (Won the best poster award.)

14. Dissociative Electron Attachment studies on N_2O and CO_2 by Velocity Map Imaging

Dhananjay Nandi, **Vaibhav S. Prabhudesai**, and E. Krishnakumar

XV National Conference on Atomic & Molecular Physics (NCAMP-XV), from 21st December to 24th December, 2004, Physical Research Laboratory, Ahmedabad, India.

15. Dissociative Electron Attachment studies on NO by Velocity Map Imaging

Dhananjay Nandi, **Vaibhav S. Prabhudesai**, and E. Krishnakumar

XV National Conference on Atomic & Molecular Physics (NCAMP-XV), from 21st December to 24th December, 2004, Physical Research Laboratory, Ahmedabad, India.

16. Dissociative Electron Attachment Study of Molecules using Velocity Map Imaging of Fragment Ions.

E. Krishnakumar, Dhananjay Nandi, and **Vaibhav S. Prabhudesai**

8th European Conference on Atomic and Molecular Physics (ECAMP VIII), Universite De Rennes, Rennes, France, 6-10 July, 2004.

17. Dissociative Electron Attachment to Formic Acid.

R. Parajuli, Dhananjay Nandi, **Vaibhav S. Prabhudesai**, Aditya H. Kelkar, and E. Krishnakumar

Fourth National Conference on Science and Technology, Tribhuvan University, Kathmandu, Nepal, March 23-26, 2004.

18. Negative Ion Formation in Molecules through Rydberg Electron Capture.

Vaibhav S. Prabhudesai, Dhananjay Nandi, V. S. Ashoka and E. Krishnakumar

XIV National Conference on Atomic & Molecular Physics (NCAMP-XIV), from

28th January to 1st February, 2003, Viswa-Bharati, Santiniketanl, India.

19. Negative Ion Formation by Rydberg Electron Attachment from Laser Irradiated Molecules.

Vaibhav S. Prabhudesai, Dhananjay Nandi, V. S. Ashoka and E. Krishnakumar

National Laser Symposium-2002 (NLS-2002), November 14-16, 2002, Sree Chitra Tirunal Institute for Medical Science and Technology, Thiruvananthapuram, Kerala, India.

20. Velocity Map Imaging in Dissociative Electron Attachment

Vaibhav S. Prabhudesai and E. Krishnakumar

ISAMP newsletter November 2005.

Synopsis

Negative ions in their ground and excited states are of interest from fundamental as well as application point of view. The relevance of these species spans a wide spectrum of interest starting from plasma studies, useful in the semiconductor industry, to astrobiology apart from fundamental physics. Although of such a wide interest, not much has been accomplished towards the understanding of the dynamics and the nature of the negative ion excited states. On the theoretical front the problem of potential energy surface calculations for the excited negative ion state is beyond any quantum chemical computation that exists. There has been some headway in scattering type calculations for diatomic molecular negative ions. However the problem becomes quite complicated for the polyatomic molecular negative ions due to the many-body nature of the species involved. On the experimental front the study of these excited molecular negative ion states is very difficult, if not impossible, using the optical techniques. The main reason is the unstable nature of the negative ion species due to relatively smaller lifetimes ($<10^{-12}$ sec) of the states as compared to the typical radiative lifetimes ($\sim10^{-9}$ sec). Moreover, photon based studies are more restricted to the dipole allowed transitions.

The phenomenon of free electron attachment to a neutral molecule is not restricted to just the dipole allowed transitions. In the plane wave approximation of the incoming electron beam, capture of different partial waves (depending on the selection rules for the negative ion formation) is possible giving direct access to many non dipole transitions. Hence, studies based on free electron attachment can give a better access to the understanding of these excited negative ion states. On the other hand, Rydberg electron attachment process gives access to those negative ion states that may not be formed by free electron attachment. Such attachment process has very large cross section due to the size of the Rydberg orbital. These processes become more relevant in the high pressure conditions that resemble the actual environment encountered in various practical applications and where the collision probabilities are higher. Most of the work reported so far is on the basis of the Rydberg electron transfer to molecules in the ground state except for few reports on the molecules

excited to their high Rydberg states. Such process for the excited state of molecules can give access to different negative ion excited states allowing different parts of the negative ion potential energy surface to be probed. The work reported in this thesis is carried out with the intention of obtaining a better understanding of the ground and excited states of negative ions and various processes that are involved in their formation and decay using free and Rydberg electron attachment.

In the low energy regime of the electron molecule collisions (electron energies below 20eV), electrons can get resonantly captured depending on the electron energy and the type of molecule involved. The transition from the neutral state to the negative ion resonant (NIR) state is considered to be instantaneous (of Franck-Condon type). That is, the nuclear co-ordinates are considered to be frozen during the capture process. Thus the electron attachment gives direct access to the part of the negative ion potential energy surface that falls in Franck-Condon overlap with the initial neutral molecular state.

The NIR states are categorized in terms of the dynamics of the electron capture process. The electron-molecule interaction potential is generally dominated by the polarization and centrifugal terms. The centrifugal term contributes only for electrons with angular momentum, $l > 0$. The combination of attractive polarization and repulsive centrifugal terms could create a local potential minimum with a barrier in which the incoming electron may get trapped. This type of resonance is known as *single particle shape resonance*. If the incoming electron has sufficient energy to electronically excite the neutral target molecule, the electron capture takes place along with such electronic excitation. This is known as a *core* or *valence excited resonance*. These resonances are of *two-particles, one-hole* type transitions where a vacancy is created in one of the valence orbitals of the molecule by electronic excitation and the incoming electron also enters one of the unoccupied excited orbitals. There are two possible types of valence excited resonances. If the incoming electron gets trapped in the shape of the local potential well formed by the polarization and the centrifugal forces between the incoming electron and excited molecule, the resonance is known as a *valence excited shape resonance*. Here, the total energy of the negative ion is greater than that of the corresponding neutral excited molecule. In the second kind of valence excited resonance, the incoming electron gets occupied in one of the excited state orbitals that lower the overall energy of the system. This type of resonance is known as a *valence excited Feshbach resonance*. In this case the negative ion state

has lower energy than the parent excited state of the neutral molecule. The major difference between the valence excited shape resonance and valence excited Feshbach resonance is that the former can decay by autodetachment to the excited neutral state (hence also known as the open channel resonance) whereas the latter cannot decay to the excited neutral as it is not energetically possible (hence also known as the closed channel resonance).

The dominant mechanism of decay of the NIR state is through the ejection of the excess electron. This process is termed as autodetachment. The second mode of decay is the dissociation of negative ion in which one of the fragments retains the excess electron forming a stable negative ion. The entire process starting from electron attachment to dissociation is known as dissociative electron attachment (DEA). Due to the competition with autodetachment, the DEA cross section is very sensitive to the nuclear coordinates even for a diatomic molecule. For a triatomic or polyatomic NIR, the fragmentation pattern is governed by its potential energy surface along different bonds within the molecule and the life time against autodetachment. The dependence of autodetachment lifetime on the nuclear coordinates and its competition with the dissociation process makes the DEA process in molecules very unique. This provides scope for selective fragmentation of molecules using mode selective excitation by a laser or other means prior to electron collision. More significantly, as we show in the thesis, this property of the NIR leads to site selective fragmentation of molecules even without any mode selective excitation before the electron collision. Such a site specific fragmentation in the DEA process to ground state molecules is reported for the first time.

Measurements of the kinetic energies along with the angular distribution of the fragment negative ions provide information on the energy, dissociation limit and quantal states of the negative ions that have been accessed. The kinetic energy and angular distribution data also leads to the understanding of the overall dissociation dynamics of the negative ion resonance. During dissociation of the negative ion state, part of the excess energy can go to the internal excitation of fragments and the remaining energy is carried by the fragments as their translational energies. The excess energy released is shared between the fragments in the inverse ratio of their masses. The amount of kinetic energy released in the fragment negative ion quantifies the internal excitation of the two fragments. This information is the direct indication of the dissociation limit of the negative ion state addressed. Hence by measuring

kinetic energy of the negative ion fragment one can gather information about the different dissociation limits of the negative ion states addressed. In the case of many body break-ups, the kinetic energy released will be a continuous distribution, and relatively low. Knowing the energy threshold for the formation of fragment negative ion and the electron energy, such effects can be identified.

The angular distribution of the fragment ion is dependent on the symmetry of the resonant state and the angular momenta of the attached electrons. As the DEA takes place in the vibrational time scale which is much shorter than the rotational time scale, the angular distribution information of the fragment negative ion gives information about the orientation of a specific bond that is broken with respect to electron beam. In the case of diatomic molecules, for a given electron incident momentum $\boldsymbol{k}$, the ion intensity I at the angular co-ordinates (θ,φ) is given by the expression [1],

$$I(k,\theta,\phi) = \sum_{|\mu|} |\sum_{l=|\mu|}^{\alpha} a_{l\mu}(k) Y_{l\mu}(\theta,\phi)|^2$$

Here $a_{l\mu}(k)$ is energy dependent expansion coefficient and $Y_{l\mu}(\theta,\varphi)$ are the spherical harmonics with $\mu = \Lambda_f - |\Lambda_i|$ and $l \geq |\mu|$. In the case of polyatomic molecules considering the diatomic like dissociation i.e. two body break-up, the expression becomes [2],

$$\boldsymbol{I(k,\theta,\phi) \propto |\sum_{l,m,\varepsilon} i^l \exp(i\delta_l) a_{lm}^{\varepsilon}(k) X_{lm}^{\varepsilon *}(\theta,\phi)|^2 \, d\phi}$$

Here, X_{lm}^{ε} is basis function for the irreducible representation of the group of the molecule. These functions are in the dissociation frame of molecule. Hence knowing the angular distribution of the fragment negative ion and the symmetry of the initial ground state, the information about the quantal state of the negative ion resonance can be retrieved.

In order to study the dynamics of the negative ion states as well as that of the DEA process in molecules, we have carried out several systematic experiments using both free and Rydberg electrons. The free electron attachment study is broadly based on two types of experiments, (a) measurement of cross sections for the electron

attachment process (b) measurement of kinetic energy distribution and angular distribution of the fragment ions.

The cross sections are measured using an apparatus that is optimized for complete collection and mass analysis of all ions irrespective of their mass and initial energy. In this experiment a pulsed and magnetically collimated electron beam is crossed at right angles with an effusive molecular beam from a capillary array. Typical electron beam energy resolution from the electron gun is found to be 500meV. The ions formed in the intersection of the two beams are extracted by a 200 V/cm pulsed field applied in the interaction region with some delay with respect to the electron beam. This pulsed field pushes the ions into a *segmented* time of flight mass spectrometer (TOFMS). The segmented TOFMS consists of a flight tube with four segments that can be floated at different voltages giving electrostatic lens action for the extracted negative ions. This provides a unique advantage of transporting all the ions that are extracted from the interaction region to the detector irrespective of the initial kinetic energies and angle of ejection with respect to the flight tube axis. The absolute cross section for the formation of various ions is determined by using the *relative flow technique* [3]. In this procedure the relative cross sections are made absolute by comparing the yield of the ion of interest to that of another one for which reliable cross section data exist. The procedure relies on the fact that the effusive beam from a capillary under strict molecular flow conditions does not change its characteristics when one gas is replaced by another.

In order to measure the kinetic energy of the fragment negative ions and their angular distribution with respect to the electron beam, Velocity Map Imaging (VMI) technique is used. In the VMI technique all the ions present in a given volume in the interaction region and moving with a specific velocity are made to arrive at identical position on a 2-dimensional position sensitive detector (PSD). This is achieved using appropriate combination of the electric fields in the interaction region as well as in the time-of-flight setup [4]. In the conventional VMI arrangement, the arrival time of the ions at the detector is not recorded and the 3D velocity sphere (Newton sphere) of the ion cloud is projected on the 2D plane of the detector. By using the spatial symmetry of the collision process, the 3D distribution is retrieved from the 2D image using appropriate inversion algorithms. By suitably stretching the time of arrival of a given Newton sphere at the detector and recording arrival time of its each part, it is possible to isolate the central slice of the sphere which contains all the relevant information.

This is known as Velocity Slice Imaging (VSI). These ion imaging techniques were originally developed for studying various processes induced by photons or fast moving ions and could not be used for low energy electron collisions. We have developed a new technique based on VMI that could be used for electron collisions. In this VMI spectrometer we use a pulsed electron beam followed by a pulsed ion extraction. This allows the use of fairly high ion extraction field without disturbing the electron beam. Apart from the pulsed electron gun, the apparatus consists of a pair of extraction electrodes namely *pusher* and *puller* flanking the interaction region, followed by a lens electrode and a small flight tube at the end of which a PSD is used for the ion detection. The PSD is made up of three micro channel plates (MCPs) in z-stacked assembly. A wedge and strip anode situated on the back of the MCPs is used for the determination of the position of the ions striking the detector. The data is stored in a *list mode* where the x, y position of each ion striking the detector and its time of arrival is recorded. Since the orientation of molecules is isotropic there exists cylindrical symmetry in the DEA process about the electron beam direction. Hence any slice of the Newton sphere that contains the electron beam direction will have all the necessary information of the velocity distribution that we are seeking. Among these the slice that is perpendicular to the ion extraction direction and parallel to the detector plane will arrive at the detector at the same time. From the list mode data we select all those ions arriving at this particular time and plot their position on the detector to get the time sliced velocity map images. The radii of these velocity map images are proportional to the speed of the fragment ions at the time of formation and thus give their kinetic energy spectra and the intensity along the polar direction provides the angular distribution. The performance of the system is verified by measuring the angular distribution for O^- from DEA to O_2 and comparing it with that existing in literature which was obtained using the conventional turn-table technique.

Though the VMI experiment appears to work well for imaging the relatively heavier and hence slower moving ions like O^-, we find that for imaging lighter and swifter ions like H^-, the strength of the imaging electric field has to be increased further. In order to avoid the field penetration in the interaction region from the acceleration region in the high field situation, a fine wire-mesh is put on the *puller* electrode. The new voltage condition is optimized using ion trajectory calculations as well as actual experimentation. The performance of the VMI set-up with wire mesh is verified by comparing the results for O^- from O_2 as well as H^- from H_2O with

corresponding existing data. It is also found that the presence of wire-mesh improves the expected quadratic dependence of the ion kinetic energy on the radii of the velocity map images. These experiments are carried out under single collision conditions, in a vacuum chamber with an ultimate vacuum of $5x10^{-9}$ Torr.

During the course of testing the VMI set up using O_2, we noticed an important feature in our results, which appears to settle a long standing problem in the electron scattering process in O_2. The existing measurements on angular distribution of O^- from O_2 were carried out in the angular range of 20^o to 160^o. These data show that the NIR accessed corresponds to the $^2\Pi_u$ negative ion state. Following the theory of O'Malley [1] for angular distribution in the DEA process, the neutral ground state of O_2 ($^3\Sigma_u^-$), no molecules oriented along the electron beam direction could capture the electron to form the $^2\Pi_u$ negative ion state. However, our results which cover the entire 2π angles show finite cross sections in the forward and backward directions, though it agrees well with the previous results in the 20^o to 160^o range. After carrying out extensive measurements under varying experimental conditions, we conclude that the cross sections are finite in the forward and backward directions. This observation appears to settle a critical discrepancy existing between the inelastic electron scattering data and the DEA angular distribution data in O_2. The electron scattering data had shown clear indication of a $^4\Sigma_u^-$ negative ion state at about 9 eV with long enough lifetime against autodetachment [5]. The long lifetime should make it observable in the DEA channel in the forward and backward directions, based on selection rules for electron attachment. Since the previous angular distribution data discounted this possibility, the observed electron scattering behavior has remained a puzzle. We believe that the DEA contribution from the $^4\Sigma_u^-$ state being small, previous measurements could not pick up its presence in the limited angular range in which the measurements were made. The only way such a small contribution could be identified is by making measurements in the forward and backward angles, which could not be done till now due to the geometrical constraints in a turn-table experiment. This also highlights the importance of the new technique that we have developed for kinetic energy and angular distribution measurements in DEA. Our identification of the $^4\Sigma_u^-$ state in the DEA channel may help in providing simpler explanations for some of the results on electron stimulated desorption of O^- from O_2 in the condensed phase [6].

We have used a combination of cross section measurements and velocity map imaging to unravel the dynamics of negative ions states in small organic molecules. Here the angular distributions measured for different resonances are for the two body kind of break ups i.e. diatomic like dissociation processes. Electron attachment to organic molecules is an area which is finding increasing interest due to radiation damage in biological tissues as well as the observation of large number of organic molecules in astrophysical environments. Being building blocks of bigger molecules, the DEA process in smallest carboxylic acids has been reported recently [7]. But these studies failed to observe the presence of H^- in the fragmentation channel. This was a surprising result since H^- has been observed from several other bigger molecules like DNA bases and from organic molecules adsorbed on surfaces by electron collision. We realized that the above measurements on carboxylic acids could suffer from discrimination against H^- ions which are likely to be formed with relatively large kinetic energies. Considering this, we carried out systematic measurements on DEA to HCOOH, CH_3COOH and C_2H_5COOH using the apparatus that is optimized for complete collection and mass analysis of all ions irrespective of their mass and initial energy.

We identify three resonances at 6.7, 7.7 and 9.1eV respectively corresponding to the formation of H^- in the carboxylic acids. A comparison of the absolute cross sections for the formation of other ions from these molecules show that H^- is one of the dominant channels of DEA in these carboxylic acids. The relatively large cross section for the formation of H^- could have important bearing on the chemical reactions occurring in the interstellar dust near various astrophysical objects like nebulae and tail of comets where these molecules are present. Moreover, being the lightest fragment, H^- will carry almost all the excess energy available as its kinetic energy. The relatively large kinetic energy of these hydride ions may have additional significance to various electron induced chemical processes relevant to astrobiology. We have also determined the absolute cross sections for the other fragments observed in the DEA process in these molecules.

One notable feature of the resonance patterns in the H^- channel from the carboxylic acids is their striking similarity. This tends to indicate a general but simple underlying rule for the DEA process. We have investigated this further by carrying out measurements on other simple organic molecules like small alcohols and an amine and some of their partially deuterated counterparts. The measurements of H^- and D^-

signals as a function of electron energy from partially deuterated compounds clearly indicate that different resonances correspond to ejection of the hydride ions from different sites within the molecule. This shows that by just changing electron energy one can selectively address different sites on the same molecule. For example, with 6.7eV electrons we break only the O-H bond, whereas with 9.1eV electrons we predominantly break the C-H bond. We find that this behavior is applicable to alcohols also. A comparison of these results with existing data on H_2O and CH_4 shows that the resonances seen in the O-H and C-H parts of the acids and alcohols are similar to the resonances seen in H_2O and CH_4 respectively. Further measurements on n-propyl amine showed resonances in the H^- channel as seen in NH_3 and CH_4 clearly showing that the site specificity arises from a hitherto un-noticed functional group dependence of the DEA process. This phenomenon, which we have identified for the first time, arises from the fact that the functional groups like hydroxyl, amine and alkyl maintain the electron attachment properties seen in their respective precursor molecules like water, ammonia and methane respectively. The fact that all these resonances lie well above the threshold energies for the breaking of O-H, C-H and N-H bonds in the respective molecules, points to a site specificity of the DEA process being beyond the threshold energy based site specificity known in the DEA process. This has important implications since using low energy electrons, different bonds (at least those associated with Hydrogen) in a molecule can be addressed by tuning the energy of the electron. This opens up a new chapter in the electron induced chemistry and points towards the possibility of controlling chemical reactions using low energy electrons.

In order to understand the dynamics and kinematics of the process that leads to the site specificity of fragmentation in DEA to these molecules, we have carried out the angular distribution and kinetic energy measurements of the H^- ions at various resonances. As mentioned earlier, measurements of the kinetic energies along with the angular distribution of the fragment negative ions provide information about the dissociation limit and quantal states of the negative ions that are accessed. The kinetic energy and angular distribution data also leads to the understanding of the overall dissociation dynamics of the negative ion resonance. This information is also essential to evaluate the potential of the electron beam based chemical control that we have identified above.

We have investigated the structure and dissociation dynamics of the three resonances in methanol and acetic acid to understand the site specific fragmentation and energy partitioning in the products by recording the velocity map images of fragment ions. In order to separate out the contribution from the CH and OH sites, we have used partially deuterated compounds (CH_3OD and CH_3COOD). At all the three resonances, D^- ions are found to be with higher kinetic energies and narrow energy spread ruling out the three body breakup of the molecules for this channel. Also at the first resonance i.e. at 6.4eV in methanol and at 6.7eV in acetic acid the angular distribution shows similarity with that from water at 6.5eV. All these differential cross-sections peak at around 100° with respect to electron beam. This shows that at this resonance the O-H bond being at specific orientation with respect to the electron beam is preferred and this preference is independent of the overall symmetry of the molecule involved. Such orientation specificity is also found for the first time.

The acetic acid molecule belongs to C_s symmetry group. The ground state of acetic acid is $1^1A'$. From the angular distribution that peaks at 100° i.e. close to 90°, the information about the negative ion state can be retrieved. Using the selection rules for the electron capture process in the polyatomic molecule of C_s symmetry it can be shown that the angular distribution that is observed for the first resonance corresponds to the $A' \rightarrow A'$ type of transition. The recent experimental and theoretical studies on the excited states of acetic acid show a valence transition in its absorption spectrum around 7eV that corresponds to the excitation of valence electron to the 14a′ orbital [8]. This orbital is known to be highly localized on the O-H bond in the molecule. The second resonance shows some loss of anisotropy but the differential cross section peaks at 90° for D^- signal indicating similar type of transition.

At the third resonance, which we find to be predominantly due to the C-H bond breakage, very little kinetic energy is observed in the H^- channel indicating possible scrambling and many body break-up. However, the small amount of D^- observed at this resonance show fairly large kinetic energy and specific angular distribution. These results point to two possibilities. Either some curve crossing is taking place within the negative ion states at this energy or two different kinds of closely lying negative ion states are addressed. The one responsible for the D^- signal is accessed by a valence transition and the one giving H^- is through Rydberg transition. The valence excitations being antibonding would result in faster

dissociation and hence the formation of the energetic D^- ions, whereas the Rydberg state excitation would be nonbonding resulting in slower dissociation. The slow dissociation process gives enough time for redistribution of the excess energy into different vibrational modes and subsequent multiple fragmentation. The absorption spectra of these molecules show large number of overlapping Rydberg as well as valence transitions in this energy range i.e. near 9eV. Also the presence of other fragments like CH_2^- in the case of acetic acid and O^- in the case of methanol around this resonance supports the scrambling type of mechanism playing vital role in this resonance.

In several situations the negative ion resonance formed by electron attachment may have large lifetime against autodetachment. And if these states are stable against dissociation, one could observe these parent negative ions directly. The long lifetime against autodetachment arises when the electron attachment process is not Franck – Condon type and energy of the incoming electron gets distributed in the vibrational modes of the molecule during electron attachment. This makes electronic part of the negative ion state lower in energy as compared to the neutral state preventing the decay through electron ejection. The decay takes place after relatively long time when the vibrational energy is transferred to the electronic energy. This type of resonance is called nuclear excited Feshbach resonance. Low energy electron attachment to C_{60} is an example of this.

Electron attachment to C_{60} is an interesting problem from the unique nature of the potential that it presents to an incoming electron. Several theoretical and experimental studies have been reported on electron attachment to this molecule. However, the results of the measurements in the low energy region have been inconsistent [9]. Although all those experiments were confirming the longevity of the C_{60} anion formed by the electron attachment up to 10eV, there was a disagreement about the electron attachment near zero eV and the kind of process involved at these energies. Some reports suggested the s-wave capture process sighting the 0 eV electron attachment while others suggested p-wave capture showing the threshold for the electron capture in the range of 150 to 260meV. These experiments used either free electron attachment technique or the Rydberg electron transfer technique (from atomic Rydberg states). The only difference in all these experiments was the temperature of the C_{60} beam used. In order to resolve this issue we have carried out detailed measurements on free electron attachment using the electron beam with

narrow energy spread. We have also studied the temperature dependence of the C_{60}^- ion signal.

For these experiments the electron beam energy resolution is improved using a newly built trochoidal monochromator. The basic principle used in this device is the velocity dependent force arising from the crossed electric field-magnetic field configuration. The electron beam with poorer energy resolution (0.5eV) gets dispersed in the direction transverse to both electric field and magnetic field in their mutually perpendicular configuration. A very narrow aperture (0.4mm diameter) beyond the trochoidal region is used to select a part of the dispersed electron beam. This improves the energy resolution of the outgoing electron beam. This way we could improve the electron energy resolution to about 130meV.

Our results on electron attachment to C_{60} show a peak around zero energy. The data thus show no threshold for the C_{60}^- formation process, confirming the s-wave capture process playing a role in the electron capture. In fact, we have observed the strongest relative signal of C_{60} anion near zero eV electron energy as compared to the resonant peaks seen at higher energies. We have used the earlier reported Vogt-Wannier (V-W) model [10], based on the capture of electron in the polarization potential of C_{60} to estimate the s-wave contribution to the near zero eV electron capture process. We have also estimated the absolute cross section of the C_{60}^- formation at zero eV energy using this model to be about $10^{-14}cm^2$.

The results of the temperature dependence of electron attachment to C_{60} show no effect of C_{60} vapor temperature on the intensity of the C_{60}^- peak at around zero eV electron energy. However, we have found that the lifetime of the C_{60}^- ions formed by electron capture above 2eV decreases with increase in temperature. We have also shown that the temperature dependence of the C_{60}^- observed above 2eV electron energy qualitatively supports the theoretical model based on the thermionic emission process [11]. This model had been used earlier to explain the decrease in cross section at larger energies for a given temperature of C_{60} vapor. All these findings point towards an interesting property of the C_{60} anion that the anion has excited states lying up to 10eV above the ground state. The relatively long lifetime of the C_{60}^- for the electron energies as high as 10eV and the absence of any fragment negative ion from C_{60}^- up to 15eV electron energy clearly indicate the presence of many bound anion states in the Frank-Condon overlap region with the neutral ground state. The ionization potential of C_{60} is 7.53eV. This means that both capture and ionization

simultaneously take place between 7.5 and 10eV. The presence of long-lived negative ion states lying well above the ionization potential makes fullerenes a unique system. We have also found that the cross section of the formation of the parent negative ion with considerable life time at these electron energies to be quite high (~10^{-15}cm^2) as compared to the electron impact ionization cross sections (10^{-17} cm^2 at 10eV to 10^{-15} cm^2 at the peak). These findings point to the need for more theoretical and experimental investigation of this interesting ionic species.

Apart from free electron attachment, the negative ions are also obtained by attaching the electrons excited to the Rydberg states of the atoms and molecules. In the high Rydberg states of atoms and molecules, the electron is very loosely bound and may be considered as quasi-free. When these species collide with an atom or molecule which has positive electron affinity, the loosely bound Rydberg electron could be transferred forming a negative ion. The energy needed to release the Rydberg electron is provided by the positive electron affinity of the electron acceptor. Since the Rydberg electron attachment needs some energy to be transferred from the electron acceptor, the negative ion formed is lower in energy as compared to the neutral ground state and thus gives it more stability. Hence many negative ions that are not accessible or highly unstable in the free electron attachment process could be accessed through this process. For example, CS_2^- is not observed in the free electron attachment to the ground state of CS_2, whereas this ion is observed in the Rydberg electron transfer from low lying atomic Rydberg states. A variation of the Rydberg electron attachment may occur when an electronically excited molecule collides with an atom or molecule in the Rydberg state. The Rydberg electron attachment in this case leads to the formation of negative ions in an excited state. The subsequent decay of this state through autodetachment or dissociation is identical to that in the free electron attachment case.

In the case of atomic or molecular Rydberg states the electron in the Rydberg orbital is loosely bound to the screened positively charged ion core. Because of the presence of many degrees of freedom in the ionic core, each ro-vibrational state of the molecular core has its own Rydberg series. This indicates the possibility of Rydberg states that can lie energetically above the first ionization potential of the neutral molecule. Here the excess energy above ionization potential is distributed among various degrees of freedoms in the ionic core. Such Rydberg states are called core excited Rydberg states. The role of these Rydberg states in the negative ion formation

in gases subjected to fairly intense laser beams has been shown in a few experiments in recent times [12]. In these experiments the enhancement of the fragment negative ion formation is reported by attaching the free electrons to molecules in the high Rydberg states. We have directed our efforts to explore the presence of these high Rydberg states and to understand their role in the negative ion formation by the Rydberg electron transfer to the electronically excited molecule in order to understand the effect of such excitation on the electron capture process.

The Rydberg electron attachment experiments are carried out by focusing a laser beam in a collision cell or gas beam under relatively high pressures. The laser beam excites some of the molecules to the Rydberg excited states through multi-photon absorption and these molecules then collide with other molecules transferring the Rydberg electron. The electron acceptor molecules may be in their ground or excited states. We have carried out the experiments using a single species of molecules or for a selected pair of molecular species. Since the experiment employs relatively higher pressures, we had to build an apparatus that uses a differential pumping arrangement. This pumping arrangement provides relatively higher pressure condition in the interaction region while maintaining the high vacuum in the flight tube and detector region. The interaction region is differentially pumped, through an aperture on the *puller* electrode of the linear TOFMS, using an assembly of a diffusion pump backed by a rotary pump. The differential pressure with the ratio of around 10^3 is maintained in the set up. The pressure in the interaction region is in the range of 10^{-2} to 10^{-4} Torr with the gas load whereas that near the detector is in the range of 10^{-5} to 10^{-7} Torr. The set-up has an additional provision of pumping the interaction region using an oil free pumping system employing a turbo molecular pump backed by a scroll pump. In that case the ultimate pressure in the interaction region is found to be in low 10^{-7} Torr range. The experiments are performed by focusing the laser beam of 308 nm (4.03eV) wavelength from the *Lambda Physik* XeCl *Excimer* laser on a gas cell with relatively higher pressures using a convex lens in the direction perpendicular to the TOFMS axis. Proper care has been taken to avoid the production of secondary electrons from the electrode surfaces. In some experiments, a molecular beam has been used instead of a gas cell. In this case the molecular beam is kept perpendicular to both laser beam and the TOFMS axis. The effect of small magnetic field as well as DC electric field in the interaction region on the negative ion intensities is also studied.

To begin with, we performed the experiment with SF_6 gas cell as this molecule is well known as a low energy electron scavenger. Previous Rydberg electron attachment experiments on SF_6 using state selected Rydberg atoms has been found to produce only SF_6^- ions. In our experiment, F^- and SF_5^- are also found to be produced along with SF_6^-. The formation of F^- and SF_5^- needs additional energy (~3eV for F^-/SF_6) to break the respective bonds. The ionization potential of SF_6 (~15.5eV) is too high to give photoelectrons from the processes associated with less than 4-photon absorption and the intensity used in the experiments is not sufficient for such processes to provide significant amount of free electrons. The role of free secondary electrons in the negative ion formation process is further ruled out by observing no effect of the magnetic field in various directions on the negative ion signal. The negative ion signal is found to be suppressed by applying small DC electric field in the interaction region. This effect is found to be independent of the direction of the field pointing to the role of high lying Rydberg states in the negative ion formation process. Using the flight-time measurements under different operating conditions the origin of the SF_5^- fragment is found to be due to the collisional dissociation of SF_6^- ions at the entrance aperture to the flight tube. No such conclusion could be drawn for the F^- fragment. The pressure dependence studies of these ions clearly indicated the role of impurity background gases in the process. In order to have a better control on the electron donor molecules the contribution from the background gases is eliminated by evacuating the interaction region to high vacuum using an oil-free pumping system. Under such conditions no negative ions are seen from pure gas samples. The same experiments are carried out by adding molecules having relatively low ionization potentials like aniline (I.P. 7.7eV) or cresol (I.P. 8.3eV) to the molecules under study. A two-photon absorption by aniline at 308 nm leads to excitation of Rydberg states lying just above the first ionization potential whereas in the case of cresol those lying below the ionization potential are excited. We find the formation of SF_6^- by laser light irradiation of a mixture of SF_6 with each of these molecules. For aniline + SF_6 mixture, we find a clear, though weak signal of F^- ion whereas no such signal is found in the case of cresol + SF_6 mixture. Rydberg electron attachment to ground state SF_6 cannot lead to the formation of F^-since the necessary energy to break the S-F bond is not available. The only way F^- could be produced is by Rydberg electron attachment to excited SF_6 molecules. The SF_6 molecule is

electronically excited to the state near 8eV (accessed by two-photon excitation) and captures the Rydberg electron from the donor species to form an excited negative ion state, which then dissociates to give F^-. In the case of cresol the Rydberg state is 0.3eV below the ionization limit and hence it would not have as large a principal quantum number as in aniline which could be in super excited Rydberg states. This makes the cross section for electron transfer from aniline Rydberg state accessed by two 308nm photons much larger than from that of cresol under the same photo-excitation condition. The absence of F^- from laser irradiated cresol + SF_6 mixture could be explained as due to this difference. It also highlights the importance of super excited Rydberg states in the negative ion chemistry in plasmas.

We have also studied CS_2 in similar experimental conditions. CS_2 shows single photon absorption at 308nm. The formation of S^- ion on free electron attachment to electronically excited CS_2 by 308nm photon has been investigated in our lab earlier. This process is found to have finite cross section at the electron energies around zero eV. Under relatively impure vacuum conditions we note that focusing 308 nm into a gas cell containing CS_2 gives rise to S^- through the Rydberg states of background impurities. Like in the case of SF_6, we repeated the measurements in clean high vacuum conditions using pure CS_2 and mixtures of CS_2 with aniline or cresol respectively. We find that in the case of pure CS_2 as well as cresol+CS_2 mixture no negative ions are formed, whereas aniline+CS_2 mixture gives rise to the formation of S^-. Here again we note that the super excited Rydberg states in aniline excited by two-photon process is the electron donor to the excited CS_2 molecules.

In summary, we have studied the formation and decay dynamics of molecular negative ion states using free and Rydberg electron attachment. We have discovered a general rule for DEA in organic molecules. Our observations show that most of the resonances seen in these molecules could be broken up in terms of the various functional groups present in these molecules. This functional group dependence also gives rise to site specific fragmentation of these molecules leading to the exciting possibility of controlling chemical reactions using low energy electrons. The dynamics of this fragmentation process is studied using the newly developed VMI technique. The VMI data show that the functional group dependence is retained even to the extent of orientation specificity of the group to the incoming electron. High

resolution electron attachment measurements to C_{60} as a function of temperature identify the dominance of *s-wave* resonance in the process near zero energy. We identify electron attachment from super excited Rydberg states to electronically excited molecules as a possible mechanism for fragment negative ion formation in laser irradiated gases.

The thesis will be comprised of a general introduction to electron-molecule resonances and various techniques used to study them. Detailed description of the instrumentation that is developed and used in the course of the entire work reported will be discussed in the 2nd chapter. The results of VMI measurements on O_2 and its significance to gas phase electron scattering as well as electron stimulated desorption of negative ions from surfaces will be discussed in the 3rd chapter. The absolute cross section measurements along with the site specific fragmentation results will be discussed in the 4th chapter. The 5th chapter will comprise of the results obtained for DEA to –OH containing organic molecules using the VMI technique along with the detailed discussion. The 6th chapter will describe the results of the low energy electron attachment to C_{60} molecule. The details of the results obtained in the Rydberg electron transfer experiments will be discussed in the 7th chapter. The thesis will end with a description of the scope for future work in the 8th chapter.

References:

[1] T. F. O'Malley and H. S. Taylor, *Phys. Rev.* **176**, 207 (1968).

[2] R. Azria, Y. Le Coat, G. Leferve, and D. Simon, *J. Phys. B: Atom. Molec. Phys.*, **12**, 679 (1979).

[3] E. Krishnakumar and K. Nagesha , *J. Phys. B*, **25**, 1645 (1992).

[4] *Imaging in Molecular Dynamics*, edited by Benjamin Whitaker, Cambridge University Press (2003).

[5] M. Allan, *J. Phys. B : Atom. Molec. Phys.* 2**8**, 5163 (1995).

[6] Roger Azria, Léon Sanche and Luc Parenteau, *Chem. Phys. Lett.* **156**, 606 (1998).

[7] A. Pelc, W. Sailer, P. Scheier, N. J. Mason, E. Illenberger, T. D. Märk, *Vacuum* **70**, 429 (2003).

[8] Sydney Leach, Martin Schwell, Sun Un, Hans-Werner Jochims, and Helmut Baumgartel, *Chem. Phys.* **321**, 159 (2006).

[9] O. Elhamidi, J. Pommier, and R. Abouaf, *J. Phys. B* **30**, 4633 (1997).

[10] Ilya I. Fabrikant and Hartmut Hotop, *Phys. Rev. A* **63**, 022706 (2001).

[11] S. Matejčik, T. D. Mark, P. Spanel, D. Smith, T. Jaffke, and E. Illenberger, J. Chem. Phys. **102**, 2516 (1995).

[12] C. Tau and L. A. Pinnaduwage, *J. Phys. D*, **33**, 2391 (2000).

Chapter 1

Introduction

Neutral atoms and molecules in their ground state are considered stable entities, and form the building blocks of all the material objects used in the day to day life. Charge neutrality in these building blocks is known to be the main reason for their stability in general. Addition of an electron to such neutral species leads to formation of a negative ion, which in isolated conditions, like in a gaseous phase, may either lower or raise the overall energy of the system. The capacity of the species to accept the extra electron, leading to either increase or decrease in the overall energy of the system, is known as electron affinity. A positive electron affinity means the negative ion state is energetically lower than the corresponding neutral state. Although there are many species that exist with positive electron affinity, indicating energetically stable negative ion ground state, negative ions are not that abundant in nature as the interaction of these negative ions with the surroundings causes the loss of extra electron from the system.

In spite of their rarity, it is important to study negative ion systems. The importance comes from the fact that most of the matter in our solar system, and probably within the whole universe, exists in form of ionized particles. These particles can be positively charged, that are formed due to ionization of the neutrals by high energy radiations or collisions, or negatively charged, which come into existence through the low energy secondary electron interaction with neutrals. Negative ions play important role in chemical reactions, as adding or removing an electron may be considered as an intermediate step in a chemical reaction. Recently, it has been established that low energy electron interaction, through the single and double strand breaking, causes enormous damage to DNA [1]. Also, low energy electrons are very reactive as they are readily captured by many molecules, which then undergo rapid uni-molecular decompositions. The cross sections for such processes are found to be very large. Hence, the study of negative ions is of direct interest to astrobiology, as well as, to electron induced chemistry. Apart from this, the negative ions play a vital

role in plasma physics that has direct relevance in the semiconductor industry, and to various types of processing plasmas. The negative ions play important roles in gas lasers. The study of negative ions is directly relevant also in the understanding of the phenomena of global warming and air pollution, and in a number of phenomena that occur in the upper atmosphere of earth.

The simplest way one can imagine the formation of a negative ion is through the attachment of an extra electron to a naturally occurring neutral atom or molecule. In that case the kind of forces that bind the extra electron with the neutral atom or molecule are the dipole or higher order forces, which are of short range as compared to the long range Coulumbic force which exists between any two charged particles. Hence unlike neutral or positive ions, negative ions will have very few stable excited states. In practice, very few negative ions are known which have a stable electronically excited state. Thus, almost all the excited negative ion states lie in the detachment continuum corresponding to the neutral species plus free electron. Such negative ion states, also known as the 'resonant' states, can decay by ejecting the excess electron. Such a decay process is known as *autodetachment*. This process contributes to resonant elastic and inelastic scattering of electrons. The *autodetachment* happens through the coupling between the resonant state and the detachment continuum of the ground negative ion state. The resonant states have finite lifetimes, depending on the strength of this coupling.

The molecular negative ion resonant (*NIR*) states differ from the atomic *NIR* states because of the additional degrees of freedom present in the inter-nuclear motion. Hence, apart from *autodetachment*, dissociation also becomes a possible mechanism of decomposition of the molecular *NIR* state. The excess energy arising due to the addition of an electron to a neutral forming a molecular *NIR* (electron affinity plus the kinetic energy in the case of free electron) can be redistributed in the nuclear motion leading to dissociation. The process of formation of a negative ion resonance by the attachment of a free electron, and its subsequent dissociation is known as dissociative electron attachment (*DEA*). The strong interplay between the electronic and nuclear degrees of freedom in the *DEA* process makes its dynamics very complex as well interesting.

Photon spectroscopy experiments are generally performed for studying the structure and dynamics of various molecular excited states. Experiments are being carried out even to map out the motion of bound electrons in atoms and molecules in

real time using sub-femtosecond laser pulses [2]. Collisions using charged particles like electrons and ions are also used quite extensively to study the different molecular processes [3]. Though photon spectroscopy has been a dominant tool in studying molecular processes, it is not suitable to study excited states of negative ions. This is because the typical radiative lifetimes (longer than 10^{-9} sec) are much larger than the typical lifetimes of the negative ion resonances ($<10^{-12}$ sec). Moreover, photon based studies are more restricted to the dipole allowed transitions. The ability to access both dipole and non dipole transitions makes electron collision processes an ideal tool to study the *NIR* states.

On theoretical front, the approach to understand electron attachment process in general and hence the molecular *NIR* states consists of two steps. (i) Determination of the structure, including the energy, symmetry and the potential energy surfaces of such states, (ii) determination of the dynamics of the *NIR* states leading to *DEA*. The problem is particularly complex for triatomic or polyatomic molecules.

The determination of the molecular *NIR* potential energy surfaces is beyond the scope of simple quantum chemical calculations. Due to the coupling to the continuum, the size of the basis set that is required to describe the *NIR* states becomes too large. Any quantum chemistry calculation of *NIR* state that uses infinite basis set, will lead to the neutral molecular state free electron. The defuse nature of the infinite basis set pushes the extra electron to infinity. *Ab initio* calculations are applied by using limited basis sets and appropriate scaling factors. The resonant nature of the excited negative ion states implies that the potential energy surfaces of these states are characterized by a real part associated with the energy of the system, and an imaginary part associated with the lifetime of the state against *autodetachment*. The *R*-matrix calculations, generally used for describing the electron-molecule scattering processes, are used to determine the resonance positions on the energy scale. In this method the electron configuration space is divided into two regions. The inner spherical region is centered at the center of gravity of the (atom/)molecule and comprises all the *N*-electron wavefunctions of the target (atom/)molecule as well as all the possible multi-centered interactions between *N+1* electrons including exchange. In the outer region, the scattering electron can be identified and the exchange interaction is completely neglected. After solving for the two above mentioned regions, the wave functions are then matched at the boundary to obtain the correct solutions. The quality of the results of these calculations depends on the

quality of the description of the system in the inner region. This description comprises of the target configuration as well as the continuum orbitals. Such configurations are to be taken for relevant target states. Inclusion of more of such configurations implies better accuracy for the results. It is evident that the enormous nature of the computation required for these calculations restricts their usage for molecular systems. Although, for simpler diatomic systems these calculation schemes are applied with fair bit of success [4], their application to polyatomic systems has been very difficult because of many modes of nuclear motion contributing to the number of target states. There have been some efforts towards the scattering calculations, and hence the successful determination of resonances in some highly symmetric molecules like SF_6, CF_4, C_6H_6, O_3 and C_{60} [5, 6].

Generally, while calculating the potential energy surfaces for the molecular *NIR* states, the space is divided in two regions along the different inter-nuclear axes: One in which the negative ion state has a pure resonant nature i.e., around the equilibrium configuration of the neutral target state, and the second, which is also an asymptotic region, corresponding to the inter-nuclear distances. In the latter the negative ion state lies energetically below the neutral target state. In the first region pure scattering calculations like *R*-matrix calculations are required where as in the second region quantum chemistry approach is used i.e. methods like Configuration Interaction (CI) are used. The final results are obtained by joining the surfaces calculated by two methods at the boundary of two regions. There has been a recent report of calculation of the complete complex potential energy surface for the resonant negative ion state for water (H_2O) [7] in which the entire calculation of the potential energy surface is done using CI citing narrow width and hence longer life of the resonance.

The problem of determination of the dynamics of the *NIR* state leading to *DEA* has been addressed using local complex potential model [8]. The use of such model has been restricted to just diatomic systems till recent past. However, very recently, this approach has been successfully applied to determine the complete dynamics of *DEA* to water [9] and formic acid [10]. In this approach the information of potential energy surface and the width of the resonance are found to be sufficient to determine the cross section for the *DEA* process. Generally, the fixed nuclei model is used in these calculations. In the case of polyatomic molecules, there is more than one configuration that can result from a particular capture process, making vibrational as

well as rotational motion of the molecule relevant in these calculations. Also, this leads to various possible dissociation channels making the calculations complicated.

As can be seen from the above, the progress on the theoretical understanding of the *NIR* dynamics leading to *DEA* has been slow and not much has been achieved for the polyatomic molecules due to enormous complexity of the problem involved. Clearly, much more efforts are needed, in order to make these calculation schemes reliable.

1.1 Resonant Free electron attachment to molecules

In the case of electron-molecule collision at low energies (≤15eV), negative ion formation through electron capture is one of the prominent mechanisms that takes place. The negative ion so formed is relatively short lived and decomposes either by *autodetachment* or by *DEA*, as discussed earlier. The *DEA* process can be considered to be a two step process, namely formation of *NIR* state and its dissociation.

1.1.1 Formation of negative ion resonance

In general, during the course of formation of (the) resonances, the internuclear separations do not change, and hence, can in most cases be treated as *Franck-Condon* transitions. The attachment of the electron to the molecule forming the *NIR* occurs at definite energies, leading to sharp structures in the cross section. For the *NIR* state having short lifetime, the width of the state is large, as given by the uncertainty principle.

The electron trapping mechanism of the molecule can be understood considering the potential well arising from the interaction between the incident electron and the neutral molecule. In this case, the attractive polarization and repulsive centrifugal forces combine to create a potential with a penetrable barrier. When a low energy electron approaches the target molecule, the bound electrons associated with the molecule tend to relax adiabatically, thus setting up a temporary dipole moment which is proportional to the dipole polarizability of the molecule and pointed in the direction of the approaching electron. This polarization interaction

strongly influences the low energy cross sections especially for small scattering angles.

At larger distances, the polarization interaction potential along with the centrifugal potential, arising due to relative motion of two particles can be written as

$$V_{eff} \sim \frac{l(l+1)\hbar^2}{r^2} - \frac{\alpha}{r^4} \qquad (1.1)$$

where l is the angular momentum quantum number of the incoming electron, α is the polarizability of the neutral molecule, and r is the electron-molecule distance. This effective potential creates a penetrable barrier for values of $l>0$, where the incoming electron can get trapped. Thus, it is the shape of the potential which is responsible for the trapping of the particle and for the formation of resonance, and hence this type of resonance is known as *shape resonance*. It is also called as a *single particle resonance*. Most of the *shape resonances* observed so far occur at low energies, exhibiting a lifetime in the range of 10^{-15} to 10^{-10} s or even longer resulting in decay into vibrational and rotational levels of molecules and, sometimes by fragmentation by DEA, into neutrals and negative ions. Thus *shape resonances* play an important role in rotational and vibrational excitation of molecules. Resonance seen in the *DEA* to O_2 through $^4\Sigma_u^-$ state discussed in chapter 3 is an example of a *shape resonance*.

In another mechanism of electron capture and resonance formation, the incoming electron loses sufficient energy in exciting the neutral molecule while getting trapped in the molecular system. This type of resonance is known as *core excited* or *valence excited resonance*. The resonances discussed in chapter 4 and 5 fall in this category. *Valence excited resonances* thus consist of a `*hole*' in one of the orbitals normally occupied by an electron and two `*particles*' (electrons) in normally unoccupied orbitals. A *valence excited resonance* can lie either below or above of its parent i.e. the corresponding neutral excited state in energy. If the *valence-excited resonance* lies above the neutral excited state, it is called *open channel* or *valence-excited shape resonance*. This resonance is similar to the *single particle shape resonance* except it is associated with an electronically excited state. If the *valence-excited resonance* lies below its parent, it is called *valence-excited Feshbach* or *closed channel* resonance where decay into the parent state is not possible. $^2\Pi_u$ resonance observed in *DEA* to O_2 is an example of this type of resonance. A *Feshbach*

resonance can't decay into the associated excited neutral molecule via a one electron process since the decay is energetically not possible and requires a change of the electronic configuration. This results in a longer lifetime.

Finally, in several situations the negative ion resonance formed by electron attachment may have large lifetime against *autodetachment*. If these states are stable against dissociation, one could observe these parent negative ions directly. The long lifetime against *autodetachment* arises when the electron attachment process is not Franck – Condon type and energy of the incoming electron gets distributed in the vibrational modes of the molecule during electron attachment. This makes electronic part of the negative ion state lower in energy as compared to the neutral state preventing its decay by electron ejection. The decay takes place after relatively long time when the vibrational energy is transferred back to the electronic energy. This type of resonance is called *nuclear excited Feshbach resonance*. Low energy electron attachment to C_{60} discussed in chapter 6 is an example of this.

1.1.2 Decomposition of negative ion resonance

Once a resonance is formed, the most natural way of its decay is through the process of ejection of the extra electron, termed as *autodetachment,* as discussed earlier. However, for a molecule, the resonance may also have, depending on the nature of its potential energy surface and the lifetime against *autodetachment*, another mode of decay by the way of dissociation. However, for this mode of decay to occur, its lifetime against autodetachment should be larger than the vibrational time scale of the molecular motion. Thus a molecular negative ion resonance has two competing channels of decay, one through the relaxation of the electronic degrees of freedom and other through the nuclear degrees of freedom. The eventual outcome of the process strongly depends on the mutual interaction of these two degrees of freedom. The manifestation of this inter-coupling between the electronic and nuclear degrees of freedom is seldom seen in any other molecular process and has very interesting consequences like the strong isotope effect and the exceptionally large temperature dependence of the cross sections, in some molecules [11]. This inter-coupling between the electronic and nuclear degrees of freedom may pave way for controlling the dissociation pattern, and thus, the electron induced chemistry.

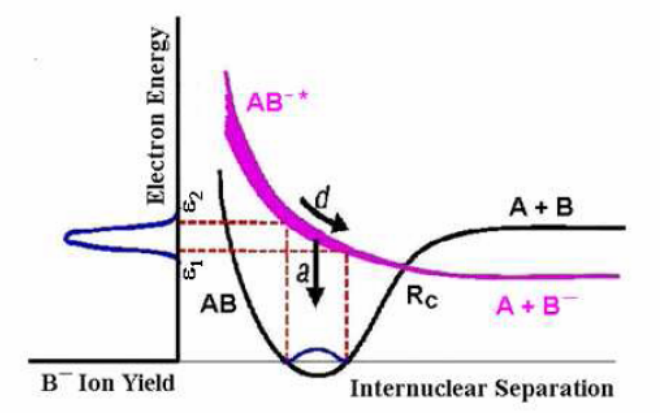

Figure 1.1: *Schematic representation of the dissociative electron attachment (DEA) from the ground state. a, d, and R_c indicate autodetachment, dissociation and critical internuclear separation beyond which the only possible channel is dissociation.*

The decay of a resonance by electron ejection can be studied only in electron scattering experiments, where one can even observe the vibrational excitation of the molecule in terms of the electron's kinetic energy loss [12]. The *DEA* process is studied by observing the negative ion mass spectrum of the products formed in the process as a function of the electron energy. In general, it is possible that depending on the detachment lifetime and stability against dissociation, a negative ion resonance may manifest in either one or both of these decay channels. Thus the electron scattering experiments and *DEA* measurements in addition to being complementary could act as a cross-check to each other.

A schematic description of the *DEA* process in terms of *Born-Oppenheimer* potential energy curves has been depicted in the Figure 1.1. According to *Franck-Condon* principle, the electronic transitions are only possible within the energy range between ε_1 and ε_2. The *autodetachment* can occur for the inter-nuclear separation, $R \leq R_c$, where R_c is called the critical distance, the crossing point of the two potential energy curves. For $R \leq R_c$, the additional electron is bound and localized to the fragment *B*, thus *autodetachment* of *NIR* is no longer possible. The cross section for *DEA* can be written as

$$\sigma_{DEA}(\varepsilon) = \sigma_C(\varepsilon) p(\varepsilon) \qquad (1.2)$$

where σ_c is the attachment (capture) cross section which depends on the symmetry properties of the molecular species and the resonant states and their *Franck-Condon* overlap; *p(ε)* is called the survival probability which depends on the mean lifetime of the resonance and the separation time (the time taken by the products to dissociate until the *autodetachment* becomes impossible) of the fragments.

Because of this resonant character of the *DEA* process, the measurement of the energy dependence for the *DEA* cross section and the peak positions allows one to determine the parameters of the *NIR* states responsible for the process at a given electron energy. Further information on the process could be obtained by determining the kinetic energy and angular distribution of negative ions with respect to the direction of the incident electron beam. The kinetic energy measurements provide information on the internal energies of the fragments and the dissociation limits of the *NIR* states involved. The angular distribution measurement provides the information about the quantal nature of the *NIR* state responsible for *DEA* process. The kinetic energy and angular distribution data also leads to the understanding of the overall dissociation dynamics of the negative ion resonance.

1.1.2.1 DEA cross section

O'Malley [13] developed a theory for the *DEA* process in diatomic molecules using the local complex potential model. The explicit formula for the *DEA* cross section has been derived assuming suitable approximations. The theory is derived from a general rearrangement formalism which is based on projection operators onto the resonance state and using *Born-Oppenheimer* approximation. In *Born-Oppenheimer* approximation, the *DEA* process is understood as an electronic transition from a continuum to a discrete electronic state which then dissociates. With this formalism, the author derived the exact transition matrix element for *DEA* in terms of the resonance and the potential scattering wave functions. Then the adiabatic approximation was considered for the potential scattering wave function in order to neglect the indirect influence of other inelastic processes on the resonance transition. And finally, the classical motion of the dissociating particles was introduced for calculating the survival probability and to derive a simple explicit formula for the *DEA* cross section from an arbitrary initial vibrational-rotational state of the molecule. The author defined a complex potential energy curve for the negative ion as *V(R)-*

$i\Gamma_a(R)/2$, $V(R)$ being the potential of the neutral and $\Gamma_a(R)$ as the *autodetachment* width which expresses the energy uncertainty due to the limited lifetime with respect to *autodetachment*. The imaginary part describes the leakage due to *autodetachment*. According to the theory of O'Malley, the *DEA* cross section for a diatomic molecule, initially in its lowest vibrational level (v=0) and with a purely repulsive *NIR* state, is given as

$$\sigma_{DEA}(\varepsilon) = \frac{4\pi^{3/2}}{(2m/\hbar^2)\varepsilon} g \frac{\Gamma_{\bar{a}}}{\Gamma_d} \exp\left(\frac{\Gamma_a^2 - 4(\bar{\varepsilon}_0 - \varepsilon)^2}{\Gamma_d^2} \right) \exp[-p(\varepsilon)] \qquad (1.3)$$

where m is the mass of electron, $\hbar$ is the Planck's constant divided by 2π, $\bar{g}$ is a statistical factor, $\Gamma_{\bar{a}}$ is the partial *autodetachment* width, Γ_a is the total *autodetachment* width, Γ_d is the *DEA* resonance width, $\varepsilon_0' = \varepsilon_0 + 1/2\hbar\omega$, ε_0 is the true electron energy at peak and $1/2\hbar\omega$ is the zero-point energy. The survival probability of the resonance state against *autodetachment* has been written as [12]

$$\exp[-p(\varepsilon)] = \exp\left[-\int_{R_\varepsilon}^{R_C} \frac{\Gamma_a(R)dR}{\hbar v(R)} \right] = \exp\left[-\frac{1}{\hbar} \int_{R_\varepsilon}^{R_C} \Gamma_a(R) dt(R) \right] \approx \exp\left(-\frac{\tau_s}{\bar{\tau}_a} \right) \qquad (1.4)$$

where $\bar{\tau}_a$ is the mean *autodetachment* lifetime and is given by $\bar{\tau}_a = \hbar/\Gamma_a$ and τ_s is the time taken by the fragments to dissociate until the *autodetachment* becomes impossible. It can be written as

$$\tau_s = \int_{R_\varepsilon}^{R_C} \frac{dR}{v(R)} \qquad (1.5)$$

with R_ε is the distance where the electronic transition takes place, R_C is the crossing point between the two potential curves and $v(R)$ is the relative velocity of separation of the fragments. For $R > R_C$, the survival probability is equal to unity; *i.e.* beyond this internuclear separation the *NIR* has to dissociate.

The situation becomes much more complicated in the case of polyatomic molecules as compared to diatomic molecules as there can be many dissociation channels available for the decomposition of the negative ion resonance. Apart from

this, the dynamics of the resonance state itself can be very complicated comprising of several effects like scrambling where the rearrangement within the molecule may take place. This further increases the number of possible dissociation channels.

1.1.2.2 Angular distribution of the fragment anions

It has been shown by detailed theoretical calculations by O'Malley and Taylor [14] and simple symmetry arguments by Dunn [15] that the angular distribution of fragment negative ions produced by *DEA* is in general anisotropic and depends on the symmetries of the initial and final molecular electronic states in the case of diatomic molecules. Assuming the plane wave picture for the incoming free electron beam, there will be certain orientation of the neutral molecules with respect to the momentum vector of the incoming electron beam in the laboratory frame that will be preferred for the electron capture process depending on the partial wave involved and the symmetry of the negative ion. In the case of diatomic molecules, under the assumption that the molecule does not rotate within the time scale of *DEA*, the angular distribution of the fragment anion will directly indicate the preference for a particular orientation the form of anisotropy in differential cross section. Knowing the initial state of the neutral molecule and this anisotropy one can determine the symmetry of the negative ion state involved in the *DEA* process.

If there are more than one *NIR* states involved in the *DEA* process, the information about their possible symmetries can be obtained from the study of the electron energy dependence of the fragment angular distribution relative to the incident electron beam direction. In the gas phase, the molecules are oriented in all directions. It follows that any dependence of the probability of the electronic transition on the direction of the incident electron and an axis of the molecule will be reflected in the angular distribution of the dissociation products. A schematic representation of the process and angular distribution of the fragment negative ions is shown in Figure 1.2.

As far as *DEA* is concerned, the incident plane wave is symmetric with respect to all rotations about $\vec{k}$ and with respect to the reflection in planes containing $\vec{k}$, $\vec{k}$ being the momentum vector of the incident electron. For a given direction of the nuclear axis of the target molecule, the initial molecular state may possess certain symmetries with respect to these operations.

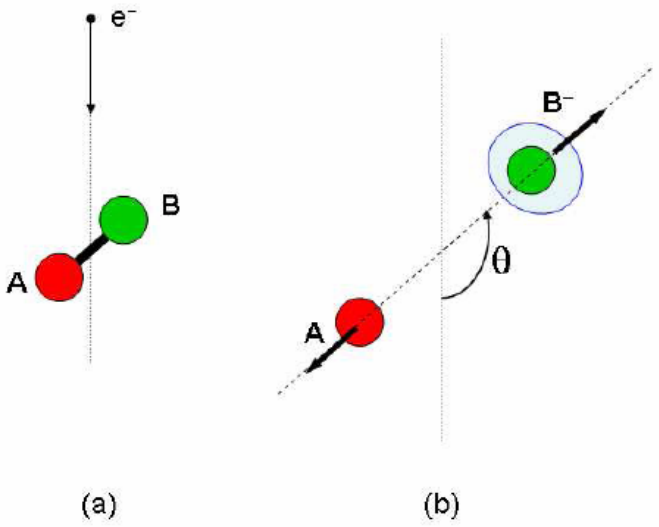

Figure 1.2: *Schematic representation of the angular dependence of the fragment negative ion produced in DEA. Panel (a) represents the situation before collision, electron's momentum vector is vertically down as shown by a down-arrow and panel (b) shows the fragmentation process, arrows show the direction of the motion of the fragments and angular dependence of the fragment ion with respect to the incident electron beam.*

The symmetry of the system before collision can be defined by (i) the initial molecular state, (ii) the electron momentum vector $\vec{k}$ and (iii) the molecular orientation with respect to $\vec{k}$. Transition to a particular final state will only be possible if it possesses these same operations or in other words, the *NIR* states should possess a symmetry which conserves the overall symmetry of the system for a particular orientation. Hence, for a particular molecular state and orientation with respect to the incident electron momentum vector, only certain negative ion states will be allowed thus defining the selection rules.

Under the assumptions that (i) there is only one resonance that contributes to the negative ion formation (ii) the negative ion state does not rotate before it decays (iii) the coupling is due to a pure electronic, spin independent, matrix element, O'Malley and Taylor [13] have shown that the differential cross section is given by

$$\frac{d\sigma}{d\Omega}(\Omega) = \frac{4\pi^3}{k_i^2}\exp(-\rho_{Jr})g\sum_{\Lambda r}\left|\sum_{l=|\mu|}^{\infty}\left\langle \chi_{Jr}\left|V_{l|\mu|}\right|\chi_v\right\rangle Y_{l\mu}^{*}(\Omega)\right|^2 \qquad (1.6)$$

in which χ_{Jr} and χ_v are vibrational wave functions and g is the spin weighting factor, exp(-ρ_{Jr}) is survival probability factor $V_{l|\mu|}$ is the electronic transition element and k_i is the incident electron momentum. Because of the conservation of the electronic axial orbital momentum there is a selection rule

$$\mu = \Lambda_f - |\Lambda_i| \tag{1.7}$$

where Λ_i and Λ_f are the electronic axial orbital angular momenta of target state and resonant state respectively. Tronc *et al.* [16] have shown that under pure resonant scattering (*PRS*) approximation the term $<\chi_{Jr}|V_{l|\mu|}|\chi_v>$ can be written as $i^l a_{l|\mu|}$; where $a_{l|\mu|}$ is a real co-efficient.If a spherically symmetric potential scattering is included (PRS-PS approximation) the $<\chi_{Jr}|V_{l|\mu|}|\chi_v>$ term becomes $i^l exp(i\delta_l) a_{l|\mu|}$ where δ_l is the potential scattering phase shift. Hence the angular dependence of the fragment anion in the case of diatomic molecule take the general form

$$I(\theta,\phi,\varepsilon) \sim \left| \sum_{l=|\mu|}^{\infty} a_{l,|\mu|} Y_{l\mu}(\theta,\phi) \right|^2 \tag{1.8}$$

The l values are restricted by

$$l \geq |\mu| \tag{1.9}$$

Furthermore, for homonuclear diatomic molecule l values are further restricted to even or odd values depending on whether the initial and final states are having the same or opposite parity with respect to inversion operation. Notice that, in *DEA*, the extra electron carries one-half unit of spin, thus there exists inherent spin selection rule

$$S_f = S_i \pm 1/2 \tag{1.10}$$

With the same assumption i.e. only one resonance contributes at a time and the coupling is purely electronic type and the dissociation takes place faster than the rotation of the molecule, Azria *et al*. [17] have adopted the similar treatment for polyatomic molecules. For both diatomic and polyatomic molecules, assuming pure electronic coupling, the angular dependence is given by the matrix element $<\Phi_r|H_e|\Phi_{kiEi}>$ in which Φ_r is the resonant wavefunction, H_e is the electronic Hamiltonian, and Φ_{kiEi} is the initial wavefunction. Also in the case of polyatomic molecules the description of the angular distribution becomes relevant only to the diatomic like dissociation i.e. two body break-up. The angular dependence comes from the fact that Φ_{kiEi} contains the incident plane wave $exp(ik_i \cdot r_e)$. For diatomic molecules this plane wave has been obtained from spherical harmonics, but in the case of polyatomic molecules, in order to introduce a selection rule, $exp(ik_i \cdot r_e)$ is expanded in linear combinations of spherical harmonics which form a basis for the irreducible representations of the point group G of the molecule. These functions are denoted by Φ_{lm}^{γ} (with m > 0 and $\gamma = \pm$ l) and are chosen real. Then one can write:

$$\exp(ik_i \cdot r_e) = 4\pi \sum_{l=0}^{\infty} \sum_{m=0}^{l} i^l j_l(k_i, r_e) \sum_{\gamma=\pm 1} \Phi_{lm}^{\gamma *}(\hat{r}_e) \Phi_{l\mu}^{\gamma *}(\hat{k}_i) \qquad (1.11)$$

This leads to the expression for the differential cross section to be

$$\frac{d\sigma}{d\Omega}(\hat{k}_i) \propto \left| \left\langle \Phi_r | H_e | \Phi_{\hat{k}_i E_i} \right\rangle \right|^2 \propto \left| \sum_{l,m,\gamma}{}' i^l \exp(i\delta_l) a_{lm}^{\gamma *} \Phi_{lm}^{\gamma *}(\hat{k}_i) \right|^2 \qquad (1.12)$$

in which δ_l is zero in *PRS* approximation. Also

$$a_{lm}^{\gamma} = \int dr \Phi_r^* H_e \Phi_i j_l(k_i r_e) \Phi_{lm}^{\gamma}(\hat{r}_e) \qquad (1.13)$$

This implies that a_{lm}^{γ} is real and equal to zero if Φ_{lm}^{γ} is not a basis for the irreducible representation $\Gamma_r \, X \, \Gamma_i$; Γ_r and Γ_i being the irreducible representations of the resonant and the target states respectively. This selection rule leads to limit the sum in (1.12) to the allowed values of l (Σ' indicates this limitation).

The expression (1.12) represents the dependence of the cross section on the orientation of $\boldsymbol{k_i}$ in the molecular frame. However one wants the dependence of the cross section on the angle θ between the direction of dissociation and $\boldsymbol{k_i}$. By using the rotation matrices one can transform the functions $\Phi_{lm}^{\gamma}\left(\hat{k}_i\right)$ into the functions $X_{lm}^{\gamma}(\theta,\phi)$ where *(θ, φ)* are the polar angles of $\boldsymbol{k_i}$ in the dissociation frame (in which the *z* axis has the direction of the bond that breaks). By averaging over the angle φ we obtain the following expression for the angular distribution in the laboratory frame:

$$I(\theta) \propto \frac{1}{2\pi}\int_0^{2\pi}\frac{d\sigma}{d\Omega}(\theta,\phi)d\phi \propto \frac{1}{2\pi}\int_0^{2\pi}\left|\sum_{l,m,\gamma}{}' i^l \exp(i\delta_l) a_{lm}^{\gamma} X_{lm}^{\gamma *}(\theta,\phi)\right|^2 d\phi \qquad (1.14)$$

For one process, the expected angular distribution is a combination of the partial distributions for each allowed value of *l.* The general shape is, however, given by a linear combination of these partial distributions with coefficients $(a_{lm}^{\gamma})^2$. The allowed values of *l* and *m* can be determined from the work of Read [18] which explains the angular distribution of the electron scattering from polyatomic molecules.

1.1.2.3 Energetics of the fragments

In general, the *DEA* process can be written as

$$e^-(\varepsilon) + AB \rightarrow AB^{-*} \rightarrow A + B^- + E^* \qquad (1.15)$$

where A and/or B is an atom or a radical, ε is the incident electron energy and E^* is the total excess energy available from the above *DEA* process. The excess available energy will be partitioned between fragments' kinetic energy and their internal energy. Thus the measurement of ion's kinetic energy can give valuable information about the distribution of excess energy available to the different degrees of freedom of the fragments.

From Figure 1.3, the energy balance for *DEA* can be written as

$$\varepsilon = [D(A\text{-}B) - E.A.(B)] + E^* \qquad (1.16)$$

where ε is the electron energy imparted to the system, *D(A-B)* is the bond dissociation energy of the molecule *AB*, and *EA(B)* is the electron affinity of the fragment *B*.

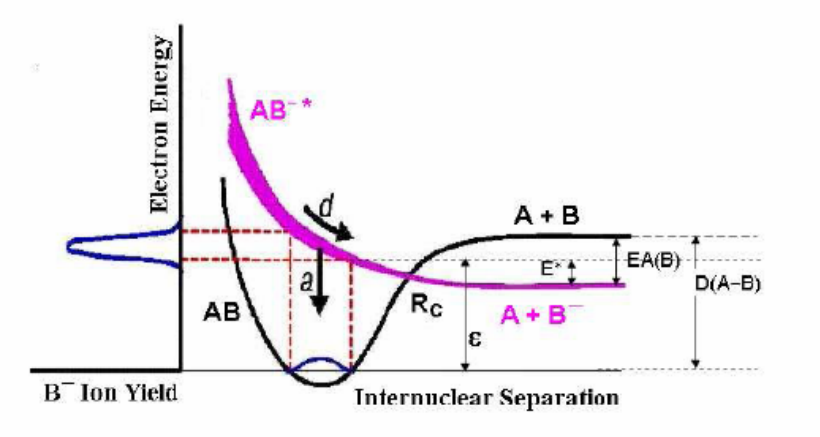

Figure 1.3: *Schematic of potential energy curve associated with DEA giving the account of the excess available energy.*

Because of the larger mass ratio of AB molecule to that of electron, the center-of-mass of the reacting system essentially coincides with the center-of-mass of the molecule and moves relative to the laboratory system with the thermal velocity of the molecule. This velocity is in general very much less than the velocity of the electron and hence can be neglected.

If the kinetic energy of the ionic fragment is measured, the total translational kinetic energy E_T can be determined from the conservation of linear momentum. Furthermore, if B^- is the atomic ion, the energy amounting $(E^* - E_T)$ must have been deposited as the internal energy in the remaining neutral fragment. Measurement of ion kinetic energy as a function of incident electron energy can provide detailed information about the distribution of the excess energy in the unimolecular decomposition of the *NIR* state.

The measurement of kinetic energy of the fragment negative ion can provide the information about the number of resonant states participating in the DEA process at given electron energy with different dissociation limits. Hence measurement of angular distribution along with the kinetic energy of the anion fragment can provide in-depth information about the dynamics of the *DEA* process such as the energy partitioning, possible many body break-ups, scrambling, number of resonances accessed etc.

1.2 Rydberg electron transfer to molecules

In another way of formation of negative ion the atoms or molecules excited to their high lying Rydberg states are made to collide with other molecules. For sufficiently large principal quantum numbers (n>20) all atoms can be considered to be hydrogen like i.e. the excited electron moves in a large orbit in a near-Coulombic field of essentially unit charge. Thus the radius of the electron orbit can be considered to be n^2a_0 following the Bohr's model where a_0 is Bohr radius. The energy of electron in such orbit is R_H/n^2 in eV where R_H = 13.6eV. Thus the electron in high lying Rydberg states is very weakly bound and can be ionized easily by electric fields. Also it is found that the radiative lifetime of the Rydberg states varies approximately as $n^{4.5}$ making these states relatively long lived in isolated conditions.

The same can be considered to be true in the case of molecular Rydberg states in which the internal structure of the molecule i.e. the additional degrees of freedom present in the ionic core can be neglected and the entire system can be treated as hydrogen like core with a loosely bound electron.

In collisions of highly excited Rydberg atoms/molecules with another molecule, the target can not interact simultaneously with both the electron and the core. The electron can be assumed to behave as if it were free. Hence, the highly excited Rydberg atom can be used as a source of low-energy "free" electron with momentum distribution characterized by particular quantum state of the Rydberg atom.

Due to large size of the Rydberg orbitals in atoms/molecules such transfer process has a very large cross section. Hence this process plays significant role in the anion formation in the high pressure conditions where atoms/molecules are excited to their Rydberg states. These are the conditions that resemble those in many of the practical applications.

In the Ryberg electron transfer a small amount of energy is needed to release the loosely bound electron from the Rydberg orbital. This energy can be provided by the positive electron affinity of the acceptor molecule. Hence this lowers the overall energy of the system making it possible to obtain some negative ion states that are not directly accessible through simple free electron attachment. For example in the case of CS_2 molecule, the parent CS_2^- ion has never been observed in free electron attachment experiments. The electron affinity of CS_2 is 0.6eV [19]. This implies that in

the free electron attachment the CS_2^- ion is always formed in its excited state which is unstable and decays either by *autodetachment* or by dissociation [20]. In the case of Rydberg electron transfer in collisions with the rare gas atoms in thie low lying Rydberg states the CS_2^- ion is observed [21].

Although there have been several reports about the Rydberg electron transfer [22-28] to ground state molecules in literature, there has been just one such report for the molecule in its excited state (high Rydberg state) [29]. Hence we have attempted to study the Rydberg electron transfer to electronically excited molecules in relatively high (~ few tens of mTorr) pressure conditions.

This thesis comprises of the following structure: detailed description of the instrumentation that is developed and used in the course of the entire work reported is discussed in the 2nd chapter. The results of *VMI* measurements on O_2 and its significance to gas phase electron scattering as well as electron stimulated desorption of negative ions from surfaces are discussed in the 3rd chapter. The results of absolute cross section measurements for *DEA* to simple organic molecules in the gas phase, particularly for the hitherto unobserved hydride ion channel and the discovery of a functional group dependence in the process resulting in the site specific fragmentation are discussed in the 4th chapter. The 5th chapter addresses the dynamics of the site specific fragmentation of *–OH* containing organic molecules using *VMI*. The 6th chapter describes the results of the low energy electron attachment to C_{60} molecule. The results obtained in the Rydberg electron transfer experiments are discussed in details in the 7th chapter. At the end a description of the scope for future work is included as the 8th chapter.

Reference:

[1] B. Boudaiffa, P. Cloutier, D. Hunting, M. A. Huels, L. Sanche, *Science* **287,** 1658 (2000).

[2] H. Njikura, F. L'egar'e, R. Hasbani, A. D. Bandrauk, M. Yu. Ivanov, D. M. Villeneuve and P. B. Corkum, *Nature*, **417**, 917 (2002).

[3] Earl W. McDaniel, *Atomic Collisions: Electron and Photon Projectiles* (John Wiley and Sons, New York 1989); Earl W. McDaniel, J. B. A. Mitchell and M. Eugene Rudd, *Atomic Collisions: Heavy Particle Projectiles* (John Wiley and Sons, New York 1993).

[4] C. J. Noble, K. Higgins, G. Woste, P. Duddy, P. G. Burke, P. J. O. Teubnor, A. G. Middleton and M. J. Brunger, *Phys. Rev. Lett.* **76** 3534 (1996) and references therein.

[5] Robert R. Lucchese, F. A. Gianturco and N. Sanna, *Chem. Phys. Lett.*, **305**, 413 (1999) and references therein.

[6] Bernd M. Nestmann, S. V. K. Kumar and Sigrid D. Peyerimhoff, *Phys. Rev. A,* **71**, 012705 (2005).

[7] Daniel J. Haxton, Zhiyong Zhang, C. William McCurdy and Thomas N. Rescigno *Phys. Rev. A*., **69**, 062713 (2004).

[8] D. T. Birtwistle and A. Herzenberg, *J. Phys. B* **4**, 53 (1971).

[9] Daniel J. Haxton, Zhiang Zhang, H.-D. Meyer, Thomas N. Rescigno and C. William McCurdy *Phys. Rev. A*., **69**, 062714 (2004).

[10] T. N. Rescigno, C. S. Trevisan and A. E. Orel, *Phys. Rev. Lett.* **96**, 213201 (2006).

[11] L. G. Christophorou (ed.), *Electron-Molecule Interactions and Their Application, Vol. 1* (Academic Press INC., London, 1983).

[12] M. J. Brunger and S. J. Buckman *Phys. Rep*. **357,** 215 (2002).

[13] T. F. O'Malley *Phys. Rev.* **150**, 14 (1966).

[14] T. F. O'Malley and H. S. Taylor, *Phy. Rev.* **176**, 207 (1968).

[15] Gordon H. Dunn, *Phys. Rev. Lett.* **8**, 62 (1962).

[16] M. Tronc, F. Fiquet-Fayard, C. Schermann and R. I. Hall, *J. Phys. B: Atom. Molec. Phys.* **10**, 305 (1977).

[17] R. Azria, Y. Le Coat, G. Leferve, and D. Simon, *J. Phys. B: Atom. Molec. Phys.*, **12**, 679 (1979).

[18] F. H. Read, *J. Phys. B (Proc. Phys. Soc.)*, **1**, 893 (1968).

[19] F. Misaizu, H. Tsunoyama, Y. Yasumura, K. Ohshimo and K. Ohmo, *Chem. Phys. Lett*., **389**, 241 (2004).

[20] E. Krishnakumar and K. Nagesha, *J. Phys. B: At. Mol. Opt. Phys.*, **25**, 1645 (1992).

[21] L. Suess, R. Parthasarathy and F. B. Dunning, *Chem. Phys. Lett.*, **372**, 692 (2003).

[22] Y. Liu, L. Suess and F. B. Dunning, J. Chem. Phys., 122, 214313 (2005) and references therein.

[23] W. D. Robertson, N. I. Hammer, J. E. Bartmess, R. N. Compton, K. Diri and K. D. Jordan, J. Chem. Phys. 122, 204319 (2005) and references therein.

[24] L. Suess, Y. Liu, R. Parthasarathy and F. B. Dunning, J. Chem. Phys., 122, 124315 (2005) and references therein.

[25] L. Suess, Y. Liu, R. Parthasarathy and F. B. Dunning , J. Chem. Phys., 121, 7162 (2004) and references therein.

[26] L. Suess, R. Parthasarathy and F. B. Dunning, J. Chem. Phys., 119, 9532 (2003) and references therein.

[27] J. Huang, H. S. Carman Jr., and R. N. Compton, *J. Phys. Chem.* **99**, 1719 (1995).

[28] J. M. Weber, M. W. Ruf, and H. Hotop, *Z. Phys. D* **37** (1996) 351; *Chem. Phys. Lett.* **361**, 277 (2002).

[29] K. Nagesha and L. A. Pinnaduwage, *J. Chem. Phys.* **17**, 7124 (1998).

Chapter 2

Experimental

Four different experimental set ups were used to carry out the measurements discussed in the thesis. They are:

- An experimental set-up dedicated to measurement of absolute cross sections for dissociative electron attachment (*DEA*).
- A Velocity Map Imaging (*VMI*) set-up to measure the kinetic energies and angular distributions of fragment negative ions arising from the *DEA* process.
- A high resolution electron attachment set-up for studying temperature dependence of the attachment process.
- Experiment to study negative ion formation through Rydberg electron attachment in gases under laser interaction.

2.1 Measurement of absolute cross sections

Measurements of the absolute cross section for *DEA* were carried out using a crossed electron beam-molecular beam arrangement. A segmented time-of-flight mass spectrometer (*ToFMS*) was used to mass analyze the negative ion fragments formed in the *DEA* process. The absolute cross section for the formation of a particular negative ion fragment was determined using a relative flow technique [1].

In order to locate the resonances on the electron energy scale the negative ion signal was obtained as a function of electron energy. The relative ion yield was then put on the absolute scale by comparing the signal from the molecules of interest under given conditions with that from a standard gas with a known cross section, by maintaining the same conditions. We used the O^-/O_2 as the standard for this purpose.

The experiments were carried out at a background pressure of 10^{-6} Torr in the interaction region in the presence of molecular beam. This ensured the pressure in the interaction volume to be not more than 10^{-4} Torr providing single collision conditions.

2.1.1 The set-up

The experimental set-up is shown in Figure 2.1. It comprises of a magnetically collimated electron gun, Faraday cup to measure the electron current, a capillary array to produce an effusive molecular beam, an ion extraction assembly and the segmented *ToFMS*. The electron beam from the gun intersects the molecular beam at right angles at the centre of the interaction region, which is flanked symmetrically by the pair of ion extraction electrodes. The electron beam emerging from the interaction region is collected by the Faraday cup. The magnetic field used for collimating the electron beam is generated using a pair of compact solenoids mounted symmetrically on either side of the interaction region. Mechanical alignment of the entire experiment is achieved by snuggly fitting the electron gun and the Faraday cup into the formers of the solenoids coaxially. The support frames holding the solenoids are also used for mounting the ion extraction grids and the segmented *ToFMS*, with appropriate mechanical alignment.

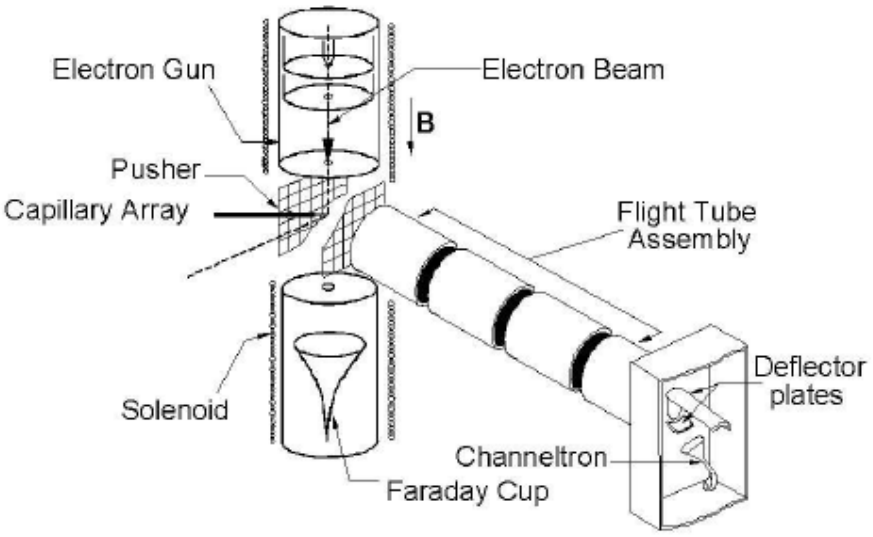

Figure 2.1: *Schematic of the experimental arrangement for making absolute dissociative electron attachment cross sections.*

2.1.1.1 Electron gun

The schematic of the electron gun assembly used in these experiments is shown in Figure 2.2. The electrons were produced by thermionic emission from a heated tungsten filament, which was kept floating on variable voltage. A cathode with Pierce geometry (Pierce element) and a grid aperture completes the three element gun.

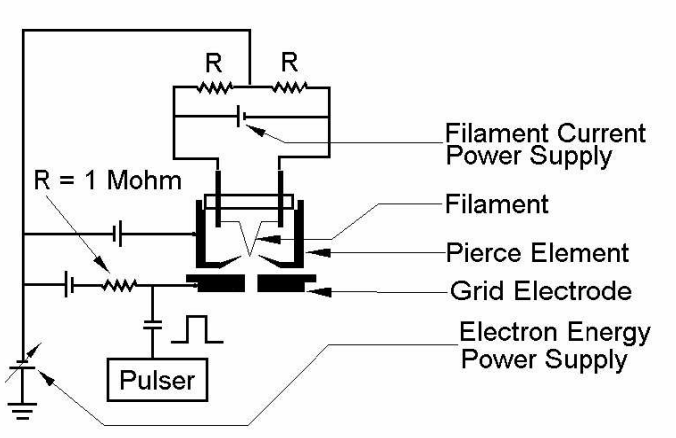

Figure 2.2: *Schematic details of the Electron Gun and the biasing mechanism.*

The cathode and the grid elements are biased with respect to the filament and the potential on these electrodes could be varied independently. This assembly was followed by an aperture at ground potential. The negative voltage on the filament with respect to ground defined the mean energy of the emerging electron beam. The geometrical divergence of the electron beam was controlled by the small apertures used on various electrodes as well as the collimating magnetic field. The filament was directly heated using a fixed current source giving a continuous current of about 2 to 2.5 amps as shown in the Figure 2.2. In most of the experiments the electron gun was operated in the pulsed mode. This was achieved by negatively biasing the grid aperture with respect to the filament (typically 3volts) and overriding it with a positive square pulse with very short rise time (rise time < 1nsec) and appropriate width (typically 250nsec). The negative bias on the grid aperture stopped the electron beam from passing through it. The overriding positive pulse created the pulses of electron beam by negating the effect of the bias on the grid aperture for duration of the pulse. The gun could be operated at different pulse repetition rates ranging from 100 Hz to 20 KHz. Typical electron beam energy resolution was restricted by the inherent spread in the electrons emitted by the filament which was ~ 0.5eV.

2.1.1.2 Faraday cup

The Faraday cup situated opposite to the electron gun was used to measure the electron current in the interaction region. The schematic of the Faraday cup is shown

in Figure 2.3. It was made of a copper tube of 75 mm length and 10 mm diameter with one end closed with a smaller copper rod cut at 45˚ that faces the electron beam.

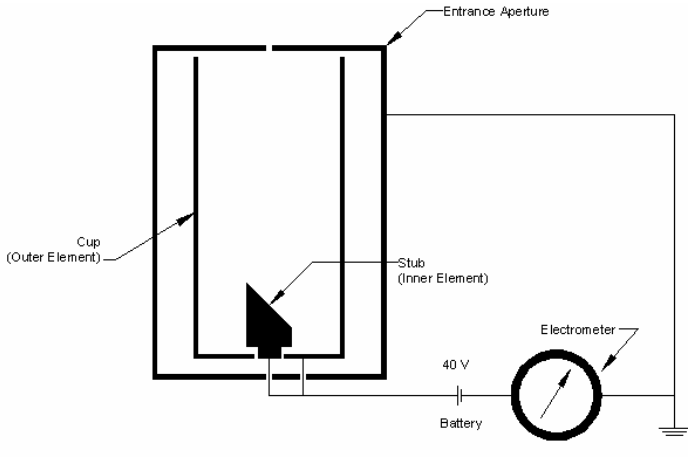

Figure 2.3: *Schematic of typical design and biasing of the Faraday cup along with the electrometer.*

The entire tube was mounted in a grounded copper tube of larger diameter and having an aperture of 3mm diameter. The inner copper tube was electrically isolated and connected to electrometer through a +40 volts bias using a well shielded battery as shown in the figure. The electron beam collected by the inner copper tube was measured by the electrometer. The positive bias on the copper tube prevents the secondary electron from escaping the Faraday cup and re-entering the interaction region. Any electron escaping the Faraday cup would be carried to the interaction region due to the collimating magnetic field present in the region. Hence this bias was critical for this type of set-up. The outer grounded tube along with the aperture in front of the Faraday cup shielded the inner tube from electromagnetic interference as well as prevented penetration of the electric field from the Faraday cup into the interaction region.

2.1.1.3 Segmented time-of-flight mass spectrometer (*ToFMS*)

The segmented *ToFMS* was used to obtain the mass spectrum of the negative ions formed in the *DEA* process. The *ToFMS* is similar to the conventional *ToFMS* with Wiley-McLaren geometry except that the single element flight tube is replaced

by four element flight tube [2]. The mass spectrometer consisted of three regions namely the interaction region, the acceleration region and the flight tube region.

(a) The interaction region

The interaction region where the molecular beam and the electron beam was made to cross each other at right angle was flanked by two electrodes namely the pusher electrode and the *puller* electrode separated by 10mm. The pusher electrode was made of a stainless steel plate with a narrow aperture at the center. The capillary array used to generate a molecular beam was placed in that aperture making the molecular beam aligned along the axis of the *ToFMS*. The puller electrode had an aperture of 20mm diameter at the center. This aperture was covered with a molybdenum wire-mesh with large transmittance. The purpose of this wire-mesh was to prevent electric field penetration from the acceleration region into the interaction region. Also the presence of the wire mesh helped in providing a uniform electric field in the interaction region.

(b) Acceleration region

The ions extracted from the interaction region were further accelerated by an electric field between the pusher electrode and the first element of the flight tube, which were separated by 5 mm. In order to define this field appropriately, a molybdenum wire-mesh was mounted on the entrance to the flight tube element.

(c) Flight tube region

The flight tube was made of four coaxially placed cylindrical elements that were isolated from each other instead of one long tube used in the conventional linear *ToFMS*. These elements could be floated at different potentials making the flight tube behave like an electrostatic lens assembly for the ions entering the flight tube region. This assembly helps in transporting all the ions that enter the flight tube region at any entrance angle to the detector. While doing so the mass resolution of the *ToFMS* worsens as the flight tube region is no more field-free unlike the conventional *ToFMS*.

The experiment was performed in pulsed mode - i.e. a pulsed electron beam was made to interact with the molecular beam and the negative ions so formed were extracted with the pulsed extraction field that was delayed with respect to the electron pulse (~100nsec). The ions formed in the interaction region were extracted using a

high voltage negative pulse (~ 200V and 1μsec width) on the *pusher* electrode making all the ions that were formed in the interaction region to enter the acceleration region. The voltages on the different flight tube segments were adjusted so that the ions were made to focus at the detector situated at the end of the flight tube region. This gave a unique advantage of complete extraction, transportation and detection of all the ions that were formed in the interaction region irrespective of their initial kinetic energies and angular distribution. This was the most essential requirement for the absolute cross section measurement for various fragment negative ions that were formed in the *DEA* process. Although it affected the mass resolution of the spectrometer, it was sufficient to separate out most of the negative ion fragments formed in the case of the molecules that we studied.

The above arrangement provided the unique advantage of complete extraction, transportation and detection of all the ions generated in the interaction region irrespective of their initial kinetic energy and angular distribution. This feature was essential in order to measure the absolute cross sections of the process under study. In fact there exists no other technique which is capable of providing reliable cross sections for the *DEA* process when the fragment ions have reasonable kinetic energies and when more than one type of ions are formed from a given molecule.

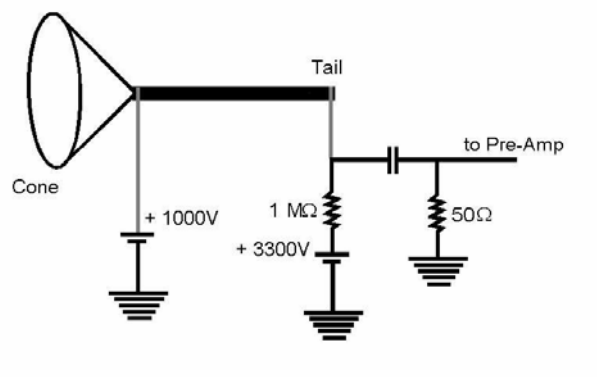

Figure 2.4: *Schematic of the biasing of the channel electron multiplier (channeltron) for negative ion detection.*

The channel electron multiplier (Channeltron) was used as the ion detector. The biases on the various electrodes in the channeltron are shown in Figure 2.4. The ion striking the front surface of the channeltron typically produces 2-3 electrons from the layer of semiconductor coating on the inner wall of the detector. These electrons were accelerated down the channels by positive bias voltage. These secondary

electrons produce more secondary electrons on striking the walls of the channels on their passage which further induce the formation of more secondary electrons on further collisions with the channel walls. The process continues till the end of the channel producing a pulse of as much as 10^7 to 10^8 electrons. For the negative ion detection the cone was operated at positive 1000 volt and the tail was operated at positive 3500 volt.

2.1.2 Making measurements

The schematic of the data acquisition system that was used to measure the absolute cross section is shown in Figure 2.5. The signal obtained from the channeltron was fed to the constant fraction discriminator (*CFD*) after appropriate amplification through fast amplifier. The out put of the *CFD* was fed as the stop pulse to the time to amplitude converter (*TAC*). The start pulse of the *TAC* was obtained from the pulse generator that provides the extraction pulse. The output of *TAC* was fed to a pulse height analyzer (*PHA*) that generated the time-of-flight spectrum.

During the experiment, the time–of-flight spectrum of the ions was obtained while the electron energy was ramped from 0 to 20 eV in order to identify various negative ions formed in the *DEA* process. A particular mass from the time-of-flight spectrum was selected by adjusting a single channel analyzer (*SCA*) window on the *TAC* and the intensity of that ion signal was measured as a function of electron energy using computer software. The curve so obtained is called the excitation function, the ion yield curve, or the relative cross section for the formation of that particular fragment ion.

A calibration of the electron energy was needed as the potential difference between the filament and the ground aperture was not the sole decider of the electron energy. The contact potentials between various electrodes of the electron gun as well as the effect of space charge present in the tiny volume in the electron gun was found to affect the electron energy. Apart from these effects the stray electric fields present in the interaction region due to the small field penetration from the acceleration region where all the fields were DC also played some role in determining the energy of electrons. Also the different surface conditions of various electrodes in the presence of different gases in the experiment could also change the electron energy as the potential seen by the electrons in the interaction region would differ as these

conditions differ. Assuming the last mentioned effect to have negligible contribution to the uncertainty of the electron energy for the gases that were studied in the course of this work, the energy calibration was carried out using the known *DEA* resonance in the H^- channel from H_2O (at 6.5eV) present in the background gases as the reference.

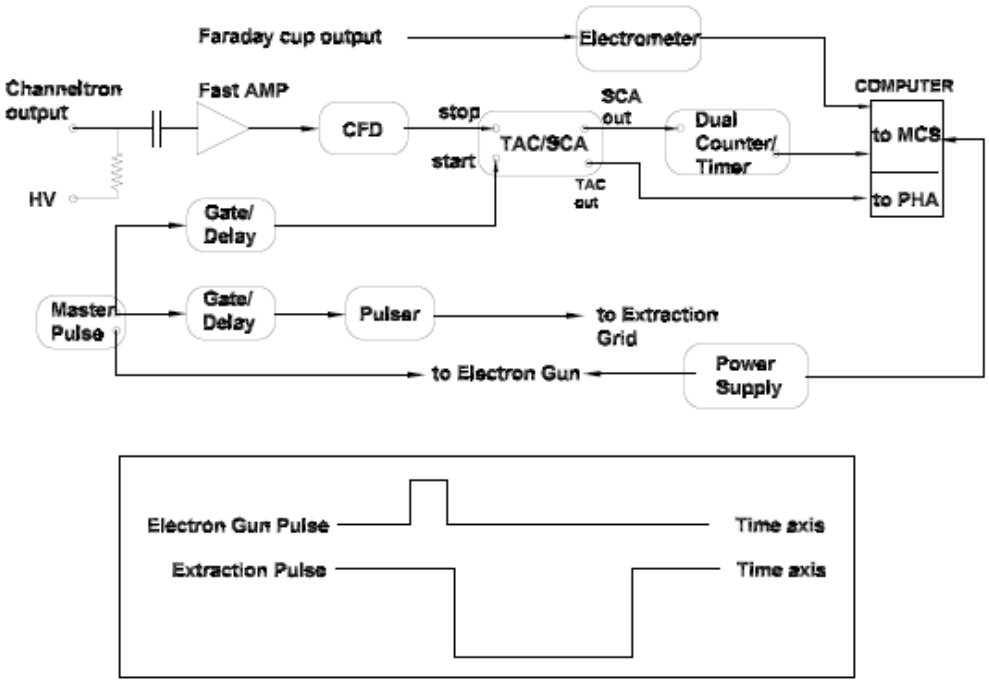

Figure 2.5: *Schematic of the data acquisition system used for the absolute cross sections measurement.*

The important aspect of the study of *DEA* to organic molecules was to look for the H^- fragment which was not reported earlier. In order to measure the absolute cross section for the formation of H^- from these organic molecules it was essential to suppress the contribution of background water to the H^- signal. For that purpose a liquid nitrogen trap was used in the pumping system near the baffle valve of the diffusion pump used in the set-up. This reduced the background water contribution to great extend. The background water contribution was completely eliminated by taking the excitation function for the H^- fragment from the background in the absence of the gas under study and subtracting it from the actual signal from the gas after the current normalization. The excitation function was put to the absolute scale using relative flow technique.

2.1.2.1 Relative flow technique

The absolute cross section measurement requires a very accurate determination of the target density and the electron current density in the interaction volume and the ion count rate of each fragment. The electron current was measured by means of a Faraday cup after passing through the interaction volume. Since the measurements were carried out under single collision conditions (chamber pressure is less than 10^{-4} mbar), the electron current density measured at the Faraday cup was essentially equal to the intensity of the electron beam. The ion count rate was strongly dependent on the various parameters like ion draw-out field, transport efficiency, detector efficiency etc. This problem could be handled experimentally. Most of the difficulty in cross beam arrangements arise from the non-uniform density of the target beam and hence in the determination of the exact volume overlap between the target beam and the electron beam. Thus a reliable determination of absolute target density in the interaction volume is a very difficult task. This difficulty is greatly overcome by appropriate normalization techniques.

The most widely accepted technique for making a reliable absolute cross section is the Relative Flow Technique (*RFT*) [1]. The basic principle of this technique is to compare the relative intensities of the species of interest with that of a standard species of known cross section measured by another method (which is useful to make absolute cross section measurement for the process where only one type of ionic species is formed). For accurate application of *RFT*, one has to be careful to ensure that the measurements for both the gases are carried out under identical experimental conditions. The crucial requirement of the technique is that the interaction volume (defined as the spatial overlap of the electron and molecular beam) should be identical for both the gases. This can be achieved by letting the gas flow through a capillary or an array of capillaries under molecular flow conditions. The capillary dimensions are to be so chosen that its length to diameter ratio is large. This ensures that the flow of molecules through it is dominated by the collisions on its walls. It has been shown that under these conditions, the molecules effusing out of it will have a specific angular distribution independent of the nature of the gas and the pressure (in the range where molecular flow condition holds) [3]. Thus replacing one gas by another does not change the effusive beam profile and hence the geometry of the interaction volume. The only change will be a constant multiplier which depends on the pressure behind

the capillary. Thus, if we flow a known gas (standard gas) producing a negative ion of mass m_s and determine the ion intensity at a particular incident electron energy (say ε_0) and flow rate, we can determine the cross section for the negative ion of mass m_u produced from the unknown gas by the following expression:

$$\sigma_u = \sigma_s x \frac{N_u}{N_s} x \frac{I_u^e}{I_s^e} x \frac{F_s}{F_u} x \left[\frac{M_s}{M_u}\right]^{1/2} x \frac{K_u}{K_s} \qquad (2.1)$$

where the subscript '*s*' and '*u*' are related to the molecular species of known cross section (standard) and that for unknown gas respectively. *N* stands for the number of ions collected for a specific time, I_e is the electron current, *F* is the flow rate, *M* is the molecular weight of parent molecule, and *K* stands for the ion detection efficiency. Thus, the experimentally measured parameters are *N*, I_e, and *F*. This is the master equation used to determine the absolute cross section for the unknown ions at particular electron energy.

For molecules of condensable vapors (which was the case for most of the molecules studied), it was difficult to measure the flow rate accurately. In these cases, instead of using flow rates, it was found that the pressures behind the capillary represented an accurate proportionality to the target densities. In this case, the expression for the determination of absolute cross section is as follows:

$$\sigma_u = \sigma_s \times \frac{I_u^e}{I_s^e} \times \frac{P_s}{P_u} \times \frac{K_u}{K_s} \qquad (2.2)$$

where *P* stands for the pressure measured behind the capillary. Notice that Eqn. 2.3 can easily be derived from Eqn. 2.2 assuming the molecular flow conditions, where the pressure is directly related to the flow rate by $P \propto \sqrt{M}$ x *F*.

In the experimental set-up the molecular beam was produced using a capillary array. The pressure behind the capillary array was controlled by a needle valve and it was measured using a capacitance manometer. The gas line behind the capillary i.e. from the vapor source to the capillary through needle valve was kept to a minimum length and was also kept warm (about 60° C) in order to reduce the condensation as

well as to avoid any possible dimer formation. The cross section for the formation of O^- from O_2 was used as standard to calibrate the cross sections in absolute scale [4].

2.2 Measuring angular distribution and kinetic energy of the fragment ions

The angular distributions of fragment ions from the *DEA* had been reported earlier for several molecules using the conventional turn table technique in which the detector was physically moved with respect to the electron beam direction. These measurements were limited to the angular range of 20˚ to 160˚ about the electron beam direction in the best case, due to physical limitations like the finite sizes of the electron gun and the detector etc. Moreover, these measurements had been limited to those cases in which the *DEA* cross section was relatively high. The measurement of kinetic energy of the fragments detected was also an additional task in these experiments lengthening the data collection time for the measurements.

Several charged particle imaging techniques had been developed in recent times for a variety of collision experiments starting from photoionization, ionization by fast projectiles and photodissociation [5]. The basic idea in all these experiments is to measure all the momentum components of one or more reaction products using appropriate coincidence techniques along with two-dimensional Position Sensitive Detectors (*PSD*). All the three velocity components are determined from the time of arrival and the position at the detector. One of the major developments in this respect has been the Velocity Map Imaging. (*VMI*) in which all the ions, with a given velocity produced in the given interaction volume, are mapped onto the same point on a two-dimensional *PSD*. This technique is capable of providing all the momentum components of the products of a reaction. We adopted this technique with appropriate modifications in order to fit in the constraints associated with the low energy electron beam experiments to measure the angular distribution of the fragment negative ions produced in *DEA*. Using this technique we were able to measure the angular distribution of the fragment ions ejected in all directions in a plane parallel to the *PSD* surface and containing the electron beam. This is for the first time the angular distribution measurement for entire 2π angle in a plane has been made for *DEA* studies. The coverage of angles, particularly in the forward and backward directions could provide a unique way of testing many theoretical results on *DEA*, which have

not been possible till now. In addition to the angular distribution the kinetic energy information of the fragment ions detected can also be retrieved from the velocity map images. This makes the technique much more powerful and efficient in these studies. The entire set-up was tested for its performance by studying the angular distribution of O^- from *DEA* to O_2 and comparing it with that reported earlier using conventional technique. The performance was found to be satisfactory.

2.2.1 Velocity Map Imaging (*VMI*)

This ion imaging technique was first developed by Eppink and Parker [6], which has become a standard method used for molecular photodissociation and reactive scattering experiments. Eppink and Parker used an inhomogeneous extraction field in order to focus the ions onto the imaging plane [6]. By projecting the expanding fragment distribution onto a two-dimensional *PSD*, the original 3D distribution may be reconstructed by means of the Abel inversion or other related algorithms.

These techniques have two inherent drawbacks: (i) the use of Abel transform requires an axis of cylindrical symmetry parallel to the imaging plane and (ii) inversion methods introduce artificial noise in the reconstructed image, especially along the symmetry axis and this can lead to a loss of experimental resolution. Thus this technique imposes limitations on the symmetry axis. In laser experiments, the laser polarization vector is generally taken as the symmetry axis. In pump-probe experiments, where it is desirable for the photolysis and probe laser polarizations to be orthogonal (for example, two-color experiments), this technique is not suitable.

In our experiments, the incident electron beam momentum vector is generally taken as the symmetry axis. But because of the relatively large size of the molecular beam and the electron beam, the effects due to the magnetic field used to collimate the electron beam and the poor energy resolution of the electron beam may make the inversion procedure inaccurate. Thus it is more convenient if we can obtain the information directly without going through an inversion procedure. Also in order to work with the low energy electrons as the generators of the ions it is essential to work with the pulsed extraction fields. During the interaction of the electron beam with the molecular beam, the interaction region is required to be field free as any stray field affects the electron energy as well as its trajectory. The only way the ions could be extracted without affecting the electron beam is by having pulsed ion extraction after

an electron pulse. But such pulsed extraction condition is found not to be appropriate to the conventional *VMI* technique as the delay in the extraction field causes the ion cloud to expand affecting the *VMI* conditions. In this context, the recent development in the area of 'velocity mapping with time slicing' was found to be suitable for us. However, this '*time slice*' technique had to be modified suitably in order to use it with the low energy electron beam.

Two different '*slicing*' ideas were introduced by different groups recently in order to bypass the need to use the inversion procedures [7, 8]. The central slice through the Newton sphere contains the full angular and translational energy information if an axis of symmetry exists for the ion formation process. Hence it is not necessary to project the entire three-dimensional sphere onto a two-dimensional detector and later try and retrieve the three dimensional information from the two-dimensional image. Thus the idea in these two slicing techniques is to detect only this slice of the Newton sphere in a plane of interest (which is made to be parallel with the detector by suitably setting up the experiment) by keeping the detector active only in the corresponding time interval. The time-gating of the detection is done by pulsing the detector bias at the appropriate time. In the first experiment of this kind, Gebhardt et al. used a pulsed electric field to extract the expanding cloud of ionic fragments following a period of field free expansion [7]. This stretches the distribution of the ion cloud (or Newton sphere) along the time-of-flight axis and thus allows the use of a sufficiently narrow time gate at the two-dimensional position sensitive detector. One drawback of this method is the use of a fine wire mesh at the extractor grid in order to create a field free expansion region. In order to eliminate possible blurring of the observed image the 'direct current (dc) slicing' technique was introduced [8]. In this technique, a dc extraction field was used in addition to an electrostatic lens in the flight path of the ions. No wire meshes were used at the apertures to eliminate image distortion due to them. By applying appropriate voltages at the lens and other electrodes the velocity mapping conditions were achieved. By using a narrow detector time gate, they were able to image only the central slice of the ion packet which contains the angular distribution information.

An outline of the experimental steps for the velocity map imaging in the photo-dissociation studies is depicted in Figure 2.6. The steps are as follows: (a) creation of the Newton spheres by photodissociation; (b) conversion of photo-fragments to ions by laser ionization; (c) projection of the ionic Newton spheres onto

a 2D position sensitive detector; and (d) recovery of the three dimensional information from the 2D image in order to get the central slice through the Newton's sphere, either by using an inversion procedure or keeping the detector active during a small time window. In our experiments the ionic Newton sphere is created due to the interaction of electron beam with the molecular beam. Thus there is only one step instead of steps (a) and (b). Our procedure for recording the ion cloud and obtaining appropriate slice of the Newton sphere also differs from steps (c) and (d).

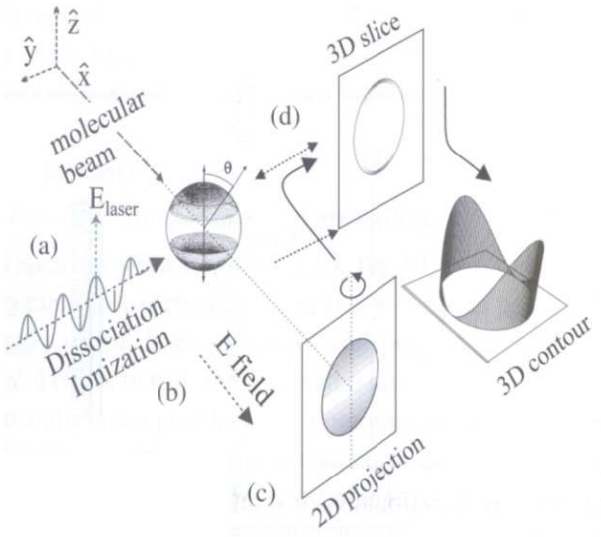

Figure 2.6: *Schematic of the experimental steps used in the photofragment imaging from photodissociation. In our experiments the Newton spheres are produced due to collision of electron beam with molecular beam. Thus the direction of the electric field of the dissociating laser will be replaced by the electron momentum vector in our experiment. The recording of the Newton sphere and retrieval of the 3D slice are also different in our experiment* [5].

In our experiments, we used time slicing technique with some modifications. A pulsed extraction was used to extract the ions formed in the interaction region. The apertures had no wire mesh to begin with and the detector bias was not pulsed. Pulsed extraction was needed to avoid disturbance to the electron beam by the ion extraction field. Unlike many of the *VMI* techniques employed in photodissociation and detachment experiments, where they use a *CCD* camera for recording the position information, we used a *PSD* with a wedge-and-strip arrangement for recording the

position information. With this arrangement we could not pulse the detector bias as is done in some of the *VMI* experiments employing time slicing. With the use of *CCD* cameras for imaging in these 'time slicing' experiments the detector is electrically isolated from the data acquisition electronics.

In the wedge-and-strip arrangement the signal is read out using charge sensitive preamplifiers. Any sudden change in the detector bias damages these amplifiers. Hence unlike other *VMI* with time slicing experiments we did not pulse the detector to select the appropriate part of the Newton sphere. However, the use of the Wedge and Strip detector allowed recording of the time of arrival of individual ions at the detector along with its position. Since the events were recorded separately, we were able to separate them out according to their time of arrival and position during off-line analysis after the experiment was over and thus carried out the necessary 'slicing'.

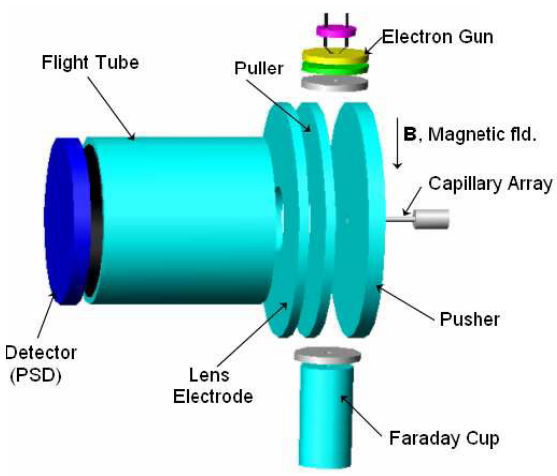

Figure 2.7: *Schematic of the experimental arrangement for angular distribution measurements using Velocity Map Imaging.*

A spread in the origin of Newton spheres introduces blurring of the image. The implementation of Velocity Mapping conditions using electrostatic lenses makes it possible to obtain better image independent of the initial spread in position. It is also important to reduce the spread in the initial velocity of the parent molecules so that it does not distort the images. This may be important when the ions are formed with relatively small kinetic energy. A velocity spread along the ion projection direction may cause less distortion of the angular distribution as compared to that when it is in the transverse direction. Considering this, the molecular beam was directed towards

the imaging detector as shown in Figure 2.7. The most important factor that can affect the resolution of the velocity mapping is the electron energy spread. This energy spread, transferred as the spread in the kinetic energy of the fragments, causes the blurring of the image. Also uncertainty of the direction of the electron momentum vector depends on the electron energy spread particularly in the low energy regime. This effect can be reduced by improving the energy resolution of the electron beam used.

Another requirement in obtaining a meaningful image is that the experiments should be performed under single collision conditions. After their formation, the ions should not undergo any secondary collisions. This requires that the experiment be done at relatively low target densities and background pressures.

The experimental set-up consisted of a magnetically collimated and pulsed electron beam, a Faraday cup to measure the electron current, an effusive molecular beam (introduced perpendicularly to the electron beam), ion optics arrangement to transport and focus the ions onto the *PSD*. The electron gun, Faraday cup, and molecular beam source were similar to that used in the absolute cross section measurements. The uniform magnetic field used for collimation of the electron beam was generated by means of a pair of coils in Helmholtz geometry. The coils were mounted outside the vacuum chamber coaxially around it. Typically 50 Gauss magnetic field at the center of the Helmholtz coil arrangement was used. The micro channel plate used in the experiment as part of the position sensitive detector had to be operated in ultrahigh oil-free vacuum. For this purpose, the entire set-up was housed in a cylindrical vacuum chamber (diameter: 70 cm and height: 50 cm) made of stainless steel and with ports having all-metal seals. The chamber was pumped down to few times 10^{-9} torr using a 2000 lt/s Turbo pump (*Varian; Turbo-V 2000HT*) and a Dry Scroll Vacuum Pump (*Varian; TriScrollTM 600*) arrangement.

The measurements were carried out in crossed electron-molecular beams geometry. The magnetically collimated electron beam was made to interact with the effusive molecular beam produced by the capillary array at right angles as shown in Figure 2.7. The ions formed in the interaction region were extracted by a pulsed electric field into the *VMI* spectrometer, which focused the ions according to their initial velocities onto different points on the *PSD*. The pulsed extraction field was created by applying a pulse having fast rise/fall time (<10 ns) to the *pusher* electrode while keeping the *puller* electrode at ground potential. The amplitude of the extraction

pulse was adjusted for optimum focusing conditions for ion imaging. Since there was no wire mesh on any of the aperture, the field due to the voltages on the *lens* electrode and flight tube tended to penetrate into the interaction region and disturb the electron beam. This problem was minimized by operating the entire *VMI* set-up at lower voltages. The length of the flight tube was chosen such that the ions expand and fill the maximum area of the detector. This provided optimum spatial resolution for imaging. The signals from the detector anode as well as from the back side of the *Micro-Channel Plates* (*MCP)* assembly were used to generate two-dimensional position and flight time data of the ions.

2.2.1.1 Ion optics

The imaging technique that we implemented required an ion optics arrangement in order to focus the ion cloud formed in the interaction region onto the *PSD*. A schematic diagram of the ion optics is shown in Figure 2.8.

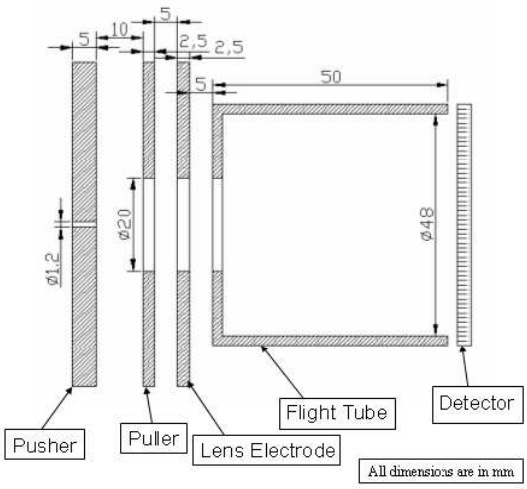

Figure 2.8: *Scaled schematic of the ion optics used for velocity map imaging.*

It consisted of a three electrode arrangement and a 50 mm long flight tube. The assembly was mounted horizontally, with its axis along the molecular beam direction and perpendicular to the electron beam. The three electrodes were made of 70 mm diameter nonmagnetic stainless steel plates. The flight tube had an inner diameter of 48 mm and was made of non-magnetic stainless steel. The first of the three electrodes (*pusher* electrode) had a central hole of 1.2 mm diameter in order to hold the capillary array. The capillary array was used to produce the effusive

molecular beam at right angles to the electron beam in the interaction region. The second electrode (*puller* electrode) and the third electrode (*lens* electrode) had 20 mm diameter apertures at their center. The flight tube had 20 mm diameter entrance aperture and 50 mm diameter exit aperture towards the detector. The separation between the *pusher* and *puller* electrodes was 10 mm, whereas the *lens* electrode was separated from *puller* electrode and flight tube by 5 mm gaps on either side.

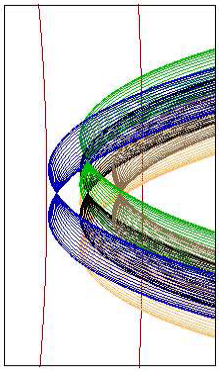

Figure 2.9: *An expanded view of the initial trajectories of the ions starting at different positions, separated by 1 mm from the center point, within the interaction volume.*

Because of the finite size of the source, it was very important to optimize the focusing conditions for the ion optics in order to get good velocity map image. This was carried out by simulating the ion trajectories using *Simion* 6.0 for O^- ion with a maximum kinetic energy of 2.0 eV as worst case and assuming an isotropic distribution. In our calculations, we have taken five different starting positions (one at the interaction point of the electron beam and molecular beam, and others 2 mm away from the interaction point) of the ions in the interaction volume as shown in the Figure 2.9. The initial energy of the ions was taken as 2 eV. All the ions were assumed to be ejected at 55˚ (lower half of the flight tube axis) and 125˚ (upper half of the flight tube axis) with respect to the electron beam direction (in our case it was vertically down). The criterion for the best focusing was to obtain the narrowest possible projection of the similar velocity cones (same apex angle and pointing in the same direction), that were spatially separated in the interaction region, on the 2D detector plane. For a given arrangement, the optimum velocity map could be achieved by adjusting the voltage ratios. In an ideal case, the voltage ratios were such that a

particle having a particular velocity would be focused onto the same point on the detector, irrespective of where they were formed in the interaction volume. In order to achieve effective slicing of the expanding ion cloud it was very important to design an apparatus, which provides sharp velocity focusing on the detector and at the same time gives a large temporal spread. This situation is shown in the Figure 2.10.

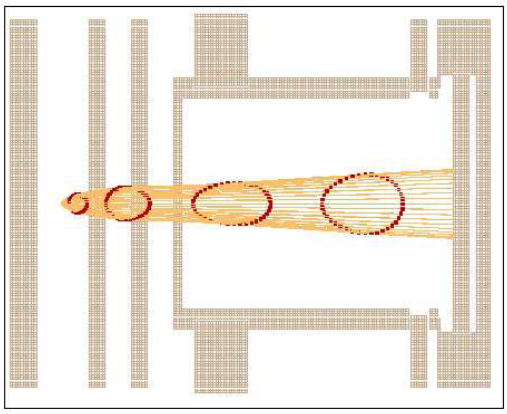

Figure 2.10: *Ion trajectory simulations for the velocity mapping showing the expansion of the ion cloud. The red markers represent the expansion of the ion cloud at 300 ns intervals for O^- ions with a translational energy of 2 eV.*

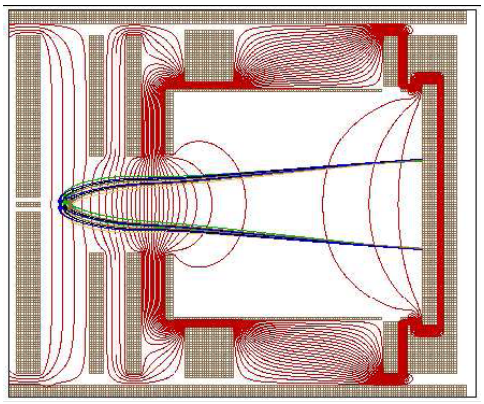

Figure 2.11: *Ion trajectory simulations for the velocity mapping set-up using Simion program.*

The initial estimate of the optimum ion optics voltages was obtained from the trajectory simulation. Figure 2.11 shows a trajectory simulation for our apparatus with pusher voltage: -24 V, puller: 0 V (ground), lens: +28 V, flight tube: +130 V and detector front: +190 V. During the experiments, the voltages on various electrodes

including flight tube were optimized in order to obtain the best velocity map image for O^- ions from O_2 at electron energy of 8 eV. The voltages thus determined were found to be pretty close to those obtained using ion trajectory calculations done prior to the experiments.

2.2.1.2 Position sensitive detector (*PSD*)

The development of *PSDs* has given an impetus to new experimental approaches for the investigation of the dynamics of atomic collisions in variety of situations in recent years. These *PSD*s are based on micro channel plates (MCP).

Figure 2.12 shows the basic structure of an MCP and the working principle for positive ion detection. For negative ion detection the polarity and the values of the voltages are different. A Micro channel plate is basically an array of large number of single channel electron multipliers. Each channel acts as an independent continuous electron multiplier. The channels are made of special glass. The typical channel diameter is in the range of few tens of microns. The inner side of each channel is coated with high-resistance semiconductor. This semiconductor coating serves as secondary electron multiplier. With the application of voltage across the array, there will be a continuous potential gradient along the length of each channel. When charge particle/radiation with sufficient energy falls on the front surface of MCP, secondary electrons are produced. The amplification of the electron cloud takes place just like in the case of channeltron discussed earlier. The eventual gain in practice is limited by three phenomena: (i) Ion feedback, (ii) Current saturation and (iii) Charge saturation.

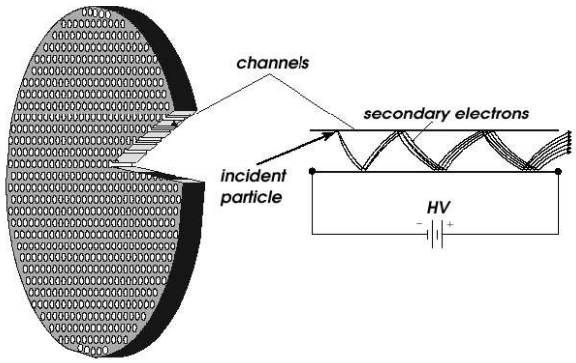

Figure 2.12: *Structural representation of a Micro-Channel Plate and its working principle for positive ion detection.*

The basic problem in electron multiplication is the ion-feedback instability at high operating voltages and high pressure. The positive ions, which are produced by the collision between electrons and residual gas atoms inside the channel, are accelerated towards the front surface of the *MCP*. These ions may strike the channel wall and if their energy is sufficient, they may produce secondary electrons. The ions striking the wall can damage the channel. The ion feedback also produces noise. The positive-ion-feedback noise depends on the gain, the pressure, nature of the residual gas and surface properties of the channel wall. This problem arises from the straight geometry of the micro channels. The problem can be minimized if the system is operated at relatively low potentials and low pressure (bellow 10^{-6} torr). It is advantageous to put two *MCP*s (*Chevron* configuration) turned 180˚ along their axis with respect to each other or three *MCP*s (*Z*-Stack configuration) to get better performance, since the positive ions get trapped at the interface of the two plates. These combinations also provide higher gain.

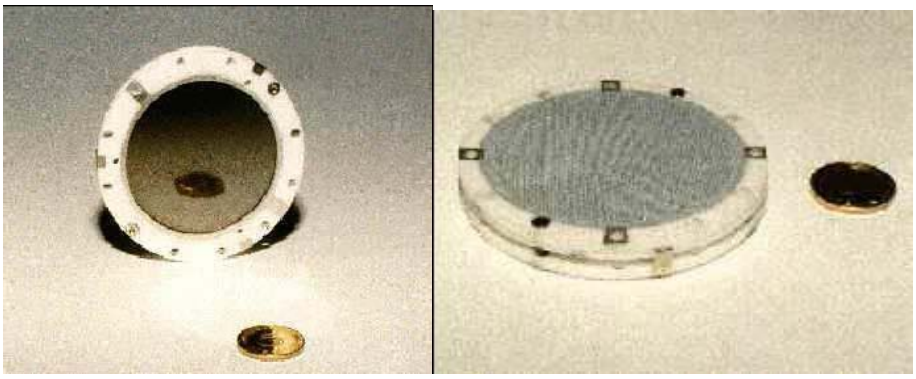

Figure 2.13: *The left panel shows the photograph of the MCP assembly, after mounting all the three MCPs between two partially metal coated ceramic rings which are held together with metal spring clamps. The right panel is the photograph of the anode plate. The front side is covered with a thin Ge-layer and back side contains the Wedge-and-Strip structure.*

The position information from the detector is read out using different schemes depending on the experiment. The simplest is the use of a phosphor anode and a *CCD* camera. The electrons coming out of the *MCP* are accelerated and allowed to fall on the phosphor screen which emits light depending on the electron current. This light is

then focused on the *CCD* camera kept outside the vacuum system. The images on the *CCD* camera are recorded. The other scheme is the use of an anode and reading out the information electrically. This is done in several ways like use of an array of small individual anodes, delay line anode or the Wedge and Strip anode. We used the Wedge and Strip anode along with three 50 mm diameter *MCP* having 48 mm effective diameter as the detector. A photograph of the *MCP* assembly after mounting all the three *MCP*s between two partially metal coated ceramic rings held together by metal spring clamps is shown at the left panel of the Figure 2.13 and on the right panel of the Figure 2.13 a photograph of the anode is shown.

The three *MCP*s were mounted as *Z*-stack configuration followed by the position sensitive anode. A voltage of 2.4-2.6 kV was applied across the *MCP* assembly. The front surface of the detector was held at + 200 V for negative ion detection. When a particle hits the *MCP*, a secondary electron cloud of typically 10^7 electrons was created, which was directly collected by the wedge-and-strip anode to be processed electronically. The wedge-and-strip anode was mounted behind the *MCP* at a distance of 3 mm and was held at + 50 V with respect to the back of the *MCP* assembly.

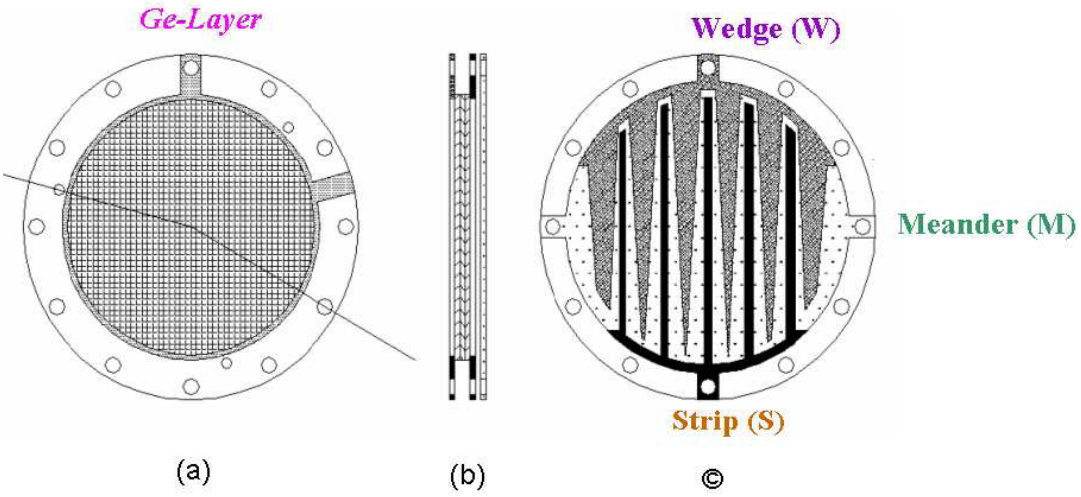

Figure 2.14: *Structural representation of the Wedge-and-Strip anode. (a): the anode coated with Ge-Layer and facing the MCP, (b): the side view of the detector and (c): the main structural form of the Wedge-and-Strip anode.*

One side of the anode, which was facing the *MCP* assembly, was coated with semiconductor germanium layer (as shown in the panel (a) of the Figure 2.14). The

other side of the anode contains three different structures, where the position information is obtained by charge division. These anode structures are `*wedge*' with increasing width from bottom to top, rectangular arrays called `*strips*' with increasing width from left to right. The space between these two structures is called `*meander*'. The basic structure of the wedge-and-strip anode with a typical periodicity of 1.5 mm is shown in the panel (c) of the Figure 2.14. The pulse heights of the signals obtained from strip and wedge electrodes were proportional to the *X* and *Y* co-ordinate of the centroid of the charge cloud, as long as the charge cloud covered an area larger than the period of the anode structure. This condition was fulfilled when the electrons were allowed to expand while traveling a distance of several mm from the *MCP* to the germanium layer. The three segments of the anode picked up the image charge created on them when the electron cloud was incident on the *Ge*-layer. The signals from each of the three structures were amplified by a set of charge sensitive preamplifiers followed by spectroscopic amplifiers. The three voltage signals were then processed using an *Analog-to-Digital Converter* (*CM60*, *4K NADC*) and given to the computer for monitoring and storing in the list mode using specially built *Linux Advanced Multi Parameter System* (*LAMPS*) software [9, 10].

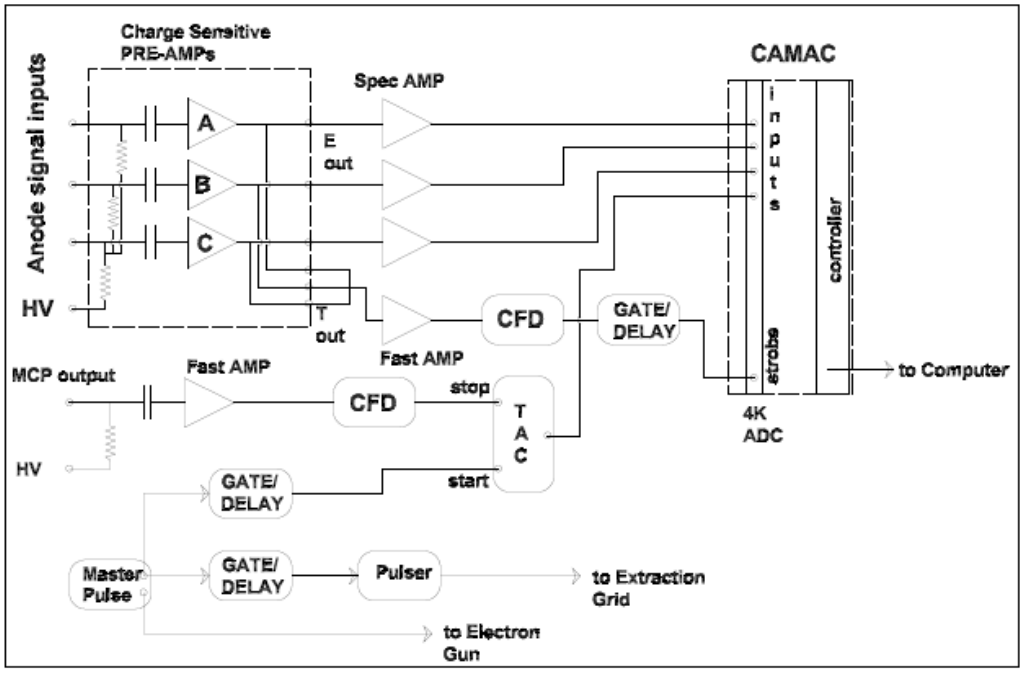

Figure 2.15*: Block diagram of data acquisition system used in Velocity Map Imaging.*

The block diagram of the data acquisition system is shown in Figure 2.15. Signals from the wedge-and-strip anode were capacitively coupled to the charge sensitive pre-amplifiers (*CASTA, RoentDek*). The ac coupling isolated the charge amplifiers from the high voltage supply connected to the anode of the detector. A fast timing amplifier was used to amplify the timing signal derived from the output of the channel plates. After discrimination, this signal was used as a *STOP* pulse of the *TAC* used for *ToF* determination. A *CAMAC* based *QUAD* nuclear *ADC* (CM60, 4K) with conversion time of 3.5 μs per input, which measured the peak height of the positive input signals, was used for data acquisition. The conversion was initiated by external fast *NIM* strobe input, which was generated from the time outputs of the pre-amplifiers. A gate width (which could be adjusted from 100 ns to 5 μs) of about 3 μs is generated, triggered by the same external strobe signal and the delay between the strobe pulse and the gate was kept ~ 250 ns. During the gate width the peak value of all four inputs were detected and stretched. It was monitored that the peak position of all inputs lied within the gate signal. The *ADC* and the controller module were held in a *CAMAC* mini crate (Kinetic System, Model: 1507) connected to a *PCI* card via a *CC 2000* crate controller. Once the charge signal was digitized, the impact position of the ions onto the detector could be calculated from simple standard expressions:

$$X = \frac{S}{S + W + M} \tag{2.3a}$$

$$Y = \frac{W}{S + W + M} \tag{2.3b}$$

where *S*, *W*, and *M* refer the charge signals measured from strip, wedge, and meander respectively. For correct imaging, the gain of the pre-amplifiers and main amplifiers in the individual channels had to be adjusted properly, such that the overall gain was same for all the three channels. The linearity of the imaging was affected by the cross talk between the anode segments. The image could be distorted due to the capacitive coupling between the discrete electrodes of the wedge-and-strip anode. If certain amount of charge was deposited onto one electrode, a charge would also be induced on the other electrodes. Thus the measured charge signal on one electrode was the sum of real charge signal deposited on it and the coupled charge from the other two

electrodes. For this reason, the position calculated by above formulae (Eqn. 2.3a and 2.3b) resulted in a distortion of the image. In order to get the correct value of the charge signals, we used an analytical method. These corrected values were used to calculate the correct *X* and *Y* position. If *S*, *W* and *M* were the charge measured from the strip, wedge and meander respectively, the real value of the charge signal would be

$$S_C = \frac{S(1-\alpha-a+b)+M(b-\beta)+W(b-\gamma)}{(1-2a+3b)} \qquad (2.4a)$$

$$W_C = \frac{W(1-\beta-a+b)+S(b-\gamma)+M(b-\alpha)}{(1-2a+3b)} \qquad (2.4b)$$

$$S_C = \frac{M(1-\gamma-a+b)+W(b-\alpha)+S(b-\beta)}{(1-2a+3b)} \qquad (2.4c)$$

where α, β and γ are the coupling constants between Meander-Wedge, Meander-Strip, and Wedge-Strip electrodes respectively. They satisfied the conditions, and $a = \alpha + \beta + \gamma$ and $b = \alpha*\beta + \beta*\gamma + \alpha*\gamma$. By choosing appropriate values for α, β and γ one can get a proper image by trial and error. In order to determine α, β and γ, the dark counts on the detector which were supposed to be uniformly distributed over the entire circular disk was collected for sufficiently long time. The oval shape image thus obtained was manipulated by adjusting α, β and γ till it became a perfect circular one. The values of α, β and γ (which were 0.04, 0.13 and 0.07 respectively) thus obtained were used for correcting the cross talk distortion in all the images.

As mentioned earlier, the data were acquired by the program *LAMPS* running on Linux operating system [9, 10]. The positions *X*, *Y* were defined as pseudo-parameters in *LAMPS* and the position spectra were displayed online. The data were collected in list mode and the same program was used in the offline analysis.

2.2.1.3 Testing set-up for oxygen ion

The velocity mapping spectrometer was tested for its performance by studying the formation of O^- from O_2 by *DEA*. The formation of O^- from O_2 is known to appear as a broad peak centered at 6.5 eV [4, 11]. These ions are formed with

considerable kinetic energies, which have been measured by several workers [12, 13]. The angular distribution of O^- from O_2 has also been reported at a number of electron energies around the resonance peak using the conventional turn-table arrangement [14]. In the present measurements, we first obtained the ion yield curve using the voltage conditions appropriate for velocity mapping and selecting the time window corresponding to O^- ions. The position of the peak obtained from the ion yield curve was used to calibrate the energy scale. The ion yield curve is shown in Figure 2.16.

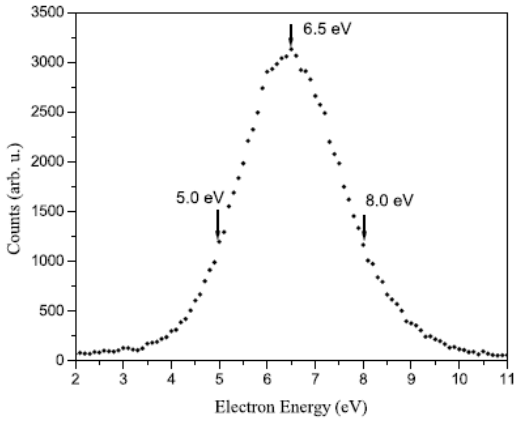

Figure 2.16: *Ion yield curve for the formation of O^- from O_2 by DEA. The arrows indicate the electron energies where the velocity map images are reported.*

The velocity map images were taken at three different electron energies corresponding to the peak in the ion yield curve and at 1.5 eV away from either side of the peak. A typical *ToF* spectrum of O^- at 6.5 eV electron energy is shown in Figure 2.17.

The ions ejected towards the flight tube appear as a clear peak in the *ToF* spectrum followed by a slight dip in the centre and a relatively broader peak corresponding to the ions ejected away from the flight tube direction. Since there was no clear-cut minimum in the *ToF* signal, which could be directly related to the ions ejected at 90˚ to the flight tube direction, we analyzed the list mode data for two-dimensional distribution with time slices of 50 ns each between the two peaks of the *ToF* distribution. This gave us time-sliced velocity images. From these images we picked the one with largest diameter, since ions ejected at 90˚ with respect to the flight tube axis would have maximum range in the detector plane. This time slice also matched fairly well with the central section of the time-of-flight distribution.

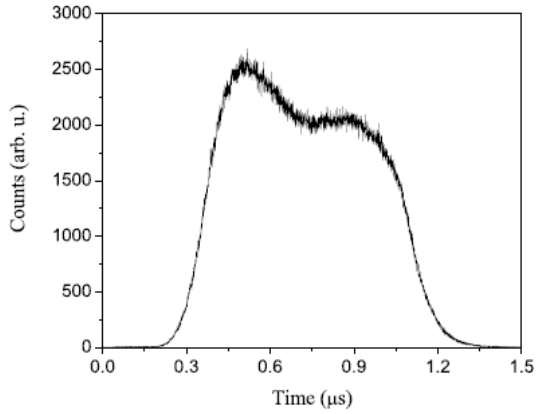

Figure 2.17: *Time-of-Flight mass spectrum of O^- from DEA to O_2 taken at 6.5 eV.*

The time-sliced images obtained at three incident electron energies along with the corresponding 3-dimensional plots with intensity as the third axis is shown in Figure 2.18. The intensity distribution along the radius of these patterns should be proportional to the speed of the ions and thus should provide information on the kinetic energy distributions of the ions. The square of the radius of the angular distribution pattern should be proportional to the kinetic energy of the ions under high enough extraction voltages where the initial energy of the ions can be neglected in comparison to the energy gained by the ions due to extraction. Since we employed low extraction voltages, the loss of linearity in the kinetic energies of the ions with the square of the radii of the annular pattern was observed.

However, the data clearly show the angular distribution of the ions with very good resolution. The uniformity of the data in both the halves about the electron beam direction emphasizes the absence of any systematic error in the imaging process, including efficiency variation on the detector surface that may arise due to the relatively small acceleration (about 200 V), that the ions underwent before they struck the detector.

The angular distribution of the ions from the time-sliced velocity map image was obtained by integrating the counts over the range of radii over which the annular ring appears. Plots of these angular distributions (for three electron energies) as a function of angle with respect to the electron beam direction and normalized with respect to the intensities at 90˚ are given in Figure 2.19. Consistent with the velocity map images, the angular distributions at all the three energies are symmetric on either side of the electron beam highlighting the quality of the data.

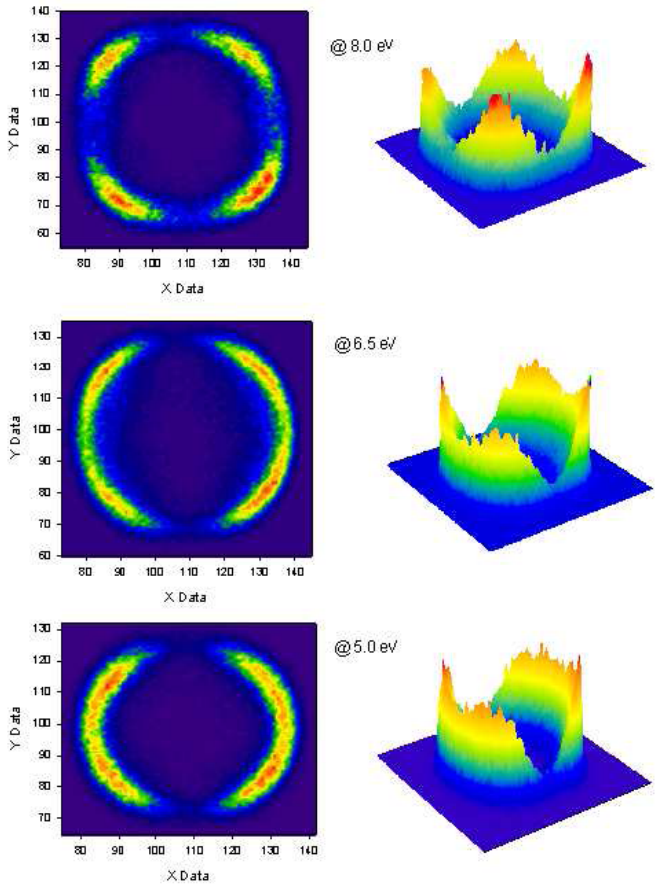

Figure 2.18: *Time sliced velocity map images of O^- from O_2 at three different electron energies. The left panel shows the 2-dimensional patterns we obtain after time slicing. Red color shows increasing intensity and blue shows least intensity. The electron beam direction is vertically down. The right panel shows the corresponding 3-d distribution with intensity as the z-axis. The distributions have been rotated through 35˚ in the counter clockwise direction for clarity.*

In order to check the performance of the experiment we compared the present data with that from the literature, obtained using the conventional method in the range of 20˚ to 160˚. This is shown in Figure 2.20. Here again the plots are normalized with respect to the intensities at 90˚. Though the two sets of data were not taken at exactly the same electron energies, they seem to agree with each other extremely well. Our data shown in this figure were collected for the duration of 2 to 3 hours.

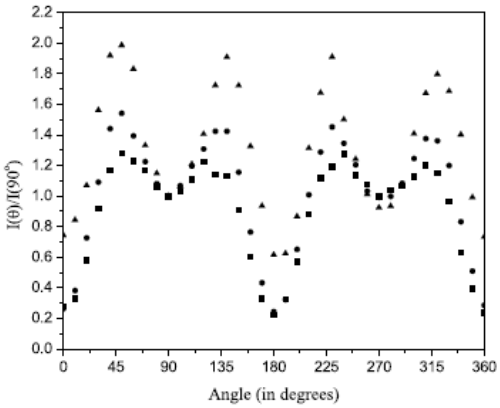

Figure 2.19: *Angular distribution of O^- from DEA to O_2 at three different electron energies. Squares, circles and triangles represent the angular distribution data for 5.0 eV, 6.5 eV and 8.0 eV electron energy respectively.*

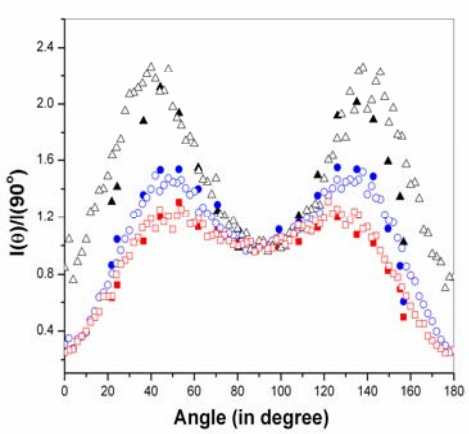

Figure 2.20: *A comparison of the angular distribution measurements of O^- with the existing data obtained using conventional technique. The open squares, circles and triangles represent the angular distribution data at electron energies of 5.57 eV, 6.70 eV, and 7.80 eV respectively taken from [14]. The filled squares, circles and triangles represent our results on the angular distribution of O^- at electron energies of 5.0 eV, 6.5 eV and 8.0 eV respectively.*

Apart from the speed of measurement, the present technique provides simultaneous measurement of the angular distribution over the entire range of angles eliminating different sources of systematic errors possible in the conventional

technique, related to the electron beam conditions and maintenance of identical geometric factors. The ability to cover the entire angular range could be very critical in the situations where there is a forward-backward asymmetry in the angular distributions as well as to pin point some transitions that have maximum contribution in the forward and backward directions. This aspect is discussed in details in the next chapter.

2.2.1.4 Performance Analysis of the *VMI* Spectrometer

In our experiments a pulsed electron beam, pulsed ion extraction and a uniform magnetic field for collimating the electron beam have been used. Thus it was very important to check the performance of the system under different combinations of these parameters. The electron energy resolution and ions kinetic energy also play a crucial role in our experiments.

The performance of our system was tested by changing the electron gun pulse width, keeping the delay between the electron gun pulse and the extraction pulse same. The gun pulse width was changed from 50 ns to 700 ns. A minimum pulse width of 50 ns was required in order to get sufficient electron current for meaningful measurements. It was found that within this range of electron pulse width, the velocity map image was not much affected for O^- from O_2. Considering this the electron pulse width of 200 ns was used for all other measurements.

The performance of the spectrometer was checked by changing the delay between electron gun pulse and extraction pulse, keeping the electron gun pulse width same (about 200 ns). The delay was changed from 25 ns to 500 ns. It was found that a minimum delay (about 50 ns) is required so as to keep the electron beam unaffected by the extraction pulse. A further delay is required to get better velocity map image. This additional delay allows the ion cloud to expand in the interaction region providing better time slicing. An optimum delay was found to be about 200 ns for the best performance.

In our experiment we use a fairly homogeneous magnetic field in order to collimate the electron beam. The ions are extracted and collected perpendicular to the magnetic field direction. So the ions will experience a Lorentz force acting on it, affecting the trajectory of the ions. The ions will land on the detector at different places depending on the magnetic field strength. It was found that with change in the magnetic field strength, the whole image gets shifted from one place to another on the

detector without any change in the shape of the image. Hence this was not a problem in the current measurements.

Another important aspect of the presence of the magnetic field in the present experiment could be its effect on the angular resolution of the experiment. The limiting angular resolution (θ) is related to the transverse energy spread (ΔE_{trans}) in the electron beam and its longitudinal energy (E_{long}) through the relation:

$$\theta = \tan^{-1}\sqrt{\frac{\Delta E_{trans}}{E_{long}}} \qquad (2.5)$$

If one considers the observed energy spread of 0.5 eV in our experiment is equally contributed by the transverse and longitudinal contributions, at the electron energy of 5 eV, the angular resolution would be about ±15^o and at lower electron energies this could be worse. The present measurements on O^- from O_2 at 5 eV did show much better angular resolution as the present data were in excellent agreement with that reported with an angular resolution of ±1.2^o [14]. Moreover, our measurements using this set-up on N_2O at energies as low as 1 eV showed that the angular resolution was reasonably good even at 1 eV. The explanation for this may be due to the fact that most of the contribution for the energy spread could be arising from the longitudinal contribution. There is no clear cut way of measuring the transverse and longitudinal energy spread separately. The upper limit of the transverse spread could be determined by carrying out a retarding potential energy measurement on the electron beam or on the *DEA* signal. Early measurements using retarding potential arrangement with similar electron guns in the presence of a magnetic field had shown the energy spread to be as low as 0.1 eV [15]. Assuming this is entirely due to transverse energy spread, the angular resolution would be about ±17.5^o at the electron energy of 1 eV. However, in our experiment, we found that the resolution was considerably better than this even at 1 eV. We believe that the small apertures in the electron beam and the pulsed extraction may be contributing to low transverse energy spread and hence correspondingly higher angular resolution. In any case, the angular resolution problem is an aspect one has to keep in mind while using this technique for magnetically collimated low energy electron beams. However the resolution could be improved with improvement in electron energy resolution.

2.2.1.5 Imaging H^- ions

The use of *VMI* set–up for imaging the lighter H^- ions needed to be carefully evaluated since the experiment involved a magnetic field over a fairly large volume, used for collimating the electron beam. Moreover, since the ions were produced continuously over an extended period of time followed by a finite time delay before they were extracted there could be a dependence on the mass of the ion that was imaged when their kinetic energies were appreciable. This problem would be worst for H^- ions due to their small mass. For example, for a given initial kinetic energy, the H^- ion cloud will bloom to a size four times that of the O^- cloud within a specific time interval. This could be eliminated by reducing the width of the electron gun pulse and by reducing delay between the electron pulse and the extraction pulse. We also found that it was necessary to increase the operating voltages, which needed further modifications of the apparatus.

As discussed earlier, because of low mass, the H^- ions moved swiftly when formed with the kinetic energies typical to *DEA* processes. Due to finite delay between the electron pulse and extraction pulse this swift movement of H^- ions caused the ion cloud to expand to four times the size of O^- ions with similar energies. As a result of which when the ions were extracted by the pulsed electric field keeping all the experimental conditions same as described earlier, they either hit the electrodes on their way to the detector or passed close to the edge of the electrodes affecting the *VMI* condition. In order to avoid this distortion one had to apply higher extraction voltages so that the H^- ions would be made to enter the *ToF* set-up at appropriate entrance angles also they would pass all the apertures away from the edges. In order to maintain the electric field configuration suitable for *VMI* with larger extraction, the increase in the *lens* and flight tube voltage became inevitable. This caused the electric field penetration from the acceleration region into the interaction region affecting the low energy electron beam.

In order to overcome these problems a fine wire mesh was fixed on the *puller* electrode. This prevented the electric field from the lens electrode from penetrating into the interaction region. Also the electron pulse width was kept at the minimum possible value (~150nsec.) that gave reasonable current with appropriate energy resolution. The delay between the electron pulse and the extraction pulse was also optimized (~150nsec.). The operating voltages were obtained by actual

experimentation and were found to be in reasonable agreement with those found using ion trajectory calculations considering H^- ions with kinetic energies up to 3eV and assuming that the initial size of the ions in the interaction region was about 3mm in radius before they were extracted.

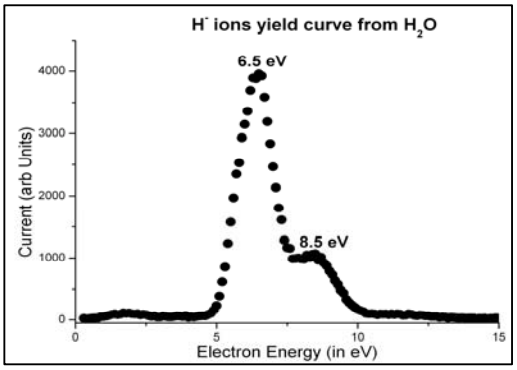

Figure 2.21: *Excitation function of H^- from water (H_2O) formed by DEA.*

The performance of the modified set-up was evaluated for the standard O^- signal from O_2. It was found to be satisfactory. No blurring effect due to the wire mesh in the path was observed within the limited electron beam energy resolution. Also due to higher extraction field the linearity in the kinetic energies of the fragment ions with the square of the radii of the annular patterns was observed for relatively higher energies as well (up to 2.5eV), showing improved performance for kinetic energy measurements as seen from the kinetic energy measurements on O^- from O_2.

The performance of the set-up to image the H^- ions was tested by imaging the H^- ions from H_2O. Water molecule shows two distinct resonances in the H^- channel at 6.5 eV and 8.5 eV with the larger cross section at 6.5 eV as shown in Figure 2.21. The H^- velocity map image was obtained at 6.5eV electron energy. The time-sliced images obtained at this incident electron energy along with the corresponding 3-dimensional plot with intensity as the third axis is shown in Figure 2.22.

As can be seen from the figure, the kinetic energy of H^- ions showed a continuous range of values starting from 0. This indicates that the remaining neutral fragment namely the OH radical was left in the vibrational excitation. Lower the kinetic energy of the H^- ion higher the excitation of OH radical. Such behavior has been reported for water [16, 17]. Though one expects to see distinct structure

corresponding to vibrational energies of OH, our data does not show the structure because of the relatively poor energy resolution of the electron beam.

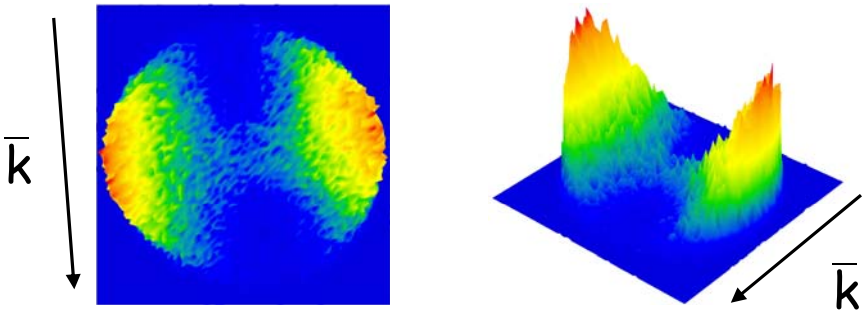

Figure 2.22: *Time sliced velocity map image of H^- from H_2O at 6.5eV electron energy. The left panel shows the 2-dimensional pattern we obtain after time slicing. Red color shows increasing intensity and blue shows least intensity. The electron beam direction is vertically down. The right panel shows the corresponding 3-d distribution with intensity as the z-axis. The distributions have been rotated through 35° in the counter clockwise direction for clarity.*

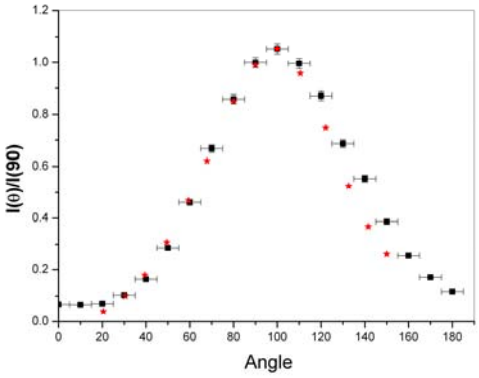

Figure 2.23: *A comparison of the angular distribution measurements of H^- with the existing data obtained using conventional technique. The stars represent the angular distribution data at 6.5eV electron energy taken from [17]. The filled squares represent our results on the angular distribution of H^- at the same electron energy.*

The polar plot shown in Figure 2.23 was obtained for the angular distribution of the H^- ions by integrating ion counts for smaller range of angles with entire range

of kinetic energies. The angular distribution and the kinetic energy distribution were compared with the existing data obtained by the conventional turned table technique [17] and were found to be satisfactory showing the ability of the set-up to image swifter H^- ions.

2.3 Improving energy resolution of the electron beam

As mentioned earlier, in order to improve the velocity map image quality as well as to obtain the well resolved kinetic energy distribution, it was essential to improve the energy resolution of the electron beam. Also in order to obtain the appearance energies, resonance positions, separate out nearby resonances and to measure cross sections more accurately, it was important to have the electron beam with as narrow energy distribution as possible. The electron gun described earlier provided an energy resolution of about 0.5 eV over the energy range of interest (0 to 20eV). In order to improve this, a trochoidal electron monochromator was built.

2.3.1 Trochoidal Electron Monochromator

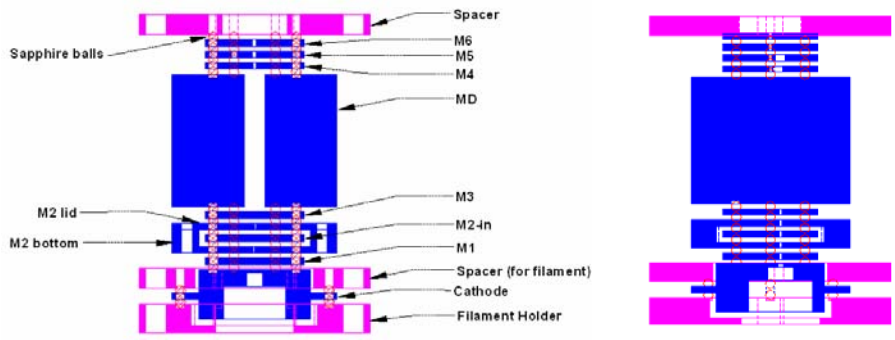

Figure 2.24: *Schematic diagram of the trochoidal electron monochromator from two different views*

The schematic of the trochoidal electron monochromator is shown in Figure 2.24. The design of the monochromator is similar to that reported by Allen [18]. All the monochromator electrodes were made of molybdenum and they were separated by 1.5mm diameter sapphire balls. The entire assembly of all electrodes was stacked

using three plates made of stainless steel (Spacer and filament holder in Figure 2.24) with three brass screws.

The schematics of all the individual electrodes are shown in Figure 2.25. The cathode consists of a 1.5 mm diameter aperture which was situated off-center by 1.5 mm. It had Pierce geometry and acted like the cathode in the simple electron gun described earlier. This element was followed by three identical electrodes namely *M1, M2-in* and *M3* with 0.5 mm aperture co-axial with that on the filament holder. The *M2-in* electrode was kept inside a molybdenum box called *M2* as shown in Figure 2.24.

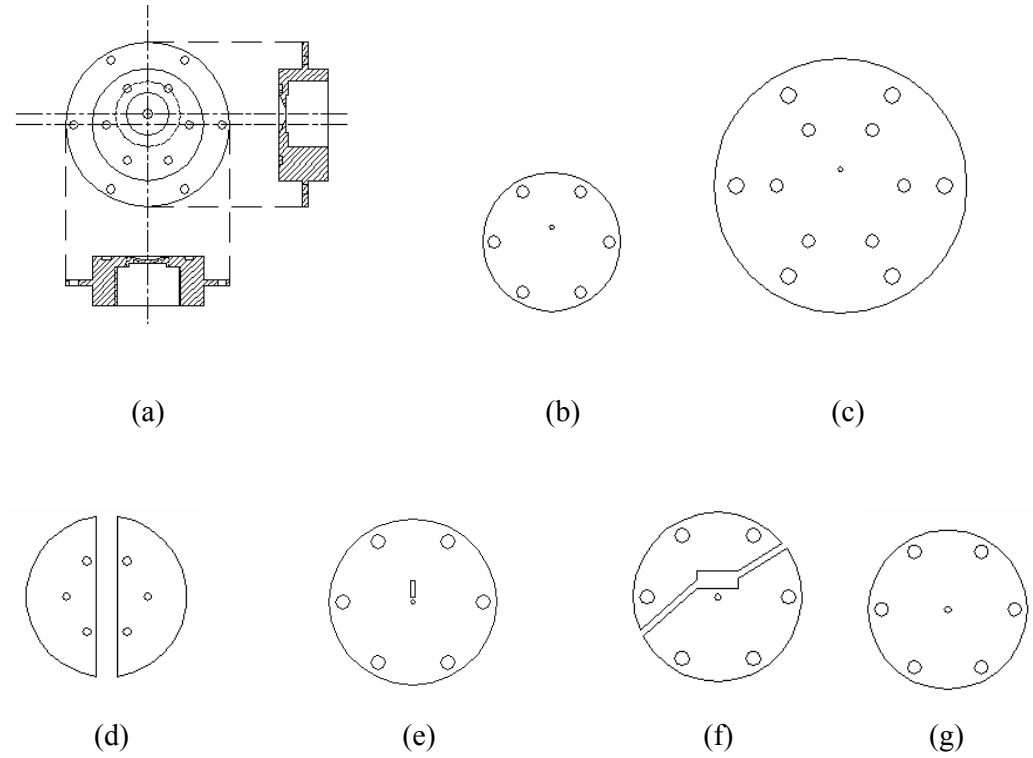

Figure 2.25: *Schematic diagram of various electrodes present in the trochoidal electron monochromator (a) Cathode (b) M1, M2-in, M3 (c) M2 (d) MD (e) M4 (f) M5 (g) M6.*

The *M2-in* is used for pulsing the electron gun and the box acts like a shield in order to prevent the other electrodes from picking up the noise from the pulses given to *M2-in*. *M2-in* electrode is equivalent to the grid in the earlier described electron gun. The *M3* is followed by the trochoidal region flanked by two '*D*' shaped electrodes separated by 10 mm gap transverse to the axis of the gun. These *D*s were

isolated from each other and from other electrodes and a small electric field could be applied in this region by putting different voltages on the *D*s. It was followed by an electrode (*M4*) that had a 0.4 mm diameter aperture at the center and a narrow slit (lying along the radius of the electrode) of 1mm length and 0.5mm thick that coincides with the apertures on *M1*. *M4* electrode was followed by an electrode (*M5*) made of two pieces that were isolated from each other as well as from other electrodes. The bigger piece had a 0.5 mm diameter aperture that matched with the central aperture on *M4*. The gap between the two parts of *M5* coincided with the slit on *M4*. A small electric field could be applied between the two parts of *M4* that prevented the fast moving undispersed electrons from contaminating the main beam on reflection from the next electrode (*M6*). This electrode i.e. *M6* was grounded and had a 1mm diameter aperture at the center. All the electrodes other than the cathode and the two Ds were 1mm thick. The separation between the adjacent electrodes was kept to be 0.75mm. All the electrodes were kept floating on the filament voltage and the voltage on the individual electrode was adjusted with respect to the filament voltage. The electrical contacts on individual electrodes were made by brazing the multi-strand wires on them.

A separate control box was made that could read the individual voltages on each electrodes and also control them. The electric field between the two *D*s could be changed in magnitude as well as in direction using two separate knobs. This provided a better control on the trochoidal condition. The energy resolution of the electron beam was measured by monitoring the full width at half maximum (FWHM) of the SF_6^- signal at electron energies close to zero eV. The voltages on various electrodes were adjusted in order to make the FWHM minimum. The best resolution was obtained to be 130meV when the gun was operated in DC mode while in the pulsed mode it was found to be about 300meV.

The operating principle of the trochoidal electron monochromator is the dispersion of the electron beam in the presence of crossed electric and magnetic field depending on the energy spread of the electrons. The electron beam was made to pass through the trochoidal region where a crossed electric and magnetic field configuration was present. The magnetic field was along the axis of the electron gun and the electric field was generated between the two Ds transverse to the electron beam. The '$\boldsymbol{E}$ *X* $\boldsymbol{B}$' force acted along the direction perpendicular to both the electric and magnetic field. This caused the electron beam to spread in the vertical direction

depending on the electron energy spread as shown in Figure 2.26. The vertical dispersion was dependent on the energy of the electrons when they are in the dispersing region. By selecting a small portion from the spatially dispersed electron beam using a small central aperture on *M3* the electron beam energy resolution was improved. The best working resolution that we got was about 130 meV with reasonable current in the DC mode. As we had to use the electron beam in the pulsed mode the monochromator was also tested for the pulsed mode operation where the *M1* electrode was treated like the grid electrode in the previously described electron gun. In the pulsed mode the best resolution obtained was about 300 meV with few tens of pico-Ampere current for 10 kHz repetition rate.

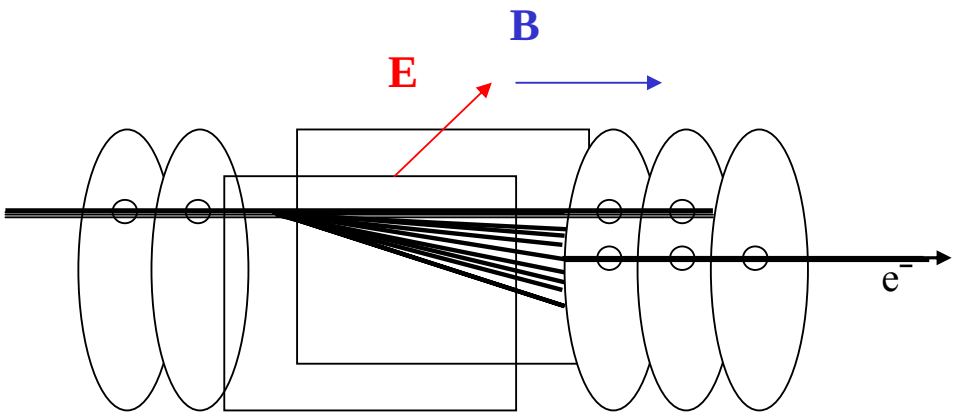

Figure 2.26: *Working principle of the throchoidal monochromator.*

Due to limited magnitude of the current given by the electron monochromator in the pulsed mode it could not be used for any measurements discussed in the thesis, except in the case of electron attachment to C_{60} for which the cross sections are fairly high.

2.4 Rydberg electron transfer

Our experiments on Rydberg electron attachment were directed at probing the formation of negative ions by laser irradiation of molecules at relatively high pressures. In order to identify the negative ions, we had to use a time of flight mass spectrometer (*ToFMS)* along with a particle detector, both of which had to be operated at high vacuum. This necessitated building a completely new experiment

different from the electron collision set up, employing a high pressure gas cell with appropriate differential pumping arrangement.

The schematic of the experimental set-up is shown in Figure 2.27. The entire set-up was pumped by a diffusion pump. In order to maintain the *ToFMS* and the detector region in high vacuum, it was necessary to reduce the gas through-put from the gas cell to a minimum. This was achieved by allowing the ions from the interaction region enter the *ToFMS* through a small aperture of diameter 3 mm in the *puller* electrode. By increasing the thickness of the puller electrode to 10 mm, the gas through-put was further reduced. Using this assembly a pressure ratio of 10^3 could be maintained between the interaction region and the flight tube and detector region. The pressure in the interaction region was measured by a capacitance manometer whereas that in the detector region was measured using ionization gauge. The gas cell was operated at not more than 10^{-2} torr range that kept the interaction region pressure upto 10^{-5} torr.

The experiment is done by focusing a laser beam into a gas cell. In order to avoid the back reflection from the quartz window into the interaction region the Brewster window is used at the outlet port for the laser beam. The ions formed in the interaction region are extracted using an electric field into a *ToFMS* and detected using a channel electron multiplier. The ion extraction field is produced between two electrodes (*pusher* and *puller*) mounted symmetrically on either side of the focal spot with a separation of 16 mm. The *ToFMS* was in the Wiley-McLaren geometry with an acceleration region of 7 mm and a flight tube of 300 mm. The ions were detected by using the channel electron multiplier in the pulse counting mode. The output of the detector was suitably amplified and fed into a constant fraction discriminator and after suitable delay was given as “stop” input into *TAC*. The “start” input for the *TAC* was generated using a photodiode which detected a part of the laser pulse. The output of the *TAC* was given to pulse height analyzer to obtain the *ToFMS*.

In some cases the count-rate of the signal from the detector was too high to be handled by the TAC based data acquisition system. In those cases the output of the detector after appropriate amplification was fed to the digital storage scope (Yokogawa Model DL7200) in order to generate the mass spectrum.

During the experiments it was found that the background gases in the interaction region were playing the major role of electron donors by getting excited to their Rydberg states (as discussed in chapter 7).

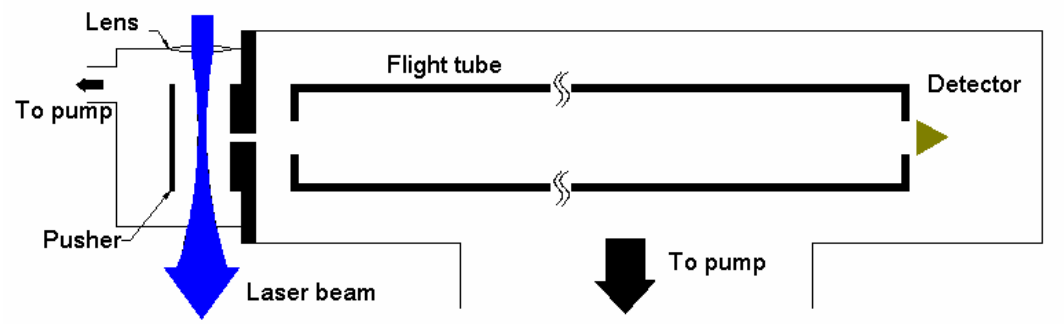

Figure 2.27: *Schematic of the experimental set-up used for the Rydberg electron attachment experiment.*

In order to understand the process involved in generating negative ions it was essential to have control on the Rydberg states that were participating in the process. For achieving this it was important to have cleaner vacuum in the interaction region before introduction of the gas under study. Hence an additional pumping arrangement was made for separate pumping of the interaction region by a dry turbo molecular pump backed by a Tri-scroll pump. Instead of the gas cell, the target gases were introduced as a molecular beam by using a capillary array which was mounted perpendicular to the both laser beam as well as the *ToFMS* axis. The gas flow in the interaction region was controlled by two needle valves situated on two different gas lines that were joined before entering the capillary array. Hence controlled mixtures of various gases of interest could also be introduced in the interaction region.

References:

[1]. S. K. Srivastava, A. Chutjian and S. Trajmar, *J. Chem. Phys.* **63**, 2659 (1975).

[2]. W. C. Wiley and I. H. McLaren, *Rev. Sci. Instrum.* **26**, 1150 (1955).

[3]. D. R. Olander, R. H. Jones and W. J. Siekhaus, *J. Appl. Phys.* **41**, 4388 (1970).

[4]. D. Rapp and D. D. Briglia, *J. Chem. Phys.* **43**, 1480 (1965).

[5]. Benjamin Whitaker (edt.), *Imaging in Molecular Dynamics: Technology and Applications* (Cambridge University Press, 2003)

[6]. A. Eppink and D. H. Parker, *Rev. Sci. Instrum.* **61**, 607 (1990).

[7]. C. R. Gebhardt, T. P. Rakitzis, P. C. Samartzis, V. Ladopoulos and T. N. Kitsopoulos, *Rev. Sci. Instrum.* **72**, 3848 (2001).

[8]. D. Townsend, M. P. Minitti and A. G. Suits, *Rev. Sci. Instrum.* **74**, 2530 (2003).

[9]. A. Chatterjee, http://www.tifr.res.in/~pell/lamps.html

[10]. A. Chatterjee, S. Kamerkar, A. K. Jethra, S. Padmini, M. P. Diwakar, S. S. Pande and M. D. Ghodgaonkar, *Pramana - J. Phys.* **57**, 135 (2001).

[11]. H. S. W. Massey, *Negative Ions* (Cambridge University Press, Cambridge, 1976).

[12]. P. N. Chantry and G. J. Schultz, *Phys. Rev.* **156**, 134 (1967).

[13]. T. Oster, A. Kuhn, and E. Illenberger, *Int. J. Mass Spectrom. Ion Proc.*, **89**, 1 (1989).

[14]. R. J. Van Brunt and L. J. Kieffer, *Phys. Rev. A* **2**, 1899 (1970).

[15]. R. E. Fox, W. M. Hickam, D. J. Grove and T. Kieldaas Jr. *Rev. Sci. Instrum*., **26,** 1101 (1955).

[16]. D. S. Belic, M. Landau and R. I. Hall, *J. Phys. B: At. Mol. Phys.* **14**, 175 (1981).

[17]. S. Trajmar and R. I. Hall, *J. Phys. B: At. Mol. Phys.* **7**, L485 (1974).

[18]. Micheal Allan, *J. Elec. Spect. Rel. Phenom.* **48**, 219 (1989).

Chapter 3

DEA to O_2: Presence of $^4\Sigma_u^-$ state

Electron collision with molecular oxygen (O_2) has been a subject of detailed studies. These studies are important due to the presence of oxygen in earth's atmosphere as well as in various plasma processes related to discharges. Also being a homonuclear diatomic molecule with open shell configuration with two unpaired electrons in the π_g orbital, it has been seen as the model system for the theoretical understanding of structure and dynamics of various bigger molecules. On the theoretical front there have been several calculations reported on the structure and dynamics of negative ion states of O_2, their potential energy curves and corresponding lifetimes including the R-matrix calculations [1–6]. On the experimental front there are many reports of electron – O_2 scattering experiments [7]. These efforts involve both elastic and inelastic scattering yielding total and differential cross sections including differential cross sections for excitation of O_2 to vibrational and electronic excited states through resonant scattering. Dissociative electron attachment (*DEA*) to O_2 has also been studied extensively in the past [8, 9]. These studies include the measurement of absolute cross section for the O^- formation through *DEA* [8] and its angular distribution for identifying the negative ion states that contributes to the *DEA* process [9]. Apart from these experiments in the gas phase, the electron scattering and electron induced desorption of O^- from O_2 condensed on various surfaces have been studied quite extensively [10–20]. These experiments were performed in order to understand electron induced processes at surfaces and in condensed phase that have enormous bearing on electron induced chemistry and radiation damage. Relatively well understood in gas phase measurements, O_2 has been sort of a prototype for these studies. The measurements on O_2 have been aimed at elucidating the lifetime, energy and symmetries of the resonant states on the surface. These states are found to play vital role in modeling the surface enhanced Raman scattering, photoemission and inverse photoemission from the surfaces [21].

In considerable number of reports existing on the electron – O_2 collision processes, there exists some inconsistency among various findings in the gas phase experiments performed at low energies (<15eV). This inconsistency has been about the lifetime of the $^4\Sigma_u^-$ state of the O_2^- ion and its possible role in *DEA*.

Based on available data, electron scattering on isolated O_2 molecules are considered to lead to four resonances – $^2\Pi_g$, $^2\Pi_u$, $^4\Sigma_u^-$, and $^2\Sigma_u^-$ below 15 eV, the first three making the majority of contribution to the electronic and vibrational excitation [1]. The $^2\Pi_u$ resonance along with $^2\Pi_g$ is found to contribute to the excitation of several low lying electronic states including the $^1\Delta_g$ and $^1\Sigma_g^+$ states [5-7, 22-23]. The $^2\Pi_g$ resonance also dominates the vibrational excitation upto $v = 4$ of the $X\,^3\Sigma_g^-$ state of O_2 below 4 eV [24]. The excitation of vibrational levels in $X\,^3\Sigma_g^-$ at higher energies shows a broad peak at about 9 eV and has been found to arise from the $^4\Sigma_u^-$ resonance [1, 25-27].

The *DEA* data from O_2 shows a single broad peak at 6.5 eV [8]. The only angular distribution measurements of O^- ions showed the $^2\Pi_u$ resonance as solely responsible for this [9]. This was also supported by the fairly large width and hence short lifetime against *autodetachment* of the $^4\Sigma_u^-$ resonance obtained in *R*-matrix calculations [1]. Since then, all analyses of electron collision data on O_2 in the free gaseous state, in clusters [12] or in condensed state [13-20] have assumed that the *DEA* process in O_2 is entirely due to the $^2\Pi_u$ state and any indication that the $^4\Sigma_u^-$ state may be contributing to the *DEA* process has been overlooked. The significant aspect of most of these experiments is the observation of new resonance peaks at about 8 eV and 14 eV in the electron stimulated desorption (ESD) of O^- ions in addition to the peak at 6.5 eV seen from the gaseous measurements. Hence in order to explain the observed large O^- yield in the electron induced desorption experiments carried out at 8 eV electron energy, mechanisms like resonance formation through forbidden transition of type Σ^- to Σ^+ have been invoked [15].

However, the observation that vibrational levels close to the dissociation limit of the $X\,^3\Sigma_g^-$ state are excited through the $^4\Sigma_u^-$ state resonance indicates the resonance to have sufficiently long lifetime to manifest in the *DEA* channel [25]. Based on the selection rules [28], the $^2\Pi_u$ resonance from a $^3\Sigma_g^-$ state will have zero contribution in the forward and backward directions, unlike the $^4\Sigma_u^-$ state, which will have finite contribution in those directions. Thus the presence of $^4\Sigma_u^-$ state is likely to manifest

unambiguously in the forward and backward directions. In the earlier reported experiment of measurement of angular distribution of O^- from *DEA* to O_2 [9], the conventional turn table technique is used. In this technique either the electron source or the detector is rotated about the interaction point in a plane and the negative ion yield is noted for a given energy of electron as a function of angle between the incident electron and the ejected ion. This technique has an inherent limitation that the ions ejected in a finite angular range in the forward and backward directions can not be detected due to geometric restriction of the apparatus. The reported O^- angular distribution data are obtained in the range of 23° to 157° [9]. Based on a fit to the angular distribution data, it was concluded that only $^2\Pi_u$ state contributes to the *DEA* process. It is probable that the lack of data in the forward and backward angles and the relatively low cross section for the $^4\Sigma_u^-$ state may have prevented it from being observed in these measurements.

As mentioned earlier, in order to address this issue it is essential to measure the angular distribution in the forward as well as backward direction. In this regard the velocity map imaging (*VMI*) technique that we developed for low energy electron collision experiments has come handy. This technique provides an efficient way of obtaining the differential cross sections for the negative ion in the entire 2π angular range.

3.1 Velocity Map Images (*VMI*) of oxygen

The excitation function of O^- from O_2 is shown in Figure 3.1. The electron energies at which the *VMI*s are taken are shown in the figure.

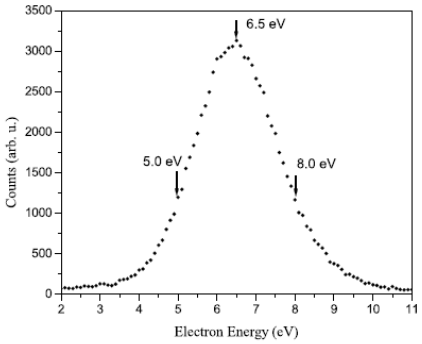

Figure 3.1: *Ion yield curve for O^- from O_2 by DEA.*

The *VMI*s at various energies (5eV, 6.5eV, 8eV, 8.8eV and 9.3eV) are shown in Figure 3.2. From this figure it is clear that the cross sections for the O^- formation in the forward and backward directions are non-zero at all the energies. For electron energies up to 8eV these cross sections are lower than that observed in the 90˚.

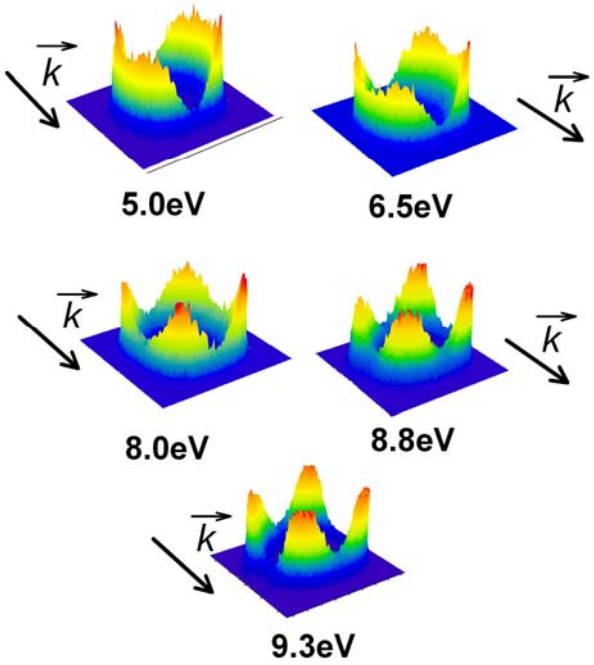

Figure 3.2: *Velocity map images of O^- from O_2 at different electron energies across the resonance. The arrow indicates the direction of electron momentum vector, $\vec{k}$.*

As mentioned earlier the polar plots in the case of all these images are obtained by integrating the ion counts for a finite range of radii of the distribution for a small angular spread about a given angle. The counts so obtained are normalized with respect to those in the 90˚ direction. These polar plots are shown in Figure 3.3 along with the earlier reported data (5.75eV, 6.7eV and 7.8eV) for the limited angular range obtained by the conventional turn table technique [9]. As can be seen from the figure, the data obtained by *VMI* is in fairly good agreement with that reported earlier with in the common angular range. But the cross sections in the forward and backward directions are found to be nonzero and also increasing with respect to that at 90˚ with the electron energy. In the case of data taken at around 9eV the cross section in the forward and backward direction are much larger than those in the 90˚ direction.

Since the $^2\Pi_u$ state alone cannot justify these nonzero cross sections in these directions, we assume that this is due to the $^4\Sigma_u^-$ state.

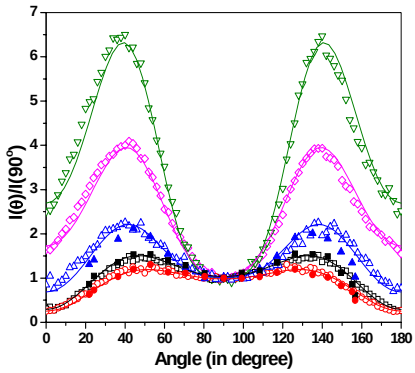

Figure 3.3: *Angular distribution of O^- at different electron energies. Open symbols: present data. o - 5 eV, □ - 6.5 eV, Δ - 8 eV, ◊ - 8.8 eV, ∇ - 9.3eV; filled symbols: from Van Brunt and Keiffer [9] ● - 5.75 eV, ■ - 6.7 eV, ▲ - 7.8 eV. The lines are the best fit given by Eq. (3.1), with coefficients as given in Table 3.1.*

In the Figure 3.3, we also provide the fits, based on the general formula for the angular distribution cross section as given by O'Malley and Taylor [29] and assuming contribution from both the $^2\Pi_u$ and the $^4\Sigma_u^-$ states. We have to include l = 1, 3, 5 partial waves to fit the data using the expression,

$$\boldsymbol{I(\theta) = A\sin^2\theta + B\cos^2\theta + C\sin^2(2\theta) + D\cos^2\theta\sin^2(2\theta) + F\sin^4(2\theta)} \quad (3.1)$$

The parameters A, B, C, D and F in equation 3.1 are determined by least square fit (Table 3.1). The last term of the fitting equation comes from the cross term in the l = 3 and l = 5 partial wave contributions. This term becomes significant only above 8 eV. The direct term from the l = 5 partial wave is not considered as its contribution to the angular distribution is negligible. We are unable to distinguish contributions from the individual partial waves due to the involvement of two states, though the presence of the $cos^2\theta$ term signifies the presence of the $^4\Sigma_u^-$ resonance.

We eliminate the possibility that the observed nonzero cross sections in the forward and backward directions are due to some artifacts in the following way. To begin with the forward and backward cross sections are found to increase with electron energy as compared to that in the 90° direction. It is expected that any artifact

due to finite angular resolution would affect both the equatorial and polar directions in the same way, which is not the case here. The possibility of a tilt of the electron beam giving rise to the observed enhancement of intensity in the polar directions is ruled out by the fact that the increase in polar directions is not seen at all energies. Moreover, our *VMI* measurements on several other molecules for which angular distribution data exist have not shown any undue increase in the polar directions.

Table 3.1: *The parameters of the various terms in Eq. 3.1 at different electron energies*

Energy (eV)	***A***	***B***	***C***	***D***	***F***
5.0	0.992	0.260	0.432	0.267	0.011
6.5	0.996	0.293	0.507	0.478	0.067
8.0	1.013	0.808	0.352	1.405	0.441
8.8	1.011	1.725	0.762	1.491	0.992
9.3	1.007	2.694	-0.263	4.028	2.427

The unambiguous presence of the $^4\Sigma_u^-$ state in the *DEA* signal brings up several issues. First of all, can its presence be seen in the total *DEA* cross sections, which have been measured by a number of authors and compare it with the data taken in the 90° direction [30]? A relatively recent measurement [27] on high resolution electron impact excitation of the $a^1\Delta_g$ and $b^1\Sigma_g^+$ states shows that the O^- yield at 90° with respect to the electron beam direction extends only up to 9 eV and is very similar in shape to the excitation cross sections for the higher vibrational levels of $a^1\Delta_g$ and $b^1\Sigma_g^+$ states. Excitation of the singlet levels will have contribution only from a doublet state and not from a quartet state. The *DEA* signal at 90° also will have contribution only from the $A^2\Pi_u$ resonance based on the selection rules [28]. Considering this the fact that the cross sections extend beyond 9 eV can only be due to the contribution from the $^4\Sigma_u^-$ state. This conclusion also appears to be consistent with the shape of the excitation cross sections measured for the high lying vibrational levels of the $X^3\Sigma_g^-$ state [27].

3.2 Estimating the lifetime of the $^4\Sigma_u^-$ state

The lifetime of the $^4\Sigma_u^-$ resonance that is estimated by the theoretical calculations must also be looked at again [1]. Since it is seen that the $^4\Sigma_u^-$ state contributes in the *DEA* signal, it is straight forward that its lifetime ought to be larger than that assumed till now. Using the potential energy curve [1] and the curve for the width for the $^4\Sigma_u^-$ state one can estimate the survival probability for the negative ion state against *autodetachment* using the formula,

$$p(\varepsilon) = \exp\left(- \int_{R_\varepsilon}^{R_C} \frac{\Gamma_a(R)}{\hbar v(R)} dR \right) \tag{3.2}$$

where Γ_a is the *autodetachment* width, R_ε and R_c are the inter-nuclear distances corresponding to the electron capture and the crossing point of the neutral ground state curve and the negative ion resonant curve. Beyond R_c no *autodetachment* is possible as the negative ion state is energetically favored beyond R_c. An upper limit of $p(\varepsilon)$ can be obtained using the available data from literature about the potential energy surfaces as the calculations of the lifetime do not exist till R_c. The *DEA* cross section can be estimated using

$$\sigma_{DEA} = \sigma_C \times p(\varepsilon) \tag{3.3}$$

where σ_c is the electron capture cross section for the $^4\Sigma_u^-$ state at the relevant electron energy. Now,

$$\sigma_C = \sigma_{DEA} + \sigma_A \tag{3.4}$$

where σ_A is *autodetachment* cross section and can be approximated to the integral cross section for the excitation of all the vibrational levels of the ground state of O_2 plus that for the excitation of the other triplet electronic states. Taking these values from the literature [7] and the calculated value of $p(\varepsilon)$ and using the relation,

$$\sigma_{DEA} = \frac{p(\varepsilon)}{(1-p(\varepsilon))} \times \sigma_A \qquad (3.5)$$

the *DEA* cross section is estimated to be $4\text{x}10^{-23}$ cm^2 for ε = 9eV. Here it is assumed that only $^4\Sigma_u^-$ contributes to the *DEA* signal at 9eV electron energy. Similar calculations for the $A^2\Pi_u$ state using the results of Noble *et al.* [1] and the experimental inelastic scattering data at the electron energy of 6.5 eV [7] gives the *DEA* cross section to be $4\text{x}10^{-19}$ cm^2 for ε = 6.5eV. In this case, it is assumed that the *DEA* at 6.5 eV is solely due to the $A^2\Pi_u$ state. From a comparison of these numbers with the measured absolute *DEA* cross sections, $9\text{x}10^{-20}$ cm^2 and $1.45\text{x}10^{-18}$ cm^2 at 9 eV and 6.5 eV respectively [8], it appears that though the calculated lifetime of the $A^2\Pi_u$ state is only marginally smaller, that of the $^4\Sigma_u^-$ state is far too small.

It is possible to get a rough estimate of the width (Γ_a) of the $^4\Sigma_u^-$ state at various inter-nuclear separations using the inelastic cross sections for vibrational excitation of the $X^3\Sigma_g^-$ state at 9 eV and assuming that there is very little contribution from the $^2\Pi_u$ state at this energy to these vibrational excitations. It is known that *autodetachment* of the $^4\Sigma_u^-$ state mostly leads to the $X^3\Sigma_g^-$ state with relatively small contribution to the $A^3\Sigma$ and $A'^3\Delta$ states [7]. Thus the change in the vibrational intensities of the $X^3\Sigma_g^-$ state can be used to obtain the Γ_a of the $^4\Sigma_u^-$ state at inter-nuclear separations corresponding to the turning points of the vibrational levels in the $X^3\Sigma_g^-$ state. We can write the integral cross section for the vibrational excitation to be

$$\sigma_V = \sigma_C \times \left(1 - e^{-\Gamma t/\hbar}\right) \qquad (3.6)$$

where Γ is the width of the state and t is the time taken by the system to roll from R_ε to R_v where R_V is the inter-nuclear separation of the oxygen atoms corresponding to the turning point of their corresponding vibrational motion. The value of Γ may be calculated using the total capture cross section, σ_c, the individual vibrational excitation cross section, σ_v and time, t under the assumption that the force between the two nuclei and the width of the resonance are constant in the range of R_ε to R_v.

We assume σ_c to be equal to the total excitation cross sections of all the triplet states below 9 eV [7], assuming the *DEA* cross section to be small. The time t is calculated using the potential energy curve for the $^4\Sigma_u^-$ state given by Noble *et al.* [1] in the formula,

$$t = \int_{R_\varepsilon}^{R_V} \frac{dR}{v(R)} \tag{3.7}$$

where $v(R)$ is the speed of separation of the two oxygen atoms moving on the potential energy surface. The results for Γ_a based on these calculations are found to be in the range of 0.6 to 0.8 eV and are substantially smaller than about 3 eV earlier reported using *R*-matrix calculations. Using these widths an upper limit of the *DEA* cross section at 9 eV due to the $^4\Sigma_u^-$ state turned out to be $5\text{x}10^{-19}$ cm^2. This is about a factor 6 higher than what has been measured [8]. The difference is not surprising since the *DEA* cross section is very sensitive to the width and considering the approximations we have used in evaluating it. In any case, it appears that the lifetime of the $^4\Sigma_u^-$ state as calculated previously is too small and more theoretical work is needed in this respect.

3.3 Possible implications of these results

As mentioned earlier, there has been large number of measurements on electron attachment to O_2 in molecular clusters [12] and in condensed state [13-20]. The significant aspect of most of these experiments is the observation of new resonances that peak at about 8 eV and 14 eV in the electron stimulated desorption (*ESD*) of O^- ions in addition to the peak at 6.5 eV seen from the gaseous measurements. It is also observed that *ESD* signal at 6.5 eV is about two orders of magnitude smaller as compared to that of the dipolar dissociation and as the O_2 coverage increases, the intensity of the 6.5 eV peak decreases with respect to other peaks.

The overall O^- signal from the ESD experiments is expected to have effects from i) perturbation in the symmetry of the electron-molecule system due to the presence of other molecules in the condensed phase ii) multiple inelastic scattering of impinging electrons (MES) before capture by molecule iii) post-dissociation

interactions (PDI) like electron detachment, reactive and non-reactive scattering by neighboring molecules, effects of image charge and polarization [17]. On the basis of the kinetic energy measurements of the O^- anions from the ESD experiments, Huels *et al.* [10] have shown that the Π_u state of O_2^- contributes to the DEA process but due to the PDI and MES its contribution to the ESD gets affected.

The ESD signal at 8 eV was interpreted as due to the $^2\Sigma_g^+$ state under the assumption that there cannot be any contribution from the $^4\Sigma_u^-$ state due to its very low *autodetachment* lifetime [16] and the fact that the previous angular distribution data of the O^- ions in gas phase did not show its presence. On the other hand, in order to have contribution from the $^2\Sigma_g^+$ state, the concept of the breakdown of the selection rule which forbids the $\Sigma^- \leftrightarrow \Sigma^+$ transition in isolated molecules had to be brought in [15]. There have been several discussions on the exact nature of the state at 8 eV, with respect to the kinetic energy measurements and the potential energy curves [10, 16, 17]. All these have been based on the assumption that the $^4\Sigma_u^-$ state is too short-lived to yield O^- ions. In the light of the present results, we propose that the peak seen at 8 eV in these measurements could be due to the $^4\Sigma_u^-$ resonance. Also it is observed that due to MES effect the ESD peaks are found to be shifted to the lower energy sides corresponding to the resonances in the gas phase.

It has been proposed that the reduction in the *ESD* yield is due to image charge effects at the metal surface [18], whereas polarization effects due to neighborhood species decrease the *autodetachment* rate and subsequently increase the *DEA* cross sections [19]. The *ESD* measurements using films of pure O_2 or mixtures of O_2 with molecules like N_2 or CO on a Platinum surface have shown that with increasing probability for a given O_2 molecule to have another O_2 molecule in its neighborhood, the intensity of the 8 eV peak increases with respect to that at 6.5 eV [20]. We argue that the peak seen at 8 eV may be due to the $^4\Sigma_u^-$ resonance. The relative increase in the intensity due to this resonance *vis a vis* that due to the $^2\Pi_u$ at 6.5 eV may be explained in terms of a relative increase of the lifetime or of the *ESD* yield or both of the $^4\Sigma_u^-$ resonance as compared to that of the $^2\Pi_u$ resonance. With increasing separation between the perturbed potential energy curves of the resonance from that of the unperturbed one, the *ESD* decreases. Also the capture cross section of the $^4\Sigma_u^-$ state in the gas phase is at least an order of magnitude larger than that for the $^2\Pi_u$ state. It is also possible that the effect of the image charge on the $^2\Pi_u$ resonance is

larger than on the $^4\Sigma_u^-$ resonance thus yielding relatively less in the *ESD* signal. A relative increase in lifetime of the $^4\Sigma_u^-$ resonance could also explain the results.

Reference:

[1]. C. J. Noble, K. Higgins, G. Woste, P. Duddy, P. G. Burke, P. J. O. Teubnor, A. G. Middleton and M. J. Brunger, *Phys. Rev. Lett.* **76** 3534 (1996) and ref. therein.

[2]. M. Krauss, D. Neumann, A. C. Wahl,G. Das and W. Zemke *Phys. Rev.* A **7,** 69 (1973).

[3]. H. H. Michels *Adv. Chem. Phys.,* **45,** 225 (1981).

[4]. C. J. Noble and P. G. Burke *Phys. Rev. Lett.* **68** 2011 (1992).

[5]. K Higgins, C. J. Noble and P. G. Burke *J. Phys. B: At. Mol. Opt. Phys.* **27,** 3203 (1994).

[6]. D. Teillet-Billy, L. Malegat and J. P. Gauyacq *J. Phys. B: At. Mol. Opt. Phys.* **20**, 3201 (1987) and D. Teillet-Billy, L. Malegat, J. P. Gauyacq, R. Abouaf and C. Benoit *J. Phys. B: At. Mol. Opt. Phys.* **22,** 1095 (1989).

[7]. M. J. Brunger and S. J. Buckman *Phys. Rep*. **357,** 215 (2002).

[8]. D. Rapp and D. D. Briglia, *J. Chem. Phy*s. **43,** 1480 (1965).

[9]. R. J. Van Brunt and L. J. Keiffer *Phys. Rev.* A **2,** 1899 (1970).

[10]. M. A. Huels, L. Parenteau, M. Michaud and L. Sanche, *Phys. Rev.* A **51,** 337 (1995).

[11]. R. E. Palmer and P. J. Rous, *Rev. Mod. Phys*. **64,** 383 (1992).

[12]. T. D. Märk, K. Leiter, W. Ritter and A. Stamatovic, *Phys. Rev. Lett.* **55,** 2559 (1985).

[13]. L. Z. Xiang and D. Lichtman *Surf. Sci*. **114**, 287 (1982).

[14]. L. Sanche *Phys. Rev. Lett.* **53,** 1638 (1984).

[15]. R. Azria, L. Parenteau, and L. Sanche *Phys. Rev. Lett.* **59,** 638 (1987).

[16]. H. Sambe and D. E. Ramaker *Phys. Rev.* A **40,** 3651 (1989).

[17]. Roger Azria, Yvonnick Le Coal, Jean-Pierre Ziesel, Jean-Pierre Guillotin, Brahim Mharzi and Michel Tronc *Chem. Phys. Lett.* **220,** 417 (1994).

[18]. H. Sambe, D. E. Ramaker, L. Parenteau, and L. Sanche, *Phys. Rev. Lett.* **59,** 505 (1987).

[19]. H. Sambe, D. E. Ramaker, M. Deschenes, A. D. Bass, and L. Sanche *Phys. Rev. Lett.* **64,** 523 (1990).

[20]. Roger Azria, Léon Sanche and Luc Parenteau *Chem. Phys. Lett.* **156,** 606 (1989).

[21]. D. P. Woodruff, *Rep. Prog. Phys.* **49**, 683 (1986), N. V. Smith and D. P. Woodruff, *Prog. Surf. Sci*., **21**, 295 (1986), A. Otto, T. Bornemann, U. Erturk, I. Morzek and C. Perrenkofer, *Surf. Sci.* **210**, 363 (1989).

[22]. A. G. Middleton, P. J. O. Teubner, and M. J. Brunger *Phys. Rev. Lett.* **69,** 2495 (1992).

[23]. M. Allan *J. Phys. B: At. Mol. Opt. Phys.* **28,** 4329 (1995).

[24]. F. Linder and H. Schmidt *Z. Naturforsch.* **26A**,1617 (1971).

[25]. S. F. Wong, M. J. W. Boness and G. J. Schulz *Phys. Rev. Lett.* **31,** 969 (1973).

[26]. T. W. Shyn and C. J. Sweeney *Phys. Rev.* A **48,** 1214 (1993).

[27]. M. Allan *J. Phys. B: At. Mol. Opt. Phys.* **28,** 5163 (1995).

[28]. G. H. Dunn *Phys. Rev. Lett.* **8,** 62 (1962).

[29]. T. F. O'Malley and H. S. Taylor *Phys. Rev.* **176,** 207 (1968).

[30]. L. G. Christophorou *Electron-molecule Interactions and Their Applications - Vol I,* (Academic Press, Orlando, Florida, 1984).

Chapter 4

DEA to simple organic molecules

Interaction of low energy electrons with organic molecules is attracting a great deal of attention currently. These studies are driven by the possibility that the major damage to DNA is caused by the low energy (<15eV) secondary electrons generated in the living cells when high energy radiation interacts with them. Recent measurements using low energy electrons on DNA in isolated conditions have shown that dissociative electron attachment plays a dominant role in single and double strand breaks and loss of super coiled DNA [1]. Several measurements on DNA bases, amino acids and their analogues as well as smaller organic molecules in gas phase as well condensed phase are being studied under low energy electron collision in order to understand the radiation induced damage in living tissues at the microscopic level [2]. In order to understand the dynamics of the process as well as to quantify the extent of the damage, we have carried out the *DEA* experiments on simple organic molecules like simple carboxylic acids, amines, and alcohols which can be used as the basic building blocks for modeling the radiation damage to bigger molecules.

These measurements were also motivated by the recent observations of the presence of small organic molecules in astrophysical objects. For example formic acid is one of the organic molecules found in the interstellar medium [3, 4]. Traces of formic acid have been detected in the coma of Hale-Bopp comet [5]. Recently traces of formic acid were observed in the extensively studied massive star forming region in Orion nebula (Orion-KL) [6, 7] and in the Orion molecular clouds (OMC-1) [8] as well as from the SGR B2 [9] which is another massive star forming region in the Sagittarius. Also the detection of formic acid and other simple organic molecules in the IRAS 16293-2422 region [10], which is a young stellar object has added to the general interest in the role of such organic molecules in the chemical processes in star forming regions. All these findings have made the study of interaction of simple organic molecules with free electrons important from astrophysics point of view. Since

carboxylic acids are part of the basic building blocks of various bio-molecular structures [11] their observation in astrophysical objects may have significance to Astrobiology. The electron collision processes on these molecules are important due to possible role of electron-induced chemistry in the formation of bigger biological molecules. Apart from this, organic acids are important atmospheric trace gases. These acids are emitted to the atmosphere from biodegradation [12, 13], biomass burning as well as from the biosphere and via motor vehicle exhaust [14, 15]. They contribute significantly to the acidity of atmospheric condensed water, acid precipitation and also play some role in chemical processes in the cloud droplets [16].

DEA process in small carboxylic acids has been reported recently [17–20]. But these studies failed to observe the presence of H^- in the fragmentation channels. This is a surprising result since H^- has been observed from several other bigger molecules like DNA bases and from organic molecules adsorbed on surfaces by electron collision [21, 22].

In the earlier studies a quadrupole mass spectrometer was used for the mass analysis of negative ions formed in the *DEA* process. The measurements were carried out using a continuous electron beam with a DC extraction field. This field had to be kept small to prevent it from affecting the electron beam. Under these conditions, it is difficult to extract energetic H^- ions. And H^- formed from these molecules, will necessarily have almost all the excess kinetic energy due to momentum conservation. Hence we felt that these measurements may have suffered from discrimination against H^- ions which are likely to be formed with relatively large kinetic energies. Since H^- ions will carry almost all the kinetic energy of the dissociation process, it is important that the presence of this channel is investigated using a different, but appropriate technique. Moreover, the possibility exists that energetic H^- ions from the acid, if present, could contribute to the chemistry of the environment in which the acid molecule is present. As described in chapter 2, we have the appropriate apparatus, using a pulsed electron beam, pulsed ion extraction and the segmented *ToFMS* that is efficient in collecting and transporting the relatively swifter ions and capable of measuring the absolute cross sections. Using this, we carried out the *DEA* measurements on some simple organic molecules namely formic acid (HCOOH), acetic acid (CH_3COOH), propionic acid (C_2H_5COOH), methanol (CH_3OH), ethanol (C_2H_5OH) and n-propylamine ($C_3H_7NH_2$).

4.1 *DEA* to formic acid (HCOOH)

The previous measurements on the *DEA* to the formic acid [17, 18] showed three different resonances peaking at energies 1.25 eV, 7.5 eV and above 8 eV yielding $HCOO^-$, OH^- and O^- respectively with a ratio of 240:10:1. Absolute cross sections were also estimated for these channels. The resonance yielding the formate ion, $HCOO^-$ was found to have a sharp onset and having structures on the high energy tail. It is not clear if these structures are due to the vibrational levels of the formate ion as suggested by them or due to different shape resonances. Another striking result of these measurements was the absence of H^- channel as mentioned earlier. We performed the *DEA* measurement on formic acid using segmented *ToFMS* to investigate the hydride ion channel of dissociation.

In our measurements, we find that H^-, O^-/OH^-, and $HCOO^-$ ions were produced depending on the electron energy. Due to poor mass resolution of the segmented *ToFMS* we are unable to separate out the O^- and OH^- mass peaks. The absolute cross sections for the formation of $HCOO^-$ and OH^-/ O^- are given in Figure 4.1 & 4.2. Previous measurements [17, 18] showed the $HCOO^-$ ion yield curve having a sharp onset at 1.15 eV with the peak position at 1.25 eV. We find the peak in the ion yield curve at 1.4 eV, and with a slower onset. This slower onset may be due to the relatively poor energy resolution in our experiment. The ion yield curve for the O^-/ OH^- ions in the present measurements show a peak at 7.6 eV followed by a shoulder at 9.3 eV. This compares well with the ion yield curves from the earlier measurements [17, 18], where they observed a peak at 7.5 eV in the OH^- channel and a peak about 9 eV in the O^- channel with an intensity of about one-tenth that of the OH^- channel. We also observe relatively weak structure for the combined O^- and OH^- channel at lower electron energies, which have not been seen in earlier reports. We find that the peak in the 4 to 6 eV region appears only when we introduce formic acid in the interaction region and hence we attribute it to be due to this molecule. The peak below 4 eV is seen even without any formic acid in the target region and hence may be due to some impurity.

The cross section for $HCOO^-$ channel at the peak energy of 1.4 eV is found to be 1.4×10^{-18} cm^2 and that for combined O^- and OH^- channels at the peak energy of 7.6 eV is found to be 6.1×10^{-20} cm^2. The cross sections for $HCOO^-$ channel and combined O^- and OH^- channels are in close agreement with the earlier estimated

cross sections which were reported to be 1.7 x 10^{-18} cm^2 for $HCOO^-$. They reported the cross section for combined signal of O^- and OH^- lesser by factor of 20 than that for $HCOO^-$ [18]**.** The peak cross section we obtained for the $HCOO^-$ ion is lower than the previously estimated cross sections. Because of the sharp onset of the ion channel, we may have underestimated the cross section for $HCOO^-$ channel due to poor energy resolution to some extent.

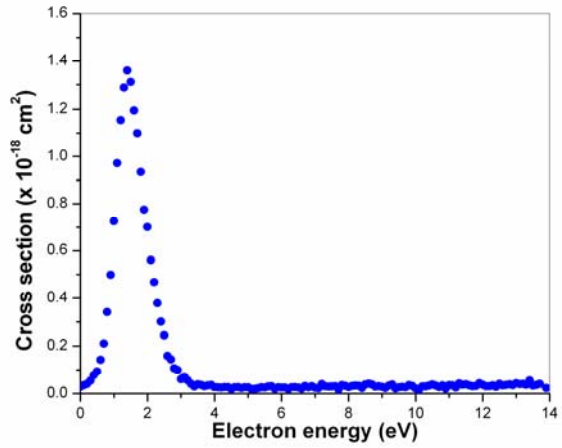

Figure 4.1: *Absolute cross-section of $HCOO^-$ from HCOOH as function of electron energy.*

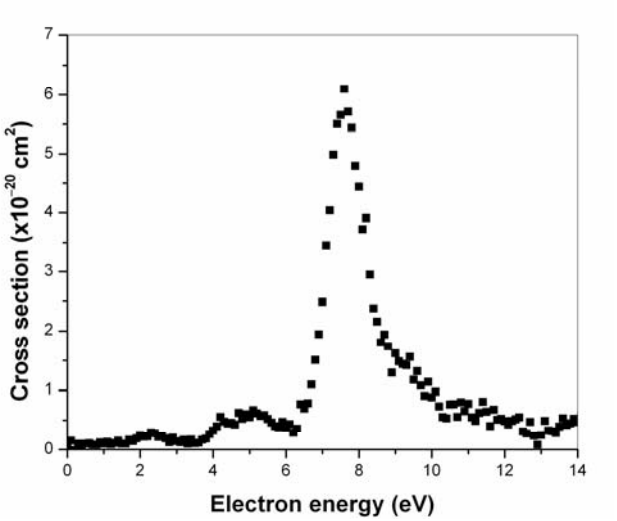

Figure 4.2: *Absolute cross section of O^- and OH^- from HCOOH as a function of electron energy.*

As compared to other channels of ion formation, we find that H^- formation is an important channel in the *DEA* process. This channel shows a main peak at 7.3 eV with a shoulder at about 9 eV as shown in Figure 4.3. The data also shows some

structure at about 6.5 eV, though it is not very conclusive. The absolute cross section for the main peak is measured to be 1.2 x 10^{-19} cm^2 and that at the high energy shoulder to be 4.9 x 10^{-20} cm^2. The absolute cross section for all the fragments from formic acid and other carboxylic acid molecules are listed in Table 4.1.

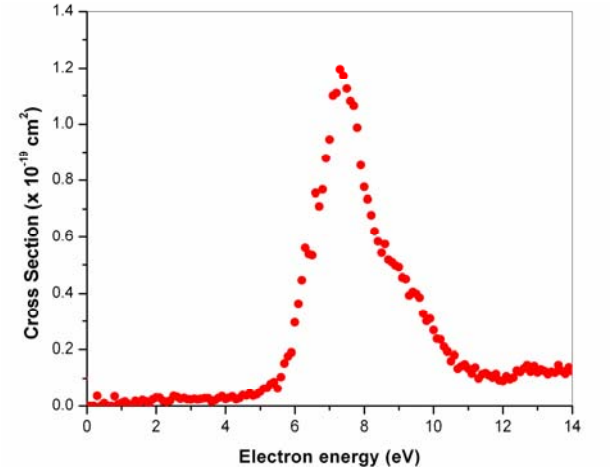

Figure 4.3: *Absolute cross-section for H^- from HCOOH as a function of electron energy.*

The uncertainty in the cross section measurements arise from the calibration technique, statistical uncertainty, uncertainty in the measurement of electron beam current and the uncertainty in the pressure measurements. The errors due to incomplete collection of ions have been eliminated by using segmented *ToFMS* along with the high extraction fields. The maximum error arising from the ion detection is estimated to be 5%. The cross section of O^- from O_2 used for the calibration has an uncertainty of 10% [23]. The uncertainty in the pressure measurements, statistical errors and those in the current measurements are estimated to be not more than 5%. Combining all these, the root mean square uncertainty in the cross section measurement is expected to be less than 15%. This number does not include systematic errors, the dominant one in this case arising from the finite electron energy resolution. The finite energy resolution tends to underestimate the cross sections for the resonances which are relatively narrow in energy.

Previous measurements by Pelc *et al.* [17, 18] showed sharp structure with an energy spacing of 340 meV in the $HCOO^-$ ion yield curve. These reports discounted the possibility of assigning this ion to $COOH^-$ due to the sharp onset seen in the ion

yield curve. Also using the isotopomers it has been shown that at this resonance the O-H bond is exclusively cleaved [24].

Table 4.1: *Absolute cross sections for DEA for various fragments from carboxylic acids (* Ref. 18, 19)*

	Electron energy (eV)	***Cross section measured (10^{-19} cm^2)***	***Cross section reported (10^{-19} cm^2) [*]***
Formic acid			
H^-	7.3	1.20 ± 0.17	
	9.0	0.49 ± 0.07	
$HCOO^-$	1.4	14.0 ± 2.00	17.0
$O^- + OH^-$	7.1	0.61 ± 0.08	<1.0
Acetic acid			
H^-	6.7	2.00 ± 0.30	
	7.7	1.70 ± 0.25	
	9.1	1.30 ± 0.19	
O^- and OH^-	10.1	0.21 ± 0.03	<0.50
CH_2^-	10.5	0.19 ± 0.03	<0.50
CH_3COO^-	1.50	1.30 ± 0.19	6.00
$CCO^- + CHCO^-$	10.0	0.40 ± 0.05	<0.50
Propionic acid			
H^-	6.8	0.78 ± 0.10	
	7.7	1.40 ± 0.19	
	9.1	0.82 ± 0.11	

Because of relatively poor resolution, we do not observe a sharp onset in the cross sections and find the peak to have shifted to 1.4 eV, instead of the 1.25 eV as observed earlier by Pelc *et al.* We are also unable to see the structure observed by them in the $HCOO^-$ ion yield curve, again due to relatively poor energy resolution. This sharp structure was attributed to vibrational excitation in the $HCOO^-$ ion, though the possibility of several closely spaced shape resonances was also not ruled out. Under the assumption that only one resonance is involved, the structure in the ion

yield curve could be attributed to either the vibrations of the resonant state or the fragments. Experimentally these two possibilities may be resolved depending on whether the ions are detected in their entirety irrespective of their kinetic energies or only those ions of near-zero energies as shown in the case of CO_2 [25]. Pelc *et al.* [17] have used similar arguments for the case of $HCOO^-$. They found that the ion extraction in their apparatus is efficient only for ions of low energy as their measurements on O^- from CO_2 yielded results similar to that obtained by Dressler and Allan [25] for the case of near-zero kinetic energy ions. However, it may be noted that in the case of *DEA* to formic acid, unlike the case of O^- from CO_2, the mass ratio of the fragments $HCOO^-$ and H are far too large and hence all the formate ions will necessarily have very little energy. For example, for a total kinetic energy of 1 eV, the formate ion will have only about 23 meV as kinetic energy, which is almost the same as thermal energy at room temperature. Thus in the measurements of Pelc *et al.* it is very likely that all the formate ions are detected. Hence the structure they observed in the ion yield curve in $HCOO^-$ cannot be due to vibrational excitation of the $HCOO^-$ fragment ion. We believe that the observed structure is due to vibrations in the $HCOOH^{-*}$ resonant state as observed in the high resolution electron transmission spectroscopy earlier [26]. The possibility that the structure is due to different resonances may also be ruled out on the basis of the study on the lowest empty orbital in HCOOH using electron transmission spectroscopy and virtual orbital calculations [27]. In fact recently reported theoretical results [28] that explain the dynamics associated with the formation of $HCOO^-$ ion from *DEA* process support, our conclusion. They conclude that the sharp structure observed on the high energy tail of the $HCOO^-$ ion yield curve is due to the reflection of the wave packets from the boundary of the vibrational levels of the parent negative ions.

4.2 *DEA* to acetic acid (CH_3COOH) and propionic acid (C_2H_5COOH)

As in the case of formic acid, *DEA* to acetic acid [19] and propionic acid [20] was also reported in the literature but without a mention of the observation of hydride anion. As in the case of formic acid we also expect these molecules to show considerable cross section in the H^- channel for *DEA*. Being bigger than the formic acid and containing more sites for the hydrogen, the cross section for hydride ion

formation through *DEA* is expected to be of the order of that observed for the formic acid if not more. Hence we have measured the absolute cross section for the H^- formation from these molecules using the segmented *ToFMS*.

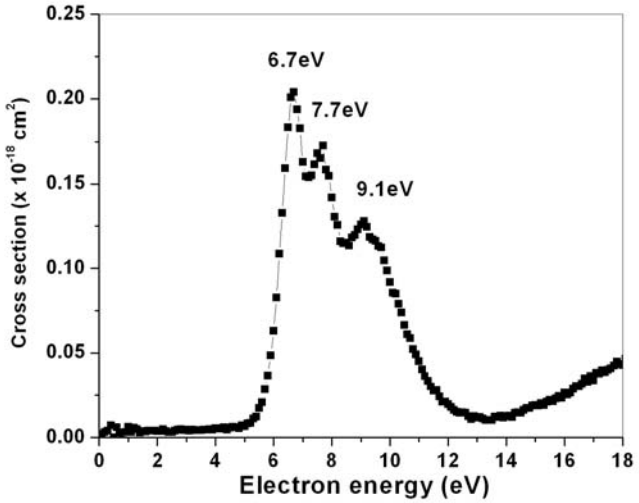

Figure 4.4: *Absolute cross-section for H^- from CH_3COOH as a function of electron energy.*

Typical mass spectrum obtained at various electron energies shows various fragments formed through the *DEA* in the case of acetic acid. The absolute cross sections measured for various fragments from acetic acid are listed in Table 4.1 along with the absolute cross sections measured for the H^- channel from propionic acid. It is clear from the Table that the formation of the hydride ion is one of the dominant channels in the relatively higher electron energy regime. The acetic acid as well as the propionic acid shows three distinct resonances in the H^- channel. In the case of acetic acid, the three resonances are situated at 6.7, 7.7 and 9.1eV. The absolute cross sections obtained at the peaks are 2.0 x 10^{-19} cm^2, 1.7 x 10^{-19} cm^2 and 1.3 x 10^{-19} cm^2 respectively as shown in Figure 4.4. In the case of propionic acid, the three resonances are found to be not as separated as those for the acetic acid. The second resonance is found to be the dominant one among the three situated at 7.7eV with two shoulders situated at 6.8eV and 9.1eV respectively as shown in Figure 4.5. The cross sections at these energies are measured to be 7.4 x 10^{-20} cm^2, 1.4 x 10^{-19} cm^2, and 8.2 x 10^{-20} cm^2 respectively.

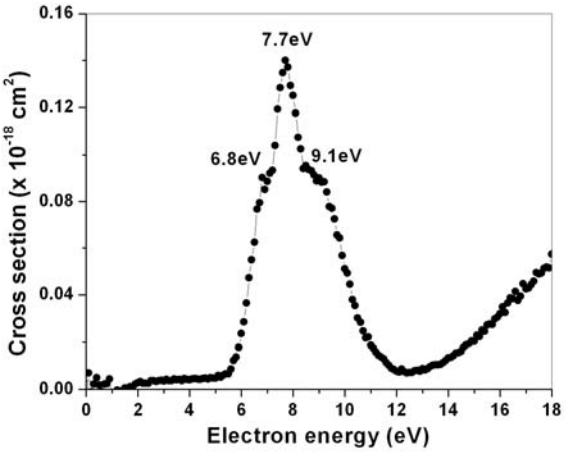

Figure 4.5: Absolute cross-section for H^- from C_2H_5COOH as a function of electron energy.

The other fragments observed in the case of acetic acid show cross sections much less than that for the H^- except for CH_3COO^- fragment that appears at 1.5eV. The resonances observed for the various other fragments in the case of acetic acid are shown in Figure 4.6 to 4.9. In these experiments, we are unable to mass separate the O^- and OH^- as well as the CCO^- and $CHCO^-$ fragments using the segmented *ToFMS*. Using the earlier reported data [19] that was obtained using the mass spectrometer with much better mass resolution, we identified the resonances corresponding to various masses that we could not separate. We have not measured the absolute cross sections for the other fragments arising from propionic acid apart from that for the hydride ions.

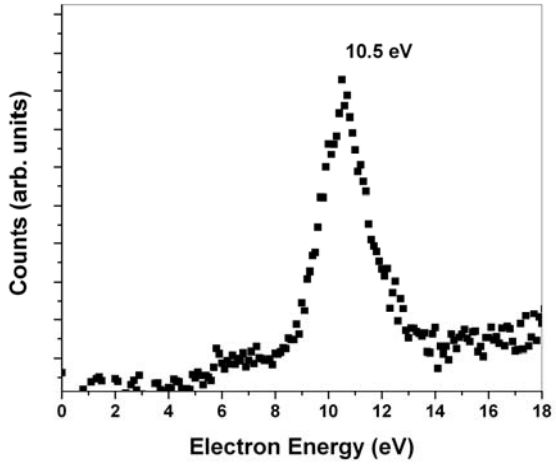

Figure 4.6: *Excitation function for CH_2^- from acetic acid.*

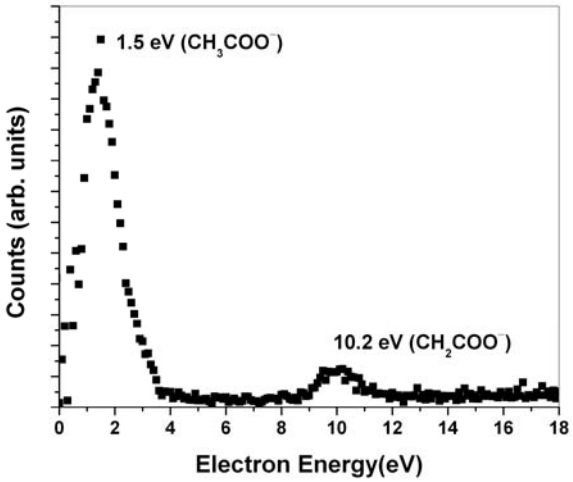

Figure 4.7: *Excitation function for CH_2COO^- and CH_3COO^- from acetic acid.*

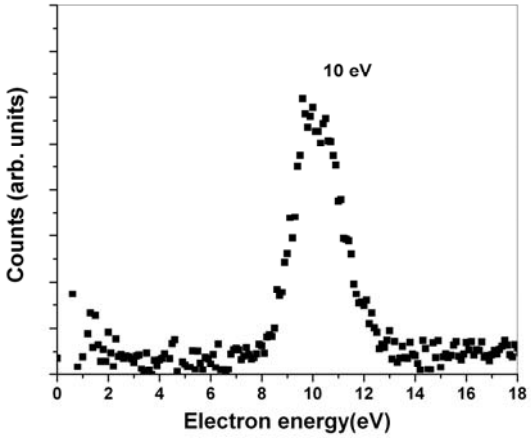

Figure 4.8: *Excitation function for CCO^- + $CHCO^-$ from acetic acid.*

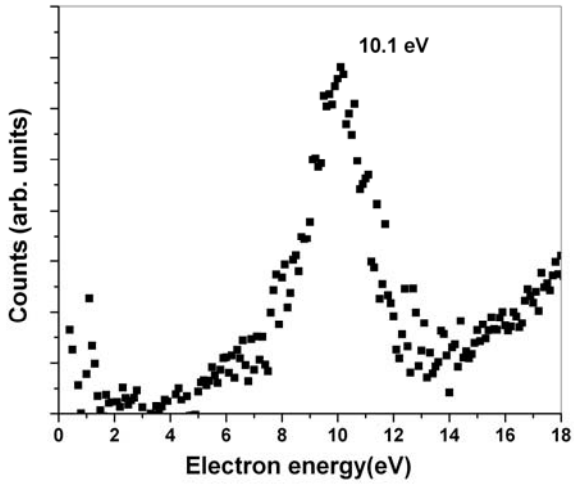

Figure 4.9: *Excitation function for O^- and OH^- from acetic acid.*

4.2.1 Functional group dependent *DEA*

The resonances obtained in the H^- channel from *DEA* to all three carboxylic acids show distinct similarity. Although the relative intensities of these resonances are different as well as the absolute cross sections are different, their positions on the electron energy scale seem to be similar. This indicates that there might exist a characteristic resonance pattern associated with these molecules in the H^- channel leading to *DEA*. Also from each of these molecules there are more than one resonances observed in the H^- channel whereas there are more than one nonequivalent sites present in each of these molecules that can contribute to the hydride ion signal. For example in the case of acetic acid there are two sites where hydrogen atom exists that are not equivalent namely methyl ($-CH_3$) and the hydroxyl part of the carboxyl group (-COOH). In order to understand the source of the hydride ions at various *DEA* resonances, we have carried out the free electron attachment experiment to partially deuterated acetic acid (CH_3COOD) and observed the resonances in the H^- and D^- channels.

The partially deuterated acetic acid is prepared by mixing the 99.9% pure acetic anhydride with 99% pure heavy water with equal molarity. The mixture is kept under magnetic stirring for one day in the sealed tube. Following reaction is expected to take place giving the partially deuterated acetic acid as the final product.

$$(CH_3CO)_2O + D_2O \longrightarrow 2CH_3COOD \qquad (4.1)$$

The purity of the final product is confirmed using the 1-D NMR signal from the sample.

The resulting ion yield curves of H^- and D^- are shown in Figure 4.10. The figure also shows the H^- ion yield curve from the undeuterated acetic acid for the comparison purpose. We note that H^- appears as a broad peak at an energy corresponding to the third peak seen from undeuterated acetic acid. Being a broad peak, its tail overlaps with second peak from the undeuterated acid, but the first peak is clearly absent. Whereas the D^- ion yield curve shows that the ions are produced predominantly at the first two resonances. The results from propionic acid also point out to the similar results. These results taken together clearly indicate that the methyl

group and the carboxyl group in these molecules retain their separate identity in the *DEA* process leading to H^- formation and that a given group behave in a similar way almost independent of the rest of the molecule.

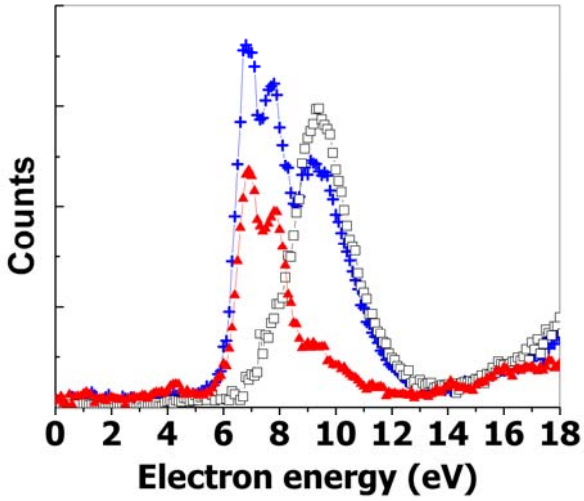

Figure 4.10: *H^- and D^- ion yield curves from CH_3COOH and CH_3COOD: (+) H^- from CH_3COOH, (▲) D^- from CH_3COOD, (□) H^- from CH_3COOD. The lines joining the points are for guiding the eye.*

That these results are the manifestation of a deeper and hence more general behavior can be concluded from a comparison of the existing data on several molecules and further measurements that we have carried out. To begin with the *DEA* behavior seen in a functional group should be seen in its parent molecule. For example, the resonance identified from the methyl group should correspond to a resonance in methane in the same electron energy range. We note that the *DEA* in CH_4 in the H^- channel is observed as a broad peak, similar to what is observed from the methyl group in the case of acetic acid centered at 9.2 eV [29]. There also appear to be further evidence that the methyl group property is retained in the *DEA* in acetic acid from the presence of a resonant peak in the CH_2^- channel at almost the same energy in both molecules (10.5 eV in acetic acid as compared to 10.3 eV in CH_4) [29]. We also note that H^- formation from H_2O by *DEA* shows similar resonant structure as seen from the carboxyl part of the acids. *DEA* with water gives rise to H^- formation at 6.5 eV and 8.6 eV respectively [30]. If the similarity between the carboxyl group and H_2O is indeed valid, a corresponding similarity should exist between alcohols, the carboxylic acids and H_2O.

We have carried out the *DEA* measurements to simple alcohols namely methanol (CH_3OH) and ethanol (C_2H_5OH) and looked for the H^- signal. In the case of methanol three distinct resonances are observed in the H^- channel as shown in Figure 4.11. These resonances are at 6.4, 7.9 and 10.2eV. We have also determined the absolute cross section for this channel from this molecule. The cross sections at the three channels are found to be 7.6 x 10^{-20} cm^2, 3.6 x 10^{-20} cm^2 and 4.3 x 10^{-20} cm^2. Only the O^- + OH^- are the other fragments observed with significant cross section.

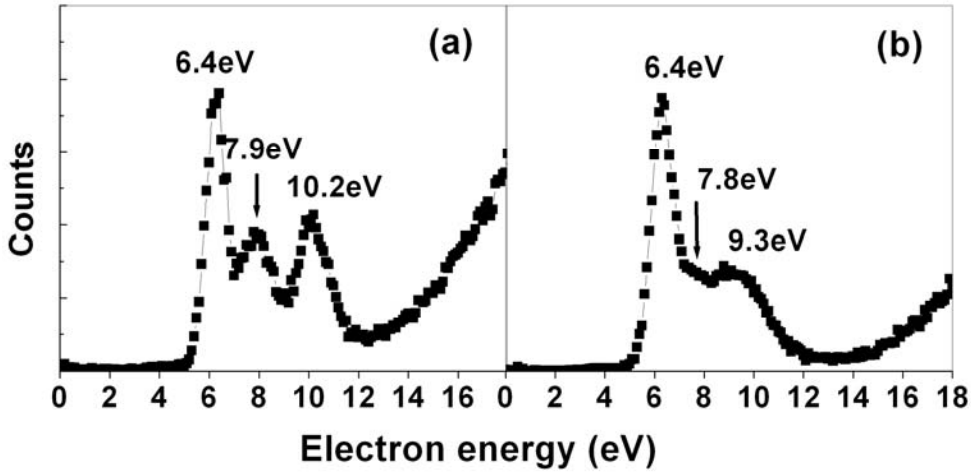

Figure 4.11: *Ion yield curves of H^- from (a) CH_3OH and (b) C_2H_5OH*

The measurements on CH_3OD reported earlier have shown that the H^- peak observed at 10.2 eV in the case of methanol originate from the C site, whereas the peaks at 6.4 eV and 7.9 eV originate from the O site [31]. In the case of ethanol a sharp resonance is observed at 6.4eV followed by an unresolved long pattern that has a shoulder at 9.3eV as seen from Figure 4.11. The absolute cross section at the 6.4eV resonance is found to be 7.5 x 10^{-20} cm^2. Here also only O^- + OH^- are the other fragments found to be present with noticeable cross section. These cross sections are tabulated in the Table 4.2. As can be seen from Table 4.2, the similarity does exist between alcohols, carboxylic acids and water as far as the first two resonances are concerned that are related to the OH part of these molecules.

The functional group dependence in the *DEA* process is further explored by studying *DEA* to n-propyl amine. Figure 4.12 gives the ion yield curve for H^- from n-propyl amine which shows a strong peak at 5.2 eV and a smaller but broader peak at 8.8 eV. The first peak can clearly be assigned to that due to the amine radical as *DEA*

to NH_3 is known to give a strong peak at 5.7 eV in the H^- channel [30]. The second peak at higher energy is expected to be a mixture of H^- from the amine group as well as the propyl part of the molecule. We have determined the absolute cross sections for the H^- channel from this molecule which are found to be 5.2 x 10^{-20} cm^2 at 5.2eV and 1.7 x 10^{-20} cm^2 at 8.8eV. The cross sections are given in Table 4.2.

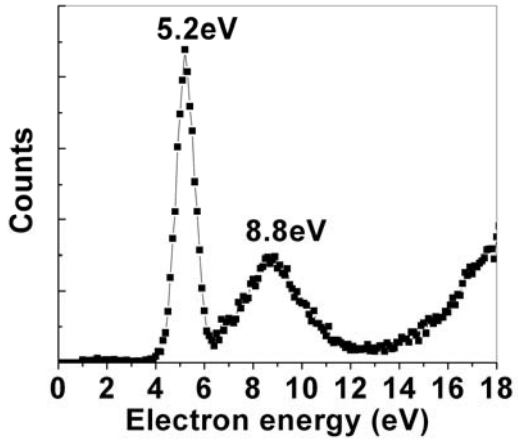

Figure 4.12: *Ion yield curve of H^- from n-propyl amine.*

Table 4.2: *Absolute cross sections for DEA for various fragments from alcohols and n-propylamine*

	Electron energy (eV)	***Cross section measured (10^{-20} cm^2)***
Methanol		
H^-	6.4	7.6 ± 1.0
	7.9	3.6 ± 0.5
	10.2	4.3 ± 0.6
$O^- + OH^-$	10.3	4.5 ± 0.6
Ethanol		
H^-	6.4	7.5 ± 1.0
	9.3	2.8 ± 0.4
$O^- + OH^-$	10.2	Negligible
n-propylamine		
H^-	5.2	5.2 ± 0.7
	8.8	1.7 ± 0.2
NH_2^- and other fragments	NEGLIGIBLE (not visible in noise)	

4.2.1.1 Our understanding of the functional group dependent *DEA*

The observed functional group dependent *DEA* can be explained qualitatively. The H^- formation in the cases we have discussed so far arises from the core-excited resonances. All these molecules show optical absorption spectra with the distinct bands present in the energy range that correspond to the above mentioned resonance positions observed in *DEA*. This implies that an electron from a specific orbital gets excited to a higher orbital along with the capture of the incoming electron. These excitations appear to occur depending on the functional groups in the molecules. This can be concluded from the striking similarity seen between their absorption spectra [32]. Now the mechanism for the functional group dependent *DEA* is led through the excitation of the electron to a fairly localized orbital from a specific valence orbital. Once this electron is excited, the corresponding atomic core will have less screening of the nuclear charge. Subsequently the incoming electron is likely be localized in the vicinity of this atom. This results in the localization of both the excess energy and the electronic charge. Since the *DEA* occurs in vibrational time scales, there will be relatively little energy redistribution. Due to the localization of energy, the fragmentation occurs at the site of core excitation and the excess charge is carried away by one of the fragments.

The above proposed mechanism seems to be playing role at least in the case of acetic acid. As can be seen from the recently reported absorption spectrum of this molecule along with the molecular orbital calculations, the absorption band present at 7.1eV has a valence nature. It is highly localized to the O-H part of the carboxyl group [33]. Hence we suggest that the resonance observed at 6.7eV is a valence excited Feshbach type resonance where the valance electron is excited to the antibonding orbital localized at the –OH site causing the H^- formation from this site in the molecule. In order to understand the dynamics of the process and nature of the negative ion resonance that plays role in the process, it is essential to measure the kinetic energy and the angular distribution of the H^- signal at various resonances from these molecules. We carried out these measurements for acetic acid and methanol and the details of these measurements are discussed in chapter 5.

It is also to be noted that in the recent results obtained on the *DEA* to bigger biologically important molecules like thymine, the resonances observed in the H^- channel are found to be consistent to the corresponding functional groups [34, 35]. For example in the case of thymine the H^- ions coming from the N-H site is found to be

at 5.5eV which is consistent with that observed from the NH_3 molecule. Similarly the H^- ions coming from the C-H sites are found to be consistent with the corresponding precursor molecules. This implies that the functional group dependent *DEA* is also observed in the bigger molecule indicating that the precursor molecules to these functional groups retain their characteristic resonances even in the bigger molecules. This highlights the importance of the discovery of the functional group dependence of *DEA* towards the understanding of the *DEA* process in the bigger molecules.

4.2.1.2 Site selective fragmentation of molecules by low energy electrons

From all these results, it is clear that in *DEA* to these simple organic molecules, the different sites on a molecule can be addressed by just tuning the electron energy as far as the bond breakage is concerned. That means depending on the functional group present, different bonds on the molecules containing the non-equivalent hydrogen atoms can be broken by just tuning the electron energy. We term this as the site specific fragmentation of molecules by functional group dependent *DEA*. More importantly this site selectivity that we have observed is different than the site selectivity in the *DEA* process reported so far which is threshold energy based [36]. In that case dissociation at a particular site contributes only when the attaching electron has sufficient energy to induce the *DEA* process at that site. As different sites within a given molecule have different thresholds for *DEA* process, they contribute in the *DEA* process at different energies giving the site selectivity. In the case of the results that we have obtained, the electron energies associated with the resonances in the H^- channel are much more than those required to break any on of the C-H or O-H bonds. That means at the energies where these resonances appear, the production of H^- ions from C-H and O-H sites are energetically possible. In spite of this the selectivity is observed in the bond breakage. Hence the site selective bond breaking is happening much beyond the threshold energies that correspond to various hydrogen containing sites within the molecule. Hence this site selectivity observed in *DEA* is way different than the one reported so far. This is for the first time that such a site selective fragmentation of molecules is observed beyond the threshold energies of different bonds.

The above results point towards the possible application of the low energy electron attachment process in controlling the chemical reactions.

Control of chemical reactions has been a long cherished dream towards which a variety of approaches have been made. The most prominent approach towards this has been the use of lasers. For molecular collisions, control has been achieved by mode selective excitation [37, 38], by stereodynamic control [39] or by control of orbital alignment [40]. In the case of unimolecular reactions, control has been achieved by quantum interference between different reaction pathways connecting the same initial and final states and by adjusting the temporal shape and spectral content of ultra-short chirped laser pulses [41, 42]. While these efforts target an ensemble of molecules, single molecule engineering using inelastic tunneling of electrons in scanning tunneling microscopes has been used to break individual bonds [43-45] and to induce as well as control molecular motion on the surface [46-50].

Soft X-rays have also been used in the context of controlling unimolecular reactions in polyatomic species. Excitation of the C *1s* electrons in acetone were found to affect the fragmentation pattern depending on whether the *1s* electron gets ionized or excited into a Rydberg-like orbital or into an antibonding π^* molecular orbital with the fragmentation occurring around the site of the carbon atom where the optical excitation took place [51]. Active control of chemical bond scission by site-specific core excitation using soft x-rays on thin films of organic polymers was also demonstrated recently [52].

All though all these efforts have provided the proof of principle involved in controlling chemical reactions, the advantage of the technique of low energy electron attachment, though passive in nature; have potential for applications on a larger scale due to its inherent simplicity.

References:

[1] B. Boudaiffa, P. Cloutier, D. Hunting, M. A. Huels, L. Sanche, *Science* **287,** 1658 (2000).

[2] Michael A. Huels, Ina Hahndorf, Eugen Illenberger and Leon Sanche, *J. Chem. Phys.* **108**, 1309 (1998).

[3] J. Ellder, P. Friberg, A. Hjalmarson, B. Hoeglund, W. M. Irvine, L. E. B. Johansson, H. Olofsson, G. Rydbeck, O. E. H. Rydbeck, *Astrophys. J.* **242,** L93 (1980).

[4] W. M. Irvine, P. Friberg, N. Kaifu, Y. Kitamura, K. Kawaguchi, *Astrophys. J.* **342,** 871 (1989).

[5] D. Bockelee-Morvan, D. C. Lis, J. E. Wink, D. Despois, J. Crovisier, R. Bachiller, D. J. Benford, N. Biver, P. Colom, J. K. Davies, E. Gerard, B. Germain, M. Houde, D. Mehringer, R. Moreno, G. Paubert, T. G. Phillips, H. Rauer, *Astron. Astrophys.* **353,** 1101 (2000).

[6] S.-Y. Liu, J. M. Girart, A. Ramijan, L. E. Synder, *Astrophys. J.* **576,** 255 (2002).

[7] S.-Y. Liu, D. M. Mehringer, L. E. Snyder, *Astrophys. J.* **552,** 654 (2001).

[8] J. M. Hollis, J. A. Pedelty, L. E. Synder, P. R. Jewell, F. J. Lovas, P. Palmer, S.-Y. Liu, *Astrophys. J.* **588,** 353 (2003).

[9] G. Winnewisser, E. Churchwell, *Astrophys. J. Lett.* **200,** L33 (1975).

[10] S. Cazaux, A. G. G. M. Tielens, C. Ceccarelli, A. Castets, V. Wakelam, E. Caux, B. Parise, D. Teyssier, *Astrophys. J. Lett.* **593,** L51 (2003).

[11] G. A. Kumar, Y. Pan, C. J. Smallwood, M. A. McAllister, *J. Comp. Chem.* **19,** 1345 (1998).

[12] N. Narkis, and S. Henfrld-Furie, *Water Res.* **12,** 437 (1978).

[13] G. Manni and F. Caron, *J Chromatogr A* **690**, 237 (1995).

[14] O. Klemm, R. W. Talbot, D. R> Fitzarald, K. L. Klemm and B. L. Lefer, *J. Geophys. Res.* **99**, 1687 (1994).

[15] K. Kawamura, L. Ng and I. R. Environ, *Sci. Technol.* **19**, 9335 (1985).

[16] J. Viidanoja, T. Reiner and F. Arnold, *Int. J. Mass Spectrom.* **181**, 31 (1998).

[17] A. Pelc, W. Sailer, P. Scheier, M. Probst, N. J. Mason, E. Illenberger, T. D. Märk, *Chem. Phys. Lett.* **361,** 277 (2002).

[18] A. Pelc, W. Sailer, P. Scheier, N. J. Mason, E. Illenberger, T. D. Märk, *Vacuum* **70,** 429 (2003).

[19] Wolfgang Sailer, Andrzej Pelc, Micheal Probst, Jumras Limtrakul, Paul Scheier, Eugen Illenberger and Tilmann D. Mark, *Chem. Phys. Lett.* **378**, 250 (2003).

[20] Andrzej Pelc, Wolfgang Sailer, Paul Scheier, Tilmann D. Mark and Eugen Illenberger, *Chem. Phys. Lett.* **392**, 465 (2004).

[21] H. Abdoul-Carime, P. Cloutier, and L. Sanche, *Radiat. Res.* **155,** 625 (2001).

[22] Hassan Abdoul-Carime and Eugen Illenberger, *Chem. Phys. Lett.* **390,** 481 (2004).

[23] E. Krishnakumar and S. K. Srivastava, *Phys. Rev. A*, **41,** 2445 (1990).

[24] Isabel Martin, Tomas Skalicky, Judith Langer, Hassan Abdoul-Carime, Grzegorz Karwasz, Eugen Illenberger, Michal Stano and Stefan Matejcik, *Phys. Chem. Chem. Phys.* **7**, 2212 (2005).

[25] R. Dressler, and M. Allan, *Chem. Phys.* **92,** 449 (1995).

[26] M. Tronc, M. Allan and F. Edard, In *Electronic and Atomic Collisions* (ed. J. Geddes, H. B. Gilbody, A. E. Kingston, C. J. Latimer, and H. R. J. Walters) (North-Holland), (1987).

[27] K. Aflatooni, B. Hitt, G. A. Gallup, and P. D. Burrow, *J. Chem. Phys.* **115,** 6489 (2001).

[28] T. N. Rescigno, C. S. Trevisan and A. E. Orel, *Phys. Rev. Lett.* **96**, 213201 (2006).

[29] T. E. Sharp and J. T. Dowell, *J. Chem. Phys.* **46,** 1530 (1967).

[30] L. G. Christophorou, Ed., *Electron-molecule Interactions and Their Applications - Vol I* (Academic Press, Orlando, Florida 1984).

[31] M. G. Curtis and I. C. Walker, J. Chem. Soc. Faraday Trans. **88,** 2805 (1992).

[32] M. B. Robin, *Higher excited states of polyatomic molecules*, *Vol. I and II* (Academic Press, New York 1975).

[33] Sydney Leach, Martin Schwell, Sun Un, Hans-Werner Jochims and Helmut Baumgartel, *Chem. Phys.* **321**, 159 (2006).

[34] Sylwia Ptasinska, Stephan Denifl, Verena Grill, Tilmann D. Mark, Paul Scheier, Sascha Gohlke, Michael A. Huels and Eugen Illenberger, *Angue. Chem. Int. Ed.* **44**, 1647 (2005).

[35] Sylwia Ptasinska, Stephan Denifl, Verena Grill, Tilmann D. Mark, Eugen Illenberger and Paul Scheier, *Phys. Rev. Lett.* **95**, 093201 (2005).

[36] Hassan Abdoul-Carime, Sascha Gohlke and Eugen Illenberger, *Phys. Rev. Lett.*, **92**, 168103 (2004)

[37] A. Sinha, M. C. Hsia, and F. F. Crim, *J. Chem. Phys.* **94**, 4928 (1991).

[38] M. J. Bronikowski, W. R. Simpson, B. Girard, and R. N. Zare, *J. Chem. Phys.* **94**, 8647 (1991).

[39] Special issue on Stereodynamics of Chemical Reactions, *J. Phys. Chem.* **101**, (No. 41) (1997).

[40] E. D. Potter, J. L. Herek, S. Pedersen, Q. Liu, A. H. Zewail, *Nature* **355,** 66 (1992).

[41] H. Rabitz, R. de Vivie-Riedle, M. Motzkus, and K. Kompa, *Science* **288**, 824 (2000).

[42] H. L. Dai, W. Ho, Ed., *Laser Spectroscopy and Photochemistry on Metal Surfaces* (World Scientific, Singapore, 1995).

[43] R. de Vivie-Riedle, L. Kurtz, and A. Hofman, *Pure Appl. Chem.* **73**, 525 (2001).

[44] B. C. Stipe, M. A. Rezaei, W. Ho, S. Gao, M. Persson and B. I. Lundqvist, *Phys. Rev.Lett.* **78,** 4410 (1997).

[45] S. W. Hla, L. Bartels, G. Meyer, and K. H. Rieder, *Phys. Rev. Lett.* **85**, 2777 (2000).

[46] Y. Kim, T. Komeda, and M. Kawai, *Phys. Rev. Lett.* **89**, 126104 (2002).

[47] D. M. Eigler, C. P. Lutz, and W. E. Rudge, *Nature* **352**, 600 (1991).

[48] B. C. Stipe, M. A. Rezaei, and W. Ho, *Phys. Rev. Lett.* **81**, 1263 (1998).

[49] T. Komeda, Y. Kim, M. Kawai, B. N. J. Persson, H. Ueba, *Science* **295,** 2055 (2002).

[50] J. I. Pascual, N. Lorente, Z. Song, H. Conrad, and H. –P. Rust, *Nature* **423,** 525 (2003).

[51] W. Eberhardt, T. K. Sham, R. Carr, S. Krummacher, M. Strongin, S. L. Weng and D. Wesner, *Phys. Rev. Lett.*, **50**, 1038 (1983)

[52] Shini-ichi Wada, Ryohei Sumii, Kouji Isari, Satoshi Waki, Erika O. Sako, Tetsuhiro Sekiguchi, Tetsuji Sekitani and Kenichiro Tanaka, *Surface Science* **528**, 242 (2003)

Chapter 5

Probing site selective fragmentation of molecules using *VMI*

The functional group dependent site selective fragmentation of molecules described in the previous chapter is a significant finding in electron induced processes. As discussed in the previous chapter, this may have a potential application in control of chemical reactions. In order to realize the potential of this possible application it is essential to know the properties of the remaining neutral fragment that is generated in the *DEA* process with the departure of the hydride ion. One important question in this respect is how the excess energy is distributed between the kinetic energy and internal energy of the fragments. Since the electron energy is known, by measuring the kinetic energy of the hydride ion it is possible to determine the internal energy of the neutral fragment. The kinetic energy and angular distribution of the hydride ion will also tell us if the dissociation is going through a two-body break up or three-body break up. Further information on the dynamics of the negative ion state like its possible structural changes, including rearrangement, if any, before it fragments may be obtained through kinetic energy measurements using partially deuterated molecules. As discussed in the first chapter, the angular distribution of the ions provides information on the symmetry of the negative ion state and the partial waves that are contributing to the capture process. Since the resonances observed through the *DEA* process are generally not very narrow, it is possible to have more than one overlapping resonances contribute at the same electron energy. In such cases, both the kinetic energy and angular distribution data may indicate whether there are more than one negative ion resonances that are participating in the *DEA* process. The dissociation limits of these states can also be estimated from the kinetic energies and angular distribution of the ions. Thus kinetic energy and angular distribution data provide information on the structure and dynamics of the negative ion resonant state. We have carried out measurements on the kinetic energies and angular distribution of negative ions formed from some of the partially deuterated organic molecules for a

better understanding of the dynamics that leads to the site specific fragmentation discussed in the previous chapter.

As discussed in chapter 2, we have adapted the velocity map imaging (*VMI*) technique to study the *DEA* process. We have tried to address most of the above mentioned questions by measuring the kinetic energy and angular distribution of the hydride ions. It was found that other ions formed at the electron energies where hydride ions appear had very small kinetic energies. Hence we do not address them.

5.1 Determination of kinetic energies and angular distribution of the hydride ions from acetic acid and methanol

In order to distinguish between the Hydride ions corresponding to different sites we have carried out the *VMI* measurements on partially deuterated samples of acetic acid (CH_3COOD) and methanol (CH_3OD). We have obtained the *VMI* of H^- and D^- ions from these molecules at different resonances.

5.1.1 Calibrating the kinetic energy scale in *VMI*

The kinetic energy scale of the *VMI* is calibrated using the images of the O^- signal from *DEA* to O_2 obtained at various electron energies. The energy threshold for the formation of the O^- from O_2 is determined to be 3.7 eV using the electron affinity of O atom (1.46 eV) [1] and the bond dissociation energy of the O_2 molecule (5.17 eV) [2]. As both the fragments are atomic fragments and the ion yield curve starts right at the threshold, it is understood that both the fragments are in their ground state. This implies that the excess energy in the system is going to get equally divided among both the identical fragments as their kinetic energy. From the known kinetic energy of O^- ions as a function of the electron energy, the radius of the velocity map image could be calibrated for the ion kinetic energy. As the size of the velocity map image on the detector is independent of the mass of the ion that is imaged and depends only on the initial kinetic energy of the ions, the scale calibrated for the O^- ion cloud can be used for the hydride ions for the same voltage conditions.

5.1.2 *VMI* of Hydride ion from acetic acid and methanol at the first resonance

5.1.2.1 Acetic acid (CH_3COOD)

The acetic acid shows three resonances in the hydride ion channel at electron energies 6.7, 7.7 and 9.1 eV as described in the previous chapter. The *VMI* taken for the first resonance i.e. at 6.7 eV is shown in Figure 5.1. It is obtained for the D^- signal as that is the only ion present at this energy. The angular distribution of the hydride (D^-) ions is determined by integrating the ion counts over the range of the radii of the *VMI* at given electron energy as well as within a small angular range of ± 5° around the given angle of ejection with respect to the electron beam.

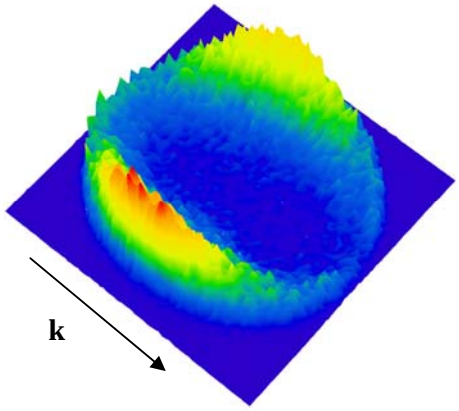

Figure 5.1: *Velocity Map Image of D^- from CH_3COOD at first resonance (6.7eV)*

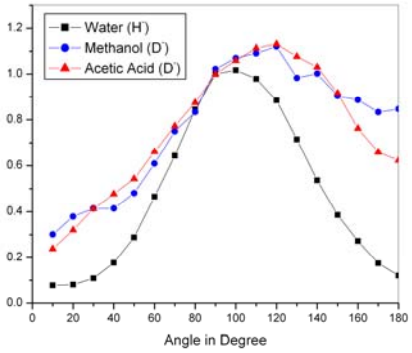

Figure 5.2: *Angular distribution of D^- from acetic acid (CH_3COOD), methanol (CH_3OD) and H^- from water at first resonance.*

The polar plot so obtained is given in Figure 5.2. As can be seen from the figure, the differential cross section peaks at around 100°. Knowing the ground state

symmetry of the molecules the symmetry of the negative ion state that contributes to the *DEA* process can be determined. The acetic acid molecule belongs to C_s symmetry group. The ground state of acetic acid is $1^1A'$. From the angular distribution that peaks at 100° i.e. close to 90°, the information about the negative ion state can be retrieved.

Using the selection rules for the electron capture process in the polyatomic molecule of C_s symmetry it can be shown that the angular distribution that is observed for the first resonance corresponds to the $A' \rightarrow A'$ type of transition [3]. The recent experimental and theoretical studies on the excited states of acetic acid show a valence transition in its absorption spectrum around 7 eV that corresponds to the excitation of valence electron to the 14a′ orbital [4]. This orbital is known to be highly localized on the O-H bond in the molecule. This explains the site selective fragmentation that occurs at the O-H site in the acetic acid molecule at this energy. It is also clear that the molecular orbital that is responsible for this result has exclusive contribution from the atomic orbitals that are contributed by the O atom and the corresponding H atom. This implies that the resonance is a characteristic one to the hydroxyl group. This explains the functional group dependent nature of the site selectivity.

The kinetic energy of the D^- ion at different electron energies around the first resonance is determined from the radii of the angular distribution obtained in *VMI*s. The appearance energy (threshold) for getting hydride ion from the O-H part of the acetic acid molecule through *DEA* can be estimated from the bond dissociation energy of $D(CH_3COO\text{-}H)$ = 4.77 eV [5, 6] and the electron affinity for H which is 0.75 eV [7]. The appearance energy for H^- is calculated to be 4.02 eV. The threshold associated with the formation of D^- ion from CH_3COOD can be assumed to be the same as that for H^- from the O-H part in the CH_3COOH molecule. The kinetic energy distribution of D^- ions at three electron energies around the first resonance is given in Fig. 5.3. The kinetic energy distributions at the resonance peak of 6.7 eV and the two lower energies appear to be almost identical. It is seen that the kinetic energy varies from 0 to 2.9 eV with maximum at around 1.2 eV. It may be noted that the energy distribution will have the electron energy spread convoluted into it. This will manifest in the high energy tail of the distribution.

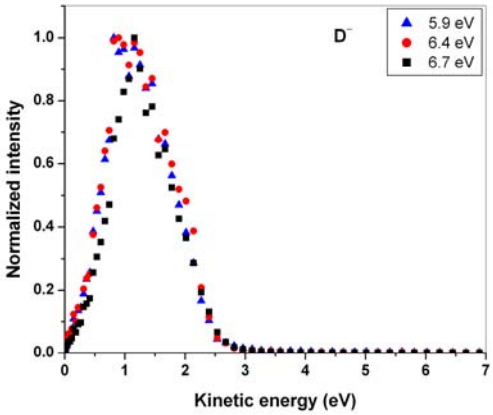

Figure 5.3: *Kinetic energy distribution of D^- from acetic acid (CH_3COOD) for electron energies about the first resonance.*

Thus the high energy tail in the distributions cannot be taken too seriously. The half-width (full width at half maximum) of the kinetic energy distribution is measured as 1.1 eV. This is higher than the energy resolution of the electron beam (0.5 eV) and appears to result from the dissociation process itself. For the most probable kinetic energy distribution of 1.2 eV as seen from the figure, and the known threshold for D^- formation, which is 4 eV, approximately 1.5 eV seems to have been left as internal excitation of the neutral fragment for the electron energy of 6.7 eV. This can be in the form of vibrational or electronic excitation of that fragment. The possibility of the three body break-up is ruled out as the excess energy is relatively small. Moreover, a three-body fragmentation is expected to give isotropic angular distribution which is not the case here.

5.1.2.2 Methanol (CH_3OD)

The methanol shows three resonances in the hydride ion channel at electron energies 6.4, 7.9 and 10.2 eV as described in the previous chapter. The *VMI* taken for the first resonance i.e. at 6.4 eV is shown in Figure 5.4. It is obtained for the D^- signal as that is the only ion present at this energy. The angular distribution of the hydride (D^-) ions is determined by the similar method that is used for acetic acid. The polar plot so obtained is given in Figure 5.2. As can be seen from the figure, the differential cross section peaks at around 115°. Knowing the ground state symmetry of the molecules the symmetry of the negative ion state that contributes to the *DEA* process can be determined.

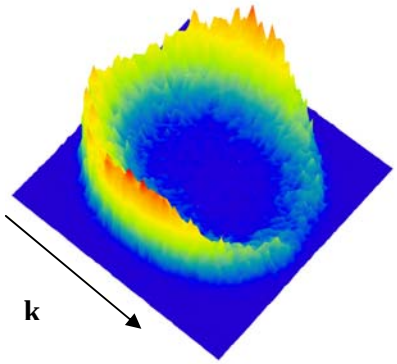

Figure 5.4: *Velocity Map Image of D^- from CH_3OD at first resonance (6.4eV)*

Methanol also belongs to C_s symmetry group. Its ground state is $^1A'$. The angular distribution of the hydride (D^-) ion shows some level of anisotropy that peaks close to 90°. From the angular distribution it is clear that the negative ion resonance state that participates in the *DEA* process is of A′ symmetry. No quantum chemical calculations are available for excited electronic states of methanol. Based on the functional group dependence that we have identified, we expect excitation of an a' state similar to the case of acetic acid.

The kinetic energy distribution of D^- ions from CH_3OD is given in Fig. 5.5. The energies are found to be in the range 0 to 2.4 eV. The distribution is found to be narrower than the one from acetic acid. At the resonance the kinetic energy distribution is found to be peaking at about 1.2 eV. The energy threshold for getting the D^- ion from the O-D site in methanol can be determined using the electron affinity of D atom (0.75 eV) and the bond dissociation energy for (CH_3O-H) (4.5 eV). The bond dissociation energy of the CH_3O-H bond is found from the thermochemical data available. The enthalpy of formation of CH_3O radical (ΔH_f (CH_3O) = 17 kJ/mol) [8], the enthalpy of formation of H atom (ΔH_f (H) = 218 kJ/mol) [9] and the enthalpy of formation of CH_3OH molecule (ΔH_f (CH_3OH) = -201 kJ/mol) [10] gives the corresponding bond dissociation energy to be 436 kJ/mol giving the value of threshold energy for H^- from CH_3O-H through *DEA* to be 3.75 eV. The threshold for D^- from CH_3O-D is expected to be very much close to that value.

From the energy threshold for this channel and the electron energy as well as the most probable value of the kinetic energy it is clear that about 1.4 eV energy has gone into the internal excitation of the remaining neutral fragment. This can appear as the vibrational or electronic excitation of that fragment. The anisotropy observed in

the angular distribution of the D^- ions rules out the three body break-up of the system in the *DEA* process.

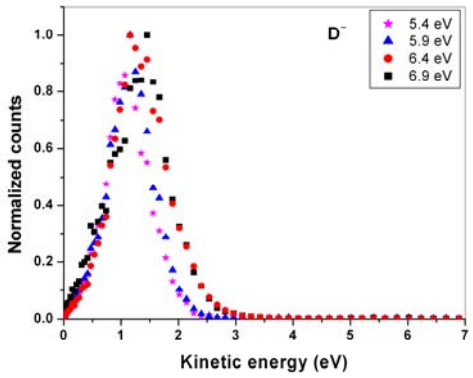

Figure 5.5: *Kinetic energy distribution of D^- from methanol (CH_3OD) for electron energies about the first resonance.*

5.1.2.3 Comparison of D^- ion angular distribution with that from water at 6.5 eV resonance

It is interesting to note that there exists a distinct similarity in the angular distribution pattern and *VMI* image of the hydride ions from acetic acid as well as from methanol at the first resonance and that from water at the resonance situated at 6.5 eV as can be seen from Figure 5.6. Assuming that the *DEA* process is localized to the bond that has broken and the molecule do not undergo substantial rotation in the dissociation timescale (which is of the order of vibrational time scale), the anisotropy in the angular distribution in a specific ion yield points out to the preference to a specific orientation of the bond that is broken in the *DEA* process towards electron capture.

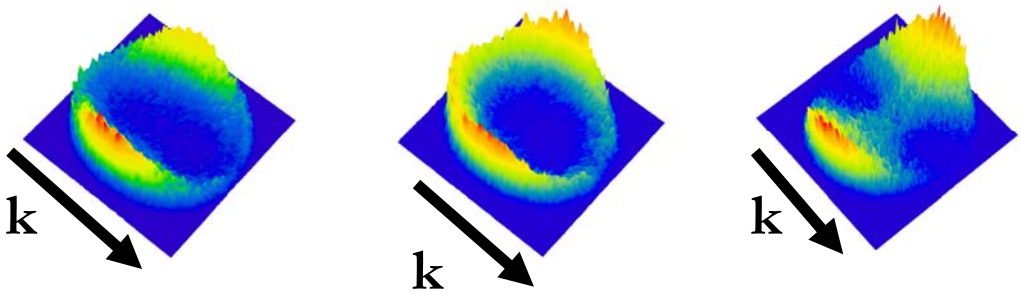

Figure 5.6: *Comparison of VMI of hydride ions at first resonance from (a)Acetic acid (b) methanol and (c) water.*

Since all the three molecules show the hydride ion formation from the O-H bond breakage, the similarity observed in the angular distribution points out to a new feature that has not been observed till now in the *DEA* process. We call it as the 'bond orientation specific *DEA*'. Here it is clear that no matter what the rest of the molecule is (i.e. independent of the overall symmetry of the molecule), it is only the orientation of the O-H bond with respect to the incoming electron beam that determines the electron capture at this energy. This seems to be the result of the site specificity of the electron attachment process which makes rest of the molecule inconsequential.

Based on this it appears that the functional group dependence of the DEA process that we observed is limited not just to the energies, it even manifests to the extent of local symmetries. Based on this, it may be possible to generalize this observation to all molecules containing O-H group that the orientation of the O-H bond with respect to the incoming electron determines its capture, irrespective of the overall size, structure and symmetry of the molecule.

5.1.3 *VMI* of Hydride ion from acetic acid and methanol at the second resonance

At this resonance the predominant contribution to the hydride ions is found to be from the O site as compared to C site (dominant D^- signal over H^- signal). The VMI of D^- ions from CH_3COOD and CH_3OD at electron energies of 7.7 eV and 7.9 eV respectively corresponding to the peaks of the second resonance is shown in Fig. 5.7.

As can be seen from the VMI, the angular distributions are distinctly different from the first resonance for both the molecules. For acetic acid, the angular distributions appear to show a maximum intensity at 120^o. For methanol the peak intensity is at 140^o. However, most noticeable is the strong forward – backward asymmetry and a clear 'hole' in the 0^o direction. Due to lack of any information on the neutral excited states and theoretical calculations, we are unable to characterize the resonances based on the angular distribution. The 'hole' in the forward direction appears to be a manifestation of the site specificity of the electron capture process and will be discussed later. We also note that angular distribution at this resonance is distinctly different from what is observed for H^- from water. Thus at this resonance,

the orientation specificity seen in the attachment process at the first resonance appear to be absent.

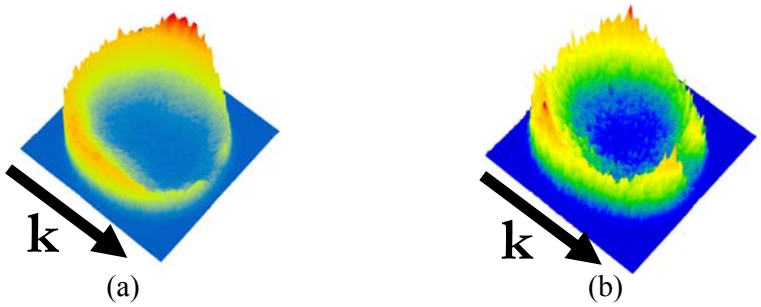

Figure 5.7: *VMI of D^- from (a) CH_3COOD and (b) from CH_3OD at the second resonance.*

The kinetic energy distribution for the D^- signal from CH_3COOD is shown in Figure 5.8. It is clear that the D^- ion energy is in the range 0 to 3 eV. The peak of the distribution appears to shift towards higher energy as the electron energy is increased within the resonance. At 7.7 eV the peak in the kinetic energy distribution is at 2 eV. Since the appearance energy for D^- is 4 eV, this corresponds to an internal energy of 1.7 eV in the neutral fragment. A comparison of this with that of the first resonance shows that the most probable internal energy of the neutral fragment is almost the same (1.5 eV vs 1.7eV) at both the resonances. This indicates that both the resonant states may have the same dissociation limits as far as the O-D bond breakage is concerned.

The kinetic energy distribution of D^- from CH_3OD at different electron energies across the second resonance is shown in Fig. 5.9. It is found that the energy distribution extends up to about 3.5 eV and peaks at about 1.5 eV. Since the appearance energy is 3.75 eV, we may conclude that on average there is about 2.7 eV of energy going into the internal excitation of the remaining neutral fragment. This is considerably higher than the corresponding partitioning of energy into the neutral fragment at the first resonance, which is about 1.4 eV. It is not clear how the 2.7 eV is being distributed into internal modes of the neutral fragment. However, the possibility exists that the second resonance in methanol could have a different dissociation limit as compared to that of the first resonance.

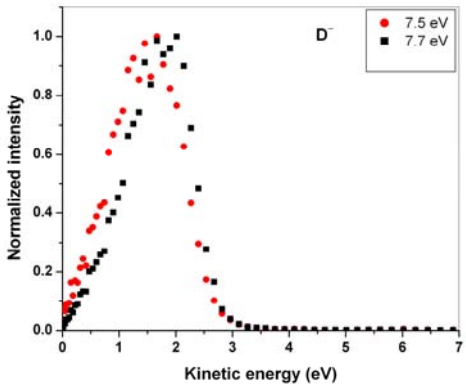

Figure 5.8: *Kinetic energy distribution of D^- from acetic acid (CH_3COOD) for electron energies about the second resonance.*

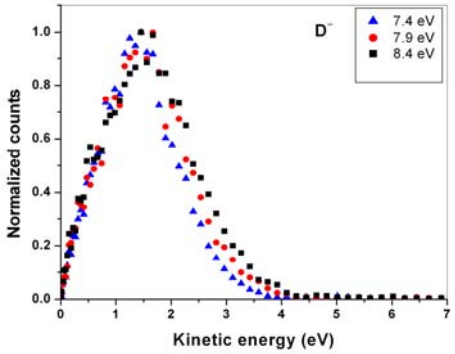

Figure 5.9: *Kinetic energy distribution of D^- from methanol (CH_3OD) for electron energies about the second resonance.*

5.1.4 *VMI* of Hydride ion from acetic acid and methanol at the third resonance

5.1.4.1 Acetic acid (CH_3COOD)

The third resonance present at 9.1 eV shows a predominant H^- signal along with a very weak D^- signal. The *VMIs* of both H^- and D^- signals at 9.1 eV resonance are shown in Figure 5.10. The angular distribution for the D^- signal clearly shows anisotropy with cross section peaking at 90˚. Using selection rules, it can be shown that the negative ion state, which is responsible for this process, is of A´ symmetry. The *VMI* of H^- shows a dominant central structure surrounded by a pattern similar to that of D^- seen at the same energy. We identify this as due to small amount of impurity CH_3COOH present in the sample.

(a) (b)

Figure 5.10: *VMI of (a) D^- and (b) H^- from acetic acid at third resonance.*

The kinetic energy distributions of the D^- and H^- ions at different electron energies across the third resonance are shown in Fig. 5.11. For D^- the energy seems to range from 0 to 4.5 eV peaking at 1.9 eV. This indicates that the remaining neutral fragment carries considerable amount of energy as its internal excitation (about 3.2 eV). From the considerable anisotropy seen in the angular distribution, one may conclude that the dissociation is still a two-body process, though considerable kinetic energy is left in the neutral fragment. Based on the energy partitioning it is safe to conclude that the resonance that leads to this *DEA* channel has a different dissociation limit than that for the first two resonances.

In the case of H^- ions the kinetic energy distribution has fairly large intensity at zero eV and extends up to 4 eV. As noted above in this case there is a contribution due to H^- formed from the O-H part of the CH_3COOH present in the sample. This will be identical to the D^- kinetic energy distribution. Thus the peak at 2 eV that is extending unto 4 eV is not from the C-H part of the molecule and hence may be ignored. The main peak at 1 eV is due to the H^- from the C-H part of the molecule.

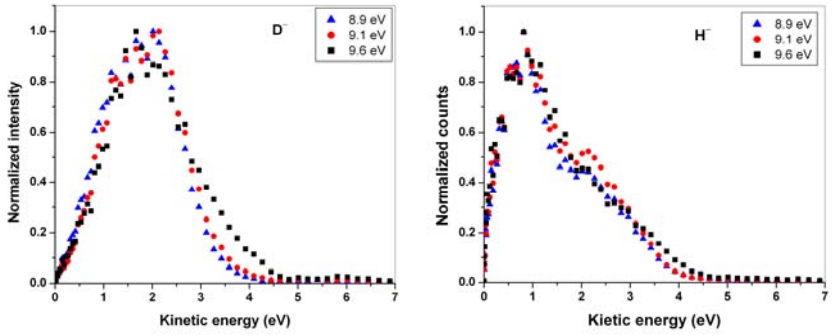

Figure 5.11: *Kinetic energy distributions of D^- and H^- from CH_3COOD at the third resonance.*

In order to determine the energy partitioning into the neutral fragment, it is required to know the appearance energy of H^- from acetic acid. We calculate it as follows. The appearance energy (threshold) for getting the hydride ion from the carbon site (C-H part of the molecule) for formic acid can be estimated from the available thermochemical data. The enthalpy of formation of $COOH^+$ i.e. ΔH_f ($COOH^+$) = 597 ± 8 KJ/mol [1] and the ionization energy of COOH is 791 kJ/mol [11]. Hence ΔH_f (COOH) becomes −194 kJ/mol. Knowing the ΔH_f (H) = 218 kJ/mol [9], ΔH_f(HCOOH) = −378.6 KJ/mol and electron affinity of H (EA (H) = 0.75 eV) [7] the appearance energy for H^- is found to be 3.43 eV. As the acetic acid is not much different from the formic acid structurally except with the hydrogen atom at the carbonyl part is replaced by a methyl group, the threshold energy for the formation of H^- from CH_3COOD can be approximated to be close to 3.43 eV (The threshold for obtaining H^- from CH_4 through *DEA* is estimated to be 3.78 eV).

Based on the appearance energy of 3.4 eV and the most probable kinetic energy of H^- measured as 1 eV, the energy deposited in the neutral fragment is 4.7 eV. This energy should be sufficient to cause further dissociation. Thus the low kinetic energy and relatively isotropic angular distribution observed in the H^- channel show the possibility of a three-body break up at this resonance.

5.1.4.2 Methanol (CH_3OD)

The third resonance situated at 10 eV for methanol (CH_3OD) shows the presence of both the ions namely H^- and D^-. The *VMI* for both the ions at this resonance is shown in Figure 5.12 and the corresponding kinetic energy distributions are given in Figure 5.13. The D^- shows highly anisotropic angular distribution with a forward backward asymmetry while that for the H^- is highly isotropic. The kinetic energy distribution is found to be within the range of 0 to 2 eV in the case of D^- ions. This distribution is found to be peaking at 0.8 eV with a narrow width. As the appearance energy for the D^- ions from the O-D site is about 3.75 eV, it is clear that the energy gone into the internal excitation of the remaining neutral fragment is about 5.5 eV which is indicative of its electronic excitation. Also anisotropy present in the angular distribution indicates the two body break-up, at least in the time scale of the D^- ejection. The large internal energy left in the neutral state indicates that the

negative ion resonance state involved in the D^- formation process has different dissociation limit as compared to the previously discussed resonance states.

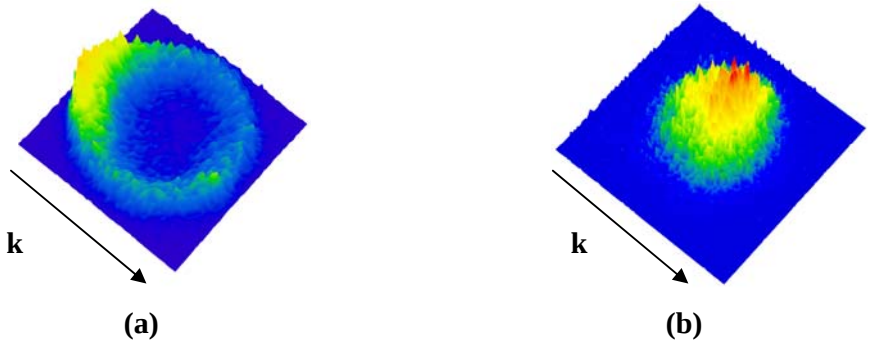

Figure 5.12: *VMI of (a) D^- and (b) H^- from methanol at third resonance*

The threshold energy for the H^- formation on electron attachment to CH_3OD is 3.5 eV (ΔH_f (CH_2OH) = -9 kJ/mol [8], ΔH_f (CH_3OH) = -201 kJ/mol [10], ΔH_f (H) = 218 kJ/mol [9] and E.A. (H) = 0.75eV [7]). In the case of H^- ions the kinetic energy distribution is found to be in the range of 0 to 3 eV peaking at 0.5 eV. Thus the excess energy remaining in the neutral fragment in this case is about 6 eV, which is quite large. The kinetic energy distribution peaking close to zero energy and the isotropic angular distribution indicate that the H^- formation is taking place at least through a three-body break up. We also note that there is relatively long tail in the kinetic energy distribution of H^- extending up to 6 eV, with a small peak at about 4 eV. This is not clearly visible in the VMI data, but nevertheless exists. Due to relatively weak intensity we are not able to obtain its angular distribution. A peak at 4 eV indicates a separate dissociation channel for the resonance.

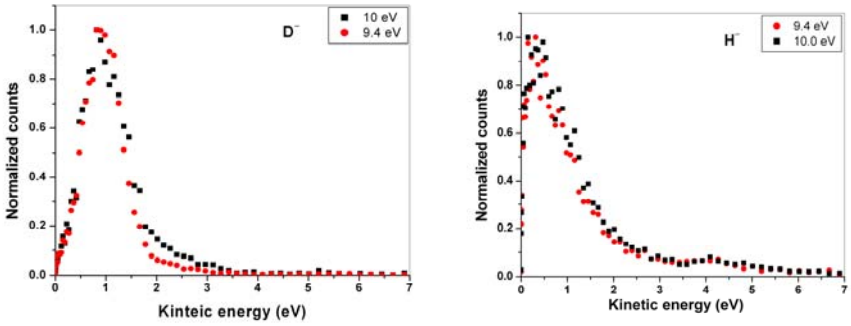

Figure 5.13: *Kinetic energy distributions of D^- and H^- from CH_3OD at the third resonance.*

It is clear from the *VMI* obtained for both H^- and D^- ions from CH_3COOD and CH_3OD molecules at different resonances that negative ion resonance states that are involved are with different symmetries as well as different dissociation limits. As can be seen from the absorption spectra of these molecules [4, 12] there are many neutral electronic transitions that exist in the relevant energy range. This points out that the resonances that are involved in the *DEA* process are valence excited resonances. The absorption spectra of these molecules are very rich in this energy range with lots of valence and Rydberg transitions overlapping with each other. Hence it is difficult to assign a particular neutral excited state as the parent state for the negative ion state that plays role in the *DEA* process at given electron energy.

On closer look at all the angular distributions in the *VMI*s for the D^- channels that correspond to the O-D bond breakage, one can notice a considerable loss of intensity around 0^0. This is very clearly evident in the second resonance for both acetic acid and methanol. This feature is something like a 'hole' in the Newton sphere in the forward direction with respect to the electron momentum vector. We can confirm that this is not an artifact as in the case of other molecules like water no such feature is observed. Also no such drop in the ion intensity is observed in the backward direction.

We know that at these resonances the dynamics that leads to this channel is associated with the electron capture at the O-D site. Also the anisotropy seen in the angular distributions of D^- is indicative of the two body kind of break-up of the parent negative ion. Hence the direction of the ejection of the D^- ion indicates the orientation of the O-D bond with respect to the electron beam direction. As a result, the D^- ions ejected in the forward direction correspond to the events in which the electrons are approaching the O-site in the molecule from the side opposite to that of O-D bond. Thus the lack of ion intensity in the forward direction in a small angular range may be indicating that for a small range of the orientation of the O-D bond with respect to the electron beam the electrons may not be able to interact with the O-site due to the presence of the remaining molecule in their way. That means the presence of this small 'hole' is indicative of a 'shadow' of the remaining molecule that is preventing the electron beam from approaching the O-site from particular angle. It is interesting to note that such shadow effect is not observed in the case of water as the O atom can be approached from the opposite side for all the orientations.

Reference:

[1] NIST chemistry webbook : http://webbook.nist.gov/chemistry

[2] S. V. Khristenko, A. I. Maslov and V. P. Shevelko, *Molecules and their spectroscopic properties*, (Springer-Verlag, Berlin, 1098).

[3] R. Azria, Y. Le Coat, G. Leferve, and D. Simon, *J. Phys. B: Atom. Molec. Phys.*, **12**, 679 (1979).

[4] Sydney Leach, Martin Schwell, Sun Un, Hans-Werner Jochims and Helmut Baumgartel, *Chem. Phys.* **321**, 159 (2006).

[5] D. Yu, A. Rauk and D. A. Armstrong, *J. Chem. Soc. Perkin Trans.* **2**, 2207 (1994).

[6] R. Yamdagni and P. Kebarle, *J. Am. Chem. Soc.* **95**, 4050 (1973).

[7] K. R. Lykke, K. K. Murray, W. C. Lineberger, Phys. Rev. A **43,** 6104 (1991).

[8] J. A. Martino Simoes, A. Greenberg and J. F. Liebmann Eds. *Energetics of organic free radicals* (Blackie Academic and Professional, London 1996).

[9] M. W. Chase Jr., *NISTJANAF Thermochemical Tables, Fourth Edition,* J. Phys. Chem. Ref. Data, Monograph **9,** 1(1998).

[10] J. Hine and K. Arata, *Bull. Chem. Soc. Jpn.* **49**, 3089 (1976).

[11] B. Ruscic, M. Schwartz, and J. Berkowitz, *J. Chem. Phys.* **91,** 6780 (1989).

[12] M. B. Robin, *Higher excited states of polyatomic molecules*, *Vol. I and II* (Academic Press, New York 1975).

Chapter 6

Electron attachment to C_{60}

One of the mechanisms that are considered to play a part in the electron attachment to bigger molecules at very low energies is nuclear excited Feshbach resonances [1]. In this process the slow moving incoming electron gets captured due to positive electron affinity of the molecule and the excess energy released in the process is redistributed in the various nuclear degrees of freedom by accessing the vibrational excited state of the anion. Fullerene (C_{60}) is one of such molecules that show this type of resonance.

Table 6.1: *Summary of the reported work on the electron attachment to C_{60} (F.E.A.: free electron attachment, R.E.T.: Rydberg electron transfer, F.A.L.P.: Flowing Afterglow Langmuir Probe).*

Threshold Behavior observed			***No Threshold Behavior observed***		
Oven Temp. (K)	***Technique used [Observation]***	***Ref.***	***Oven Temp. (K)***	***Technique used***	***Ref.***
550-600	F.E.A. (200meV) [Threshold: 240meV]	3	670	F.E.A (200meV)	2
			958	R.E.T. (n = 12-40)	5
744	F.E.A. [Threshold: 150meV]	4	725	F.E.A. (30meV)	7
			673	F.E.A. (90meV)	8
673	F.E.A. (210meV) [Threshold: 150meV]	5	-	F.E.A.	9
			853	F.E.A.	10
850	F.E.A. [Threshold: < 500meV]	6	873-923	R.E.T. (n = 20-125)	11
			940	R.E.T. (n = 30-270)	12
700	F.A.L.P. [Threshold: 260meV]	13			

Low energy electron capture by the fullerene molecule resulting in the formation of long lived anion (C_{60}^-) for electron energies ranging from close to zero eV to 10 eV has been studied by many groups in the last decade. Various techniques

like free-electron attachment [2-10], Rydberg electron transfer [5, 11-12] and Flowing Afterglow Langmuir Probe (FALP) [13] have been used for such studies.

Although the longevity of the anion product (C_{60}^-) from the above mentioned experiments is well established, there has been a major disagreement in the results among these experiments as far as the electron attachment close to zero eV is concerned. A summary of these experiments is given in Table 1. The free-electron attachment experiments by Jaffke *et al.* [3], Vostrikov *et al.* [4], Huang *et al.* [5] and Matejcik *et al.* [6] as well as the FALP experiment by Smith *et al.* [13] indicate a threshold for the electron attachment to the fullerene molecule close to zero eV. This threshold had been observed to be in the range of 150 to 260 meV. Tosatti and Manini [14] explained this behavior and estimated the threshold for the low energy electron attachment to C_{60} in the similar range using symmetry arguments. They ruled out the s-wave nature of the electron capture at electron energies close to zero eV. The threshold was obtained using the p-wave nature of the capture mechanism. These arguments were based on the oversimplification of the problem in which the inelastic cross section is substituted by the elastic cross section [5]. On the other hand, some of the free electron attachment experiments [2, 7-10] as well as the Rydberg electron transfer experiments [5, 11-12] indicated the s-wave nature of the electron attachment near zero eV. These experiments also showed the absence of an activation barrier in this phenomenon. One of the arguments given for such an absence of a threshold behavior is the presence of induced polarization in the C_{60} molecule due to the incoming electron. The argument of Tosatti and Manini is countered using the effect of rotational motion of the molecule which makes L = 0 state available for the s-wave kind of capture [11].

Gianturco and co-workers have studied the resonances in C_{60} in terms of the elastic differential cross sections [15]. Their quantum scattering calculations indicated that the threshold behaviour of the electron attachment cross sections may be due to the occurrence of a virtual state from *s-wave* scattering in the a_g symmetry and a peak in the *p-wave* scattering in the t_{1u} symmetry [16]. They have also tried to analyze the single particle resonances in the 2 to 25 eV range in terms of the dynamical trapping behind different centrifugal barriers [17]. Fabrikant and Hotop estimated the relative contribution of *s*-wave and *p*-wave for electron capture cross-section for near zero eV using Vogt-Wannier (VW) model [18]. They used the high resolution data by Elhamidi

et al. [7] and the Rydberg electron attachment rate to estimate the absolute cross sections near zero eV. Though the data by Elhamidi *et al.* is supposed to have the highest resolution, the relative intensity of the peak they observed at zero eV is much smaller than that obtained by Vasil'ev *et al*. [8]. Vostrikov *et al*. [9] had also reported a relatively higher peak near zero eV (at 0.15 eV) as compared to the attachment cross sections at higher energies. A neutral beam depletion measurement by Kasperovich *et al*. [10] also showed fairly large relative cross section at zero eV. Though the most recent measurements [7-10] and the theoretical calculations [18] indicate the presence of the *s*-wave at near zero energies, there appears to be uncertainty regarding the relative contribution of the *s*-wave to the overall attachment cross section as seen in the widely differing relative intensities at zero eV in the experiments [7-10]. In addition, there is the suspected role of temperature of the C_{60} vapor that may be responsible for the observed discrepancies. The role of temperature of the C_{60} vapor has been considered to explain the s-wave attachment near zero eV [8, 19]. The argument has been that the population in the A_g ($L=0$) vibrational state is substantial for temperatures above 600K making the s-wave capture possible [8]. Considering the discrepancies that exist in the relative cross sections, we have investigated the electron attachment to C_{60} as a function of temperature.

6.1 Electron capture near zero eV

6.1.1 Fixing zero of electron energy scale

As mentioned earlier, there have been inconsistent reports about the electron capture near zero eV in the case of C_{60}. In order to determine the threshold energy corresponding to the electron capture process the energy spread of the electron beam used must be as narrow as possible. Hence we use the trochoidal electron monochromator (discussed in Chapter 2) for making measurements on C_{60}. The energy resolution of the electron beam near zero eV was determined using the full width at half maximum of the SF_6^- peak. The typical energy width of the electron beam was found to be 130 meV when the gun was operated in DC mode with the ions being detected without mass separation. The negative ion signal from SF_6, which is dominated by SF_6^- as a function of electron energy is given in Figure 6.1 along with the electron beam current. The figure also shows the negative ion signal from C_{60}

obtained from identical electron gun conditions. The peaks in both these appear at the same energy. Also the electron current profiles remain almost identical in both cases.

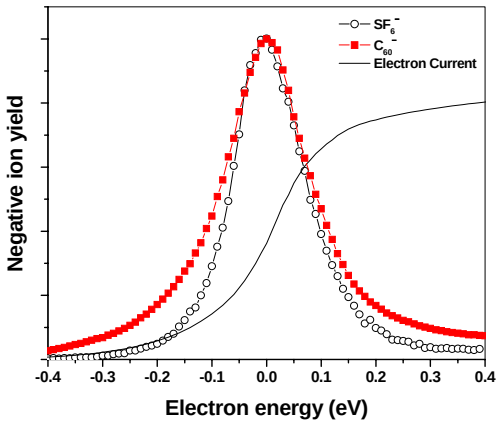

Figure 6.1: *Comparison of C_{60}^- (squares) signal with that of SF_6^- (circles) collected separately with the electron gun operated in DC mode. The two curves are normalized at the peak. Also given is the current profile of the gun during the run. [The electron energy is defined by the applied negative potential on the filament with respect to ground. The negative energy shown in the figure is due to the finite spread in the electron energy distribution.]*

A further check on the zero of the electron energy scale for the C_{60}^- excitation function is carried out using a mixture of SF_6 and C_{60}. In this case the electron gun is operated in the pulsed mode so that the two types of ions can be separated using the time-of-flight arrangement. Figure 6.2 shows the excitation functions for both SF_6^- and C_{60}^- from their mixture taken using the electron gun operated in pulsed mode. The ion yield curves and the electron beam current are measured simultaneously using the General Purpose Interface Bus (GPIB) based data acquisition system described in chapter 2. This mode of operation, though has a poorer energy resolution of 350 meV, confirms that there is no shift in the peak position of the C_{60}^- as compared to that of SF_6^- signal.

Using the time-of-flight mass spectrometer, it is confirmed that no negative ion signal is present except that due to C_{60}^- in the electron energy range 0 to 12 eV when only C_{60} vapor beam is present in the interaction region. Hence we have used the electron gun in the DC mode in order to maintain higher energy resolution. A small DC extraction field (<1V/cm) is used along with the small flight tube voltage

(20 volts) in order to detect the C_{60}^- ions. The spectrum is taken for long enough time to improve the signal to noise ratio.

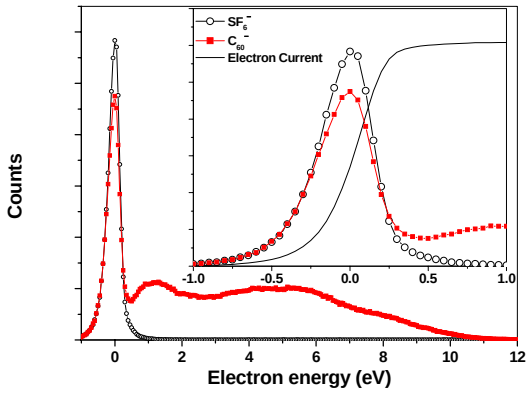

Figure 6.2: *Comparison of C_{60}^- (squares) signal with that of SF_6^- (circles) in the extended energy scale, collected together with the electron gun operating in pulse mode. The inset shows the electron gun current profile along with both the ion yield curves around zero eV.*

6.1.2 Comparing our results with those in the literature

The results of our measurements are given in Figure 6.3 along with the results from Elhamidi *et al.* [7] which were obtained at an electron energy resolution of 30 meV. Our data clearly show a strong enhancement of the zero eV peak as compared to the higher energy structures. The ratio of intensity of C_{60}^- peak near zero eV to that at higher electron energy (1 eV) is tabulated in Table 6.2 along with the ratios from the previously reported experiments.

Table 6.2: *Summary of the relative ion yield near zero eV electron energy as compared to that near 1eV*

Ref.	***Technique***	***Oven Temp. (K)***	***Electron Energy Resolution (meV)***	***Relative Ion Yield*** **($I_{C_{60}^-}$ (0eV)/ $I_{C_{60}^-}$ (1eV))**
2	F.E.A.	670	200	<1
7	F. E. A.	725	30	~1
8	F. E. A.	673	90	~7
Our Experiment	F. E. A.	723	130	8.9 ± 0.3

It appears from the ion yield curve that we obtained (Fig. 6.3) that there is no threshold behavior or the presence of activation energy for the C_{60}^- ion formation around zero electron energy. Also in spite of the energy resolution of the electron beam being on the poorer side as compared to the previously reported experiments, we see the maximum ratio of the intensity of the C_{60}^- ion peak near zero eV to that of the ion peak at higher energy. Moreover we could obtain all the structures in the higher energy part of the spectrum, which were reported in the earlier experiment performed using a better electron energy resolution, except for a small but systematic difference of 200 meV.

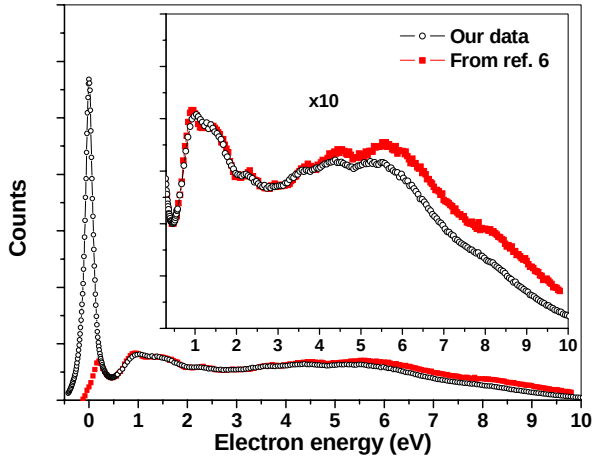

Figure 6.3: *Plot of C_{60}^- ion yield (circles) as a function of the electron energy taken at 818K. Also given are the results from Ref. [7] (squares) after its energy scale is shifted up by 200mV. The inset shows the same data multiplied by 10. The data are normalized to have the same magnitude at the valley between the first two peaks.*

We notice that such a shift is present in the extended energy spectrum given by Elhamadi *et al.* [7] (their Fig.1) as compared to their own higher resolution data in a smaller energy range (their Fig.2). Hence in Fig. 6.3 we have shifted their data by 200 meV to the higher energy side. This shift could be justified further by a comparison with other available data. The shift brings all the high energy peaks in excellent agreement in the two sets of data in Figure 6.3, with the notable difference being the difference in the zero eV peaks. The difference in the peaks at zero eV may be attributed to the difficulties associated with the use of a pure electrostatic electron gun

used by Elhamadi *et al.* [7]. The device used in their experiment was an electron spectrometer using double-hemispherical electrostatic analyzers in tandem, both in the incident and analyzer sections.

There may be a question whether the relative intensity of the peak at zero eV as compared to that at higher energies observed in our data is due to increased path-length in the presence of the magnetic field for electrons near zero eV. This is important as the previous results by Vasilev *et al.* [8] as well as the present one, both showing relatively large zero eV peaks as given in Table 2, were obtained using a magnetically collimated electron beam unlike the case of Elhamidi *et al.* [7]. In this context we provide the data collected simultaneously on SF_6^- and C_{60}^- by having both target molecules simultaneously present in the interaction region. For this purpose, the electron gun had to be operated in the pulsed mode and hence the energy resolution was poorer. The data thus obtained for the two anions along with the electron gun current profile is given in Figure 6.2. From a comparison of this figure with that of Figure 6.1, we note that as the width is reduced by a factor of 2, the relative intensity of the zero eV peak with respect to that at 1 eV of C_{60}^- increases by a factor 2. If the large intensity of the zero eV peak seen in the experiments using magnetic collimation is due to systematic error from increased path-length, the peak height should have increased much faster with improvement in resolution. We note that the zero eV peak in C_{60}^- has a finite width of 150 meV as seen in measurements by Elhamidi *et al.* [7] using an electrostatic gun with an energy resolution of 30 meV and by Vasilev *et al.* [8] using a magnetically collimated gun with an energy resolution of 90 meV. We too find a width of 170 meV, though the energy resolution as measured using SF_6^- is about 130 meV. These also point to the fact that the relatively large intensity observed in the experiments using magnetic collimation cannot be due to the increase in path length.

On a different note, the finite width of the peak could be a clear indication of the presence of higher order partial waves contributing to the negative ion signal as described by Fabrikant and Hotop [18]. Although the present electron energy resolution is not good enough to separate out the s-wave contribution from the higher order contributions, the presence of very strong C_{60}^- signal near zero eV despite the poorer energy resolution is indicative enough to support the presence of significant amount of *s*-wave capture behavior.

6.1.3 Determination of s-wave contribution and estimation of capture cross section

Fabrikant and Hotop [18] have used a *Vogt-Wannier* (*V-W*) profile to fit the cross section measured by Elhamidi *et. al.* [7] since it was the best available data in terms of energy resolution. In this model the capture is considered to be taking place into a polarization well. It is assumed that the reaction occurs with 100% probability if the electron falls into the singularity created by the polarization potential $-\alpha/2r^4$. The cross section depends only on energy and the molecular polarizability α.

Determining *s*-wave contribution

Fabrikant and Hotop [18] calculated the *V-W* cross sections for *s*-wave and *p*-wave capture and used the relation

$$\sigma = c(\varepsilon\sigma_0 + \sigma_1) \qquad (6.1)$$

where σ_0 is the *s*-wave *V-W* cross section and σ_1 is the *p*-wave *V-W* cross section and c and ε are adjustable parameters, to determine the total cross section. ε indicates the relative contribution of the *s*-wave with respect to *p*-wave whereas the parameter c scales the cross section. The value for parameter c has been obtained from the rate constants of the Rydberg electron transfer experiments [11, 12]. They averaged this cross section over a Gaussian profile of 50 meV width and normalized the data by Elhamidi *et al.* with the theoretical cross section at 0.2 eV. The best fit gave them a contribution for *s*-wave about one-tenth of the contribution from p-wave. Though the energy resolutions are poorer, both the data by Vasilev *et al.* [8] and the present one have larger intensity at the main peak (about a factor of 6 in both cases) as compared to the intensity at 0.2 eV.

We have attempted a fit similar to that given by Fabrikant and Hotop [18] by convoluting the SF_6 data (taken here as the instrument function) obtained under similar conditions as that for C_{60} with the *s*-wave and *p*-wave cross sections taken from Fabrikant and Hotop [18]. The fit as shown in Figure 6.4 gives $\varepsilon = 0.45$, showing considerable contribution due to *s*-wave. We put the cross section on the absolute scale using the absolute cross section measurement reported earlier by Vostrikov *et al.*

[4, 9]. The value of *c* obtained in this way is 0.06 as against 0.1 taken by Fabrikant and Hotop [18].

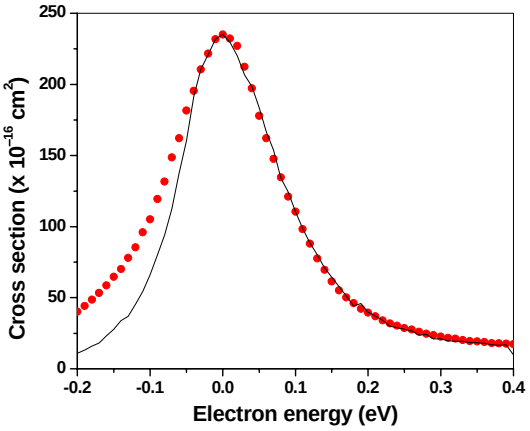

Figure 6.4: *Comparison of our data (points) at 818 K with the theoretical fit using s-wave and p-wave contributions (Ref. [18]) convoluted with the SF_6^- curve under similar conditions taken as the instrument function. The best fit needed 45% contribution from s-wave to that from p-wave. The cross sections are normalized to absolute values using the data from Vostrikov et al. [4, 9].*

Estimating the absolute cross section

The absolute scale shown in the Figure 6.4 for the cross sections is determined using the data from Vostrikov *et al.* [4, 9]. It may be noted that there are relatively few measurements of absolute cross sections for electron attachment to C_{60}. The data by Vostrikov *et al.* [4, 9] show the zero eV peak to be shifted to 0.15 eV in one measurement where they report the peak cross section of $8.0 \times 10^{-15} cm^2$ for electron capture [4]. In another set of measurement they report the peak $1.2 \times 10^{-14} cm^2$ at 0.15 eV [9]. In both cases, the experiments were carried out using a crossed electron beam - molecular beam method. The absolute cross section of electron capture by C_{60} was determined by comparing the electron energy dependence of the C_{60}^- signal with the SF_6^- signal obtained under similar conditions [9]. They used the established result for the electron attachment to polyatomic molecules near zero eV that approximates the cross section to vary as $E^{-\gamma}$ where the constant γ was determined for SF_6 to be 1.12. The cross section was calculated using the relation

$$\sigma^{-}(E) = \left(\pi a_0^2 \Big/ 2\beta E_0^{\gamma} \right) \{ 1 - \exp\left[-4\left(2\beta\alpha E_0^{\gamma-0.5} \right)^{1/2} \right] \} \qquad (6.2)$$

where σ^- is the capture cross section, a_0 is the Bohr radius, α is the molecular polarizability in a_0^3 units and E_0 is the electron energy in atomic units. Setting γ = 1.12, α = 4.41 and β = 4 for SF_6, good agreement with the experimental data for SF_6^- signal was obtained by them. Sighting the qualitative similarity between the electron energy dependence of the negative ion signal from SF_6 and C_{60}, they performed the similar calculations for C_{60} and found the absolute cross sections for the process at those energies.

The beam depletion measurements by Kasperovich *et al.* [10] give an absolute cross section of $9 \times 10^{-14} cm^2$ at 0.05 eV, though this may be considered an upper limit as it is the total scattering cross section. Due to the uncertainty in the reliability of the peak position at near-zero eV in Vostrikov *et al*. [4, 9], we have normalized our data with the average value of the cross sections they have reported at 1 eV in the two measurements, which is $3.4 \times 10^{-15} cm^2$. This gives the peak cross section of $2.4 \times 10^{-14} cm^2$ as shown in Figure 6.4 as against 4.5×10^{-15} cm^2 obtained by Fabrikant and Hotop [18]. By matching this absolute value with the theoretical fit, we get c = 0.06.

6.2 Temperature dependence of the electron capture process for energy range 0-12 eV

It is clear from Table 1 that various experiments performed over the period of time have used C_{60} vapor at different temperatures. Hence one of the possible reasons for observing the threshold near zero eV can be the temperature of the C_{60} vapor not being adequate. We have investigated this possibility by carrying out the measurements at various oven temperatures, the results of which are summarized in Table 3, where we have given the relative intensities of the negative ion signal at electron energy near zero eV to that at 1eV. We find that the ratio is independent of the C_{60} vapor temperature, though there is a reduction at 818K. However the ratio of 7 at this temperature is still much higher than what has been generally reported. We believe that our measurements rule out the possibility of temperature of the fullerene vapor having played a role in the observed disparity in the earlier measurements.

From the data obtained at different temperatures, we note a decrease in the cross sections with the increase in temperature at higher electron energies (> 7 eV). This could be seen from Figure 6.5 in which we have plotted the data obtained at various temperatures after normalization at the 1 eV peak. Though at lower temperatures there is large statistical spread, it is seen that the cross sections decrease with increase in temperature. This may be explained in terms of the decrease in lifetime of the negative ion states formed through electron attachment.

Table 6.3: *Relative C_{60}^- ion-yield at different vapor temperatures in the present experiment*

Temperature (K)	***Relative Ion Yield*** $\mathbf{I_{C_{60}^-}}$ **(0eV)/** $\mathbf{I_{C_{60}^-}}$ **(1eV)**
648	09.0 ± 1.8
668	09.0 ± 1.4
723	08.9 ± 0.3
793	08.7 ± 0.2
818	07.0 ± 0.1

Lezius has explained the electron attachment to C_{60} using a three step model [19]. These steps are namely (i) capture of electron in the induced polarization potential of C_{60} (classically it is Langevin rate and quantum mechanically it is formulated in the V-W model) (ii) electron diving from the continuum state to a bound state by transferring energy into the intramolecular excitation and (iii) loss of anions due to auto-detachment (thermionic emission). The third step is considered to be responsible for the drop in the anion signal at higher electron energies. The negative ion lifetime at higher temperature could be smaller since it becomes increasingly difficult to dissipate the energy of the incoming electron as many vibrational modes are already saturated at higher temperatures.

The autodetachment of C_{60}^- in terms of a model based on thermionic emission has been discussed by Matejčik *et al.* [6].This model was used to explain the observed drop in the C_{60}^- intensity at energies above 7 eV for fixed C_{60} temperature. In this model the incident electron energy plus the energy released during capture due to electron affinity of C_{60} is assumed to go into exciting the vibrational modes, thereby raising the temperature of the molecule. And as the temperature increases there is increasing autodetachment due to thermionic emission. Based on this model any

change in temperature whether due to the energy transferred from the electrons or by direct heating should lead to corresponding changes in the lifetime of the negative ion through the thermionic emission process.

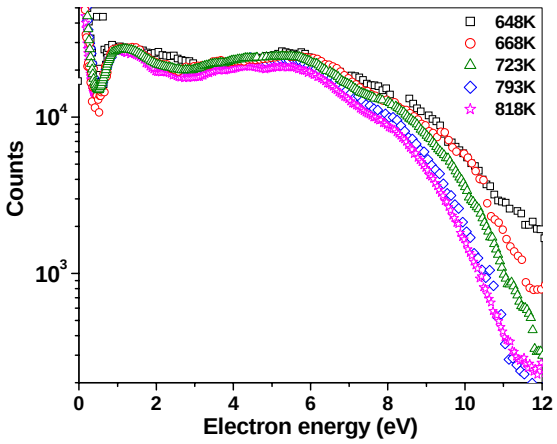

Figure 6.5: *Plots of C_{60}^- ion yield as a function of the electron energy taken at different C_{60} vapor temperatures. The plots are normalized at the peak near 1 eV. The data at 648, 668 and 723 K were smoothed to reduce the scatter.*

We have tried fitting the reduction in the anion signal due to increase in temperature with the themionic emission model. At a given electron energy (say 8 eV) we estimated the loss in the anion signal from the difference in the theoretically calculated cross section [6] and the cross section obtained in our experiment at various temperatures. The detachment rate coefficient (k_d) is determined by the relation

$$N_t = N_0 \exp(- k_d t) \qquad (6.3)$$

where N_0, N_t are the no. of anions at time $t=0$ and t. The time t is taken to be the flight time of the anion in the *ToFMS* in the experiment. Also the temperature of the C_{60} is determined from the electron energy, electron affinity and the oven temperature. The values for k_d are found to be consistent with those determined earlier for fixed temperature but different electron energies and hence at different total temperatures. Thus our observation of the temperature dependence is found to be consistent with the thermionic emission model given by Matejčik *et al.* [6].

We also note that the electron capture efficiency has been shown to go down with increase in internal energy of the molecule [7]. This may also add to a reduction in the negative ion signal with increase in temperature. Though one expects to see the temperature dependence at all energies, our data show no noticeable effect at energies below 2 eV. A plausible reason for this could be the temperature (including that transferred from the electron) not being sufficiently large to make noticeable loss due to thermionic emission.

It is interesting to note that the first ionization potential of C_{60} is 7.5 eV. Thus for electrons of energy above 7.5 eV, both capture leading to C_{60}^- formation as well as electron impact ionization leading to C_{60}^+ formation are possible. This may explain the relatively fast drop in the attachment cross section as the energy is increased beyond 8 eV. On the other hand, the existence of relatively longer lived negative ion states above first (7.5 eV) and second (8.9 eV) ionization potentials as well as the much higher cross section for the electron capture ($\sim 10^{-15}$ cm^2) as compared to that for the electron impact ionization at these energies ($\sim 10^{-16}$ cm^2) [20] makes this system a very unique one.

References:

[1] L. G. Christophorou, *Electron-molecule Interactions and Their Applications - Vol I,* (Academic Press, Orlando, Florida) (1984).

[2] M. Lezius, P. Scheier, and N. D. Mark, *Chem. Phys. Lett.* **203**, 232 (1993).

[3] T. Jaffke, E. Illenberger, N. Lezius, S. Matejcik, D. Smith, and T. D. Mark, *Chem. Phys. Lett.* **226**, 213 (1994).

[4] A. A. Vostrikov, D. Yu. Dubov, and A. A. Agarkov, *Pis'ma Zh. Tekh. Fiz.* **21**, 55 (1995); *Tech. Phys. Lett.* **21**, 517 (1995).

[5] J. Huang, H. S. Carman Jr., and R. N. Compton, *J. Phys. Chem.* **99**, 1719 (1995).

[6] S. Matejčik, T. D. Mark, P. Spanel, D. Smith, T. Jaffke, and E. Illenberger, *J. Chem. Phys.* **102**, 2516 (1995).

[7] O. Elhamidi, J. Pommier, and R. Abouaf, *J. Phys. B* **30**, 4633 (1997).

[8] Y. V. Vasil'ev, R. F. Tuktarov, and V. A. Mazunov, *Rap. Comm. in Mass Spect.* **11**, 757 (1997).

[9] A. A. Vostrikov, A. A. Agarkov, and D. Yu. Dubov, *High Temp.* **39**, 22 (2001).

[10] V. Kasperovich, G. Tikhonov, and V. V. Kresin, *Chem. Phys. Lett.* **337**, 55 (2001).

[11] C. D. Finch, R. A. Popple, P. Nordlander, and F. B. Dunning, *Chem. Phys. Lett.* **244**, 345 (1995).

[12] J. M. Weber, M. W. Ruf, and H. Hotop, Z. Phys. D **37,** 351 (1996).

[13] D. Smith, P. Spanel, and T. D. Märk, *Chem. Phys. Lett.* **213**, 202 (1993).

[14] Erio Tosatti, Nicola Manini, *Chem. Phys. Lett.* **223**, 61 (1994).

[15] F. A. Gianturco, R. R. Lucchese, and N. Sanna, *J. Phys. B* **32**, 2181 (199).

[16] R. R. Lucchese, F. A. Gianturco, and N. Sanna, *Chem. Phys. Lett.* **305**, 413 (1999).

[17] F. A. Gianturco and R. R. Lucchese *J. Chem. Phys.* **111**, 6769 (1999).

[18] Ilya I. Fabrikant and Hartmut Hotop, *Phys. Rev. A* **63**, 022706 (2001).

[19] Matthias Lezius, *Int. J. Mass Spectrom.* **223-224**, 447 (2003).

[20] B. Dunser, M. Lazius, P. Scheier, H. Deutsch and T. D. Mark, *Phys. Rev. Lett.* **74**, 3364 (1995).

Chapter 7

Rydberg electron attachment to excited molecules

Apart from free electron attachment, Rydberg electron attachment is one of the mechanisms through which a negative ion can be formed. As discussed in the first chapter, through Rydberg electron attachment process some of those negative ion states, that are not accessible through free electron attachment, can be accessed.

Electron in the Rydberg state can be considered to be a quasi free electron which is very loosely bound to the positive ion core of the parent atom or molecule. In the simple one electron excitation of the atom or molecule to Rydberg state, the excited electron resides in the Rydberg state where as the remaining positive ion stays in the ground state. Such Rydberg states lie below the first ionization potential of the corresponding neutral species. There could also exist bound Rydberg states that lie above the first ionization potential of the corresponding neutral molecules. Such states are termed as the high-Rydberg states (HR states). As can be understood from the definition itself, the positive ion core of such Rydberg state, will be in an excited state. In fact each vibrational and rotational level of the core has its own Rydberg series which comprises these HR states.

There have been several reports about the Rydberg electron attachment to the ground state molecules using Rydberg states of rare gas atoms as a function of the principal quantum numbers [1-8]. These experiments are carried out by selectively exciting atoms in specific Rydberg state with known principal quantum number in a supersonic beam and colliding them with molecules from another beam. On the other hand, several other reports have appeared in the recent past about generating negative ions by just focusing a laser beam in a high pressure gas cell [9-15]. The underlying mechanism leading to the negative ion formation in these experiments is considered to be the free electron attachment to the molecules excited to high Rydberg states i.e. Rydberg states above the first ionization potential of the molecules. In these experiments the free electrons were generated by photoionization of the molecules

under study. There have been some experiments reported in which a mixture of molecules is used where one of the molecular species in the mixture has considerably lower ionization potential acting as the electron source through photoionization. These experiments are equivalent to the free electron attachment to electronically excited molecules.

Only one experiment has been reported so far where Rydberg electron transfer to an electronically excited molecule has been studied [16]. In this experiment an ArF (photon energy 6.4eV) or KrF (photon energy 5eV) laser beam is allowed to pass through the mixture of O_2 and benzene (I. P.: 9.4eV). It was found that no negative ions were formed in the absence of benzene where as in the presence of benzene O^- and O_2^- ions were observed under different pressure conditions. The mechanism associated with this process was identified as the Rydberg electron transfer from benzene molecule in HR states to the O_2 molecule in a Rydberg state.

In general, it is interesting to study Rydberg electron transfer to excited molecules occurring at relatively higher pressures as compared to those used in regular free electron attachment experiments (beyond single collision conditions) since one encounters relatively high pressures in most of the practical applications where negative ions play a vital role. We have attempted to study the Rydberg electron attachment to electronically excited SF_6 and CS_2 in relatively high pressure conditions.

To begin with the experiments were performed with CH_3I and CCl_4 molecules. The details of the experiment that allows relatively high pressure in the collision region while maintaining necessary high vacuum in the detection region have been presented in Chapter 2. To begin with XeCl excimer laser beam (308nm i.e. 4eV photon energy) is focused on the gas cell in the interaction region. The typical energy of the pulses used is about 40mJ and a convex lens of 50cm focal length is used to focus the beam in the interaction region. The laser beam is focused to 1mm x 2mm size spot at the center of the interaction region. In order to collimate the laser beam a slit of 5mm width is used outside the chamber. The negative ions formed in the focal spot were extracted using a pulsed electric field and mass analyzed using a *ToFMS* as discussed in Section 2.4. I^- and Cl^- ions were observed from CH_3I and CCl_4 respectively. The mass spectrometer was calibrated using these ions. It is known that both CH_3I and CCl_4 attach electrons at zero energy to give rise to the respective halide negative ions [17, 18]. These molecules are also known to give I^- [19] and Cl^- [20] ions

respectively on Rydberg electron transfer. The observation of these ions in the current experiment implies that there exist either very low energy electrons or molecules excited to the Rydberg states in the interaction region. The ionization potential for CH_3I (9.54eV) and CCl_4 (11.47 eV) are too high to give free electrons on photoionization by light of wavelength 308nm (4eV), unless there is multiphoton ionization through a 3-photon process. We investigated the possibility of free electrons produced by possible multiphoton ionization or secondary electrons from surfaces giving rise to negative ion formation by applying a magnetic field in the interaction region. The magnetic field is generated in the interaction region using a pair of Helmholtz coils exterior to the chamber. The direction of the magnetic field is also varied by rotating the axis of the Helmholtz coils with respect to the *ToFMS* axis. It is observed that the presence of magnetic field in the interaction region does not affect the ion signal strength irrespective of the direction of the magnetic field. This ruled out the possibility of negative ion formation by attachment of free electrons produced by photoionization of the gases or photoemission from surfaces.

The only other mechanism for creation of the negative ions is through a Rydberg electron transfer. This was confirmed in the following way. When a small DC electric field was generated in the interaction region by the application of a small voltage to the puller electrode it is found that the signal strength decreases. It is found that the intensity of negative ion decreases rapidly with increase in electric field irrespective of its direction.

The DC electric field dependence of the negative ion signal is given in Figure 7.1. The DC electric field causes the Rydberg states to field ionize before they could react with another molecule to form the negative ions. Thus the electric field dependence of the negative ion signal confirmed that the negative ions are formed through Rydberg electron transfer.

In order to identify the precursors of the Rydberg states, we studied the intensity of the negative ions as a function of pressure. The pressure dependence of these ions showed (Figure 7.2) linear behavior in low pressure regime (<5mTorr). This indicated that the Rydberg states are not due to the CH_3I and CCl_4 molecules. The only way they could arise is by photoexcitation of the relatively large molecules present in the background gases. In these experiments we had used an oil rotary pump to evacuate the gas cell and the large molecules acting as precursors may have been due to the oil. This possibility was eliminated by evacuating the cell using a

completely oil free pumping system employing a turbo pump and an oil free tri-scroll pump. The measurements were repeated after pumping down the cell to high vacuum. These measurements yielded very little negative ions from CH_3I and CCl_4.

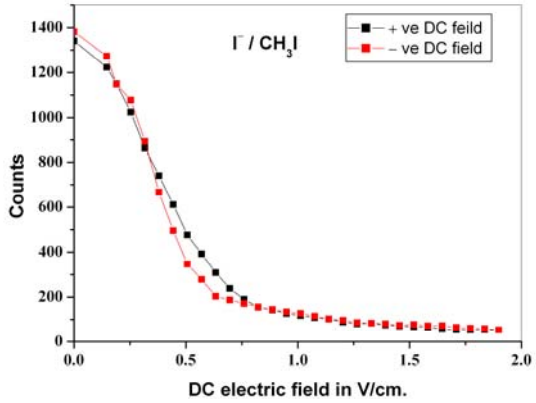

Figure 7.1: *Dependence of ion counts for I^- from CH_3I on DC electric field present in the interaction region.*

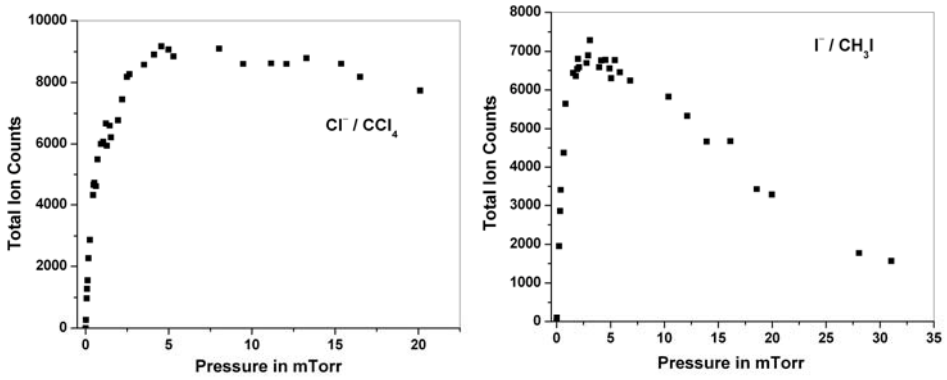

(a) **(b)**

Figure 7.2: *Pressure dependence of (a) Cl^- signal from CCl_4 and (b) I^- signal from CH_3I gas cell*

7.1 Rydberg electron attachment to electronically excited SF_6

The first set of experiments on SF_6 was carried out without using the cleaner vacuum conditions. Typical mass spectrum obtained for the SF_6 gas is shown in Figure 7.3. Ion peaks that correspond to mass 19, 25, 38, 130, and 146 can be seen. The masses 19, 38 and 146 could be identified as F^-, F_2^- and SF_6^-. Repeated

measurements under varying conditions confirmed that the peaks at mass 25 and 130 were present only with SF_6 gas. Eventually, a careful analysis in terms of the flight times of the ions showed that the ions corresponding to mass 25 are nothing but F^- ions generated by collisional dissociation of SF_6^- ions at the differential pumping aperture situated at the entrance of the flight tube of the *ToFMS* set-up. In a similar way the ion at mass 130 was also identified as SF_5^- ions formed by the above mechanism. The time of flight calculated for the other ions matched very well with the measured time of flight indicating that the origin of these ions is located at the center of the interaction region.

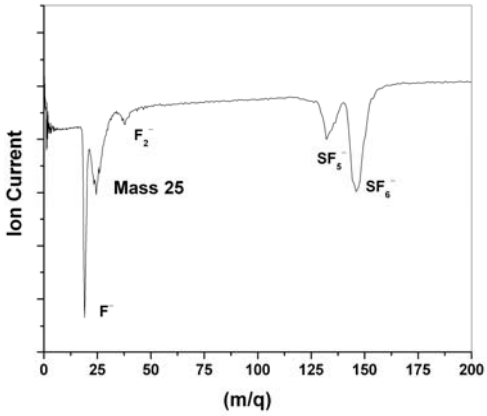

Figure 7.3: *Time of flight mass spectrum for negative ions obtained by focusing the XeCl excimer laser beam on SF_6 gas cell. The spectrum is obtained using a storage oscilloscope.*

Like in the case of CH_3I and CCl_4, we identified the source of the negative ion formation as due to Rydberg electron transfer. That free electrons formed by photoionization or photoemission are not the agents for creating the negative ions was confirmed by using an external magnetic field to deflect away the electrons. Also the laser beam size and intensity are adjusted in order to avoid the formation of any secondary electrons due to multiphoton ionization from SF_6 (I. P. 15.5eV) [21] by avoiding tight focusing. Again, as in the case of CH_3I, we could suppress the negative ion intensity by application of an electric field in the interaction region. The DC electric field dependence of the negative ion strength for different ions is given in Figure 7.4. As can be seen from Figure 7.4 the ion intensity decrement is independent of the direction of the electric field. The effect of DC electric field in the interaction

region points out that the negative ion formation is taking place through the Rydberg electron transfer. On application of DC electric field these states get field ionized and hence the negative ion signal get suppressed irrespective of the direction of the electric field.

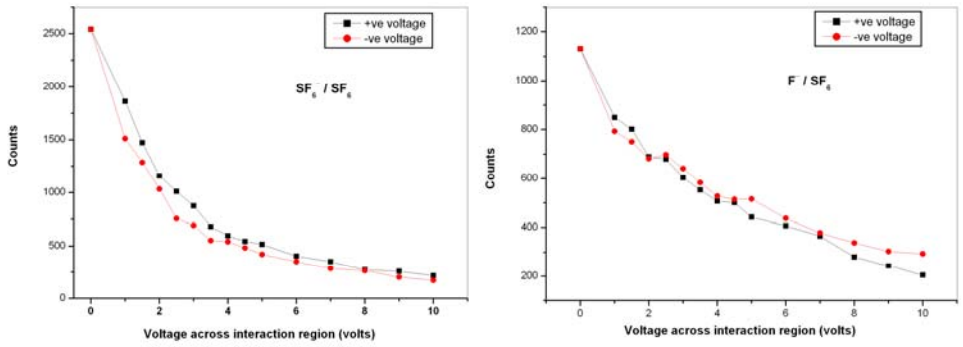

(a) (b)

Figure 7.4: *Dependence of ion counts for (a) SF_6^- and (b) F^- from SF_6 on DC electric field present in the interaction region.*

We have measured the pressure dependence of the different negative ion signals. These results are given in Figure 7.5 and 7.6 for F^- along with mass 25 and SF_6^- along with SF_5^- ions respectively. It can be seen that in the relatively low pressure region (below 10 mTorr) the signal shows a linear relation with the pressure. This implies that only one SF_6 molecule is participating in an event leading to a negative ion formation. This also shows that the source of the electron is not SF_6 molecule. Thus in this case also, the Rydberg states appear to be formed from the background gases. The pressure dependence of SF_6^- and SF_5^- show almost similar behavior except that the ion intensity for SF_6^- peaks at around 2.6 mTorr pressure where as that for SF_5^- peaks around 6.5 mTorr. The intensity of F^- peaks at about 5 mTorr, whereas that of mass 25 keeps on increasing till about 10 mTorr pressure and then saturates for some range of pressure. At higher pressure range above 20 mTorr it decreases.

We notice that the pressure dependence of the atomic negative ion fragments formed in various cases like Cl^- from CCl_4, I^- from CH_3I, F^- (including that at mass 25) from SF_6, and S^- from CS_2 (discussed later) show almost similar pressure dependence. In all these cases the ion intensity increases linearly in some pressure

range and then falls gradually at higher pressure. The overall decrement in intensity of these atomic ion signals at higher pressure is distinctly different than that observed for the molecular ions like SF_6^- and SF_5^- ions from SF_6. The ion intensity loss at higher pressure in the case of molecular ions is much rapid and almost exponential. This implies that the collisional losses that become predominant at higher pressures are more effective in the case of molecular negative ions than the atomic negative ions. This also points towards the relative stability of the negative ions which is more for the atomic negative ions than the molecular negative ions.

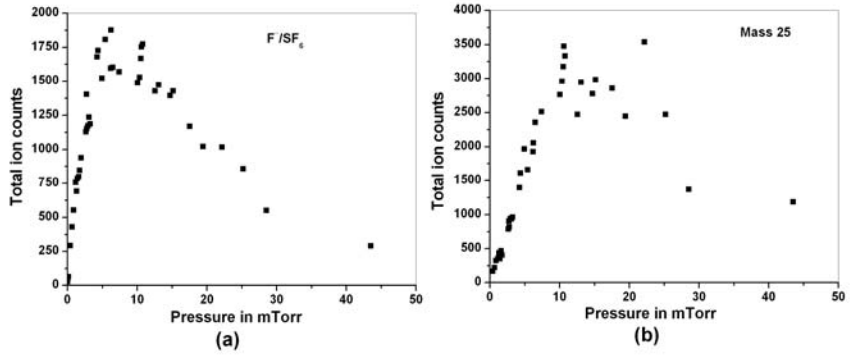

Figure 7.5: *Pressure dependence of (a) F^- signal and (b) ion signal arriving at time corresponding to mass 25 from SF_6 gas cell without pumping the interaction region with dry pump.*

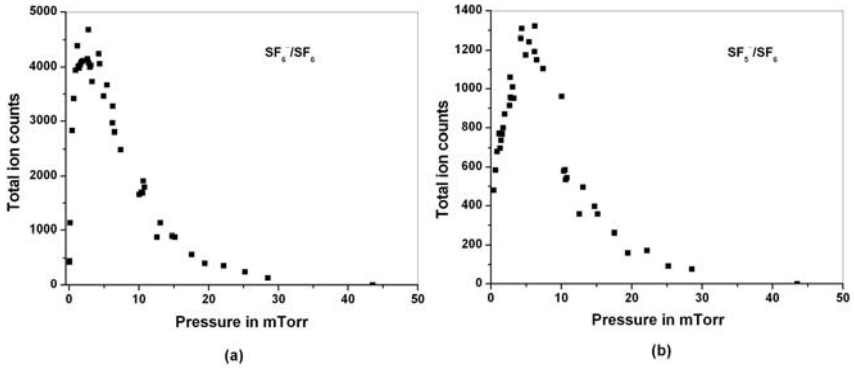

Figure 7.6: *Pressure dependence of (a) SF_6^- and (b) SF_5^- signal from SF_6 gas cell without pumping the interaction region with dry pump.*

SF_6 is known to be a low energy electron scavenger as it shows very high cross section for the zero eV electron capture. The Rydberg electron attachment experiments reported so far on SF_6 show that only SF_6^- ions are observed [22]. In these

experiments the rare gas atoms excited to their high Rydberg state are made to collide with the ground state SF_6 molecules. The free electron attachment to SF_6 in ground state show F^- and F_2^- ion signals at relatively higher electron energies (2.5eV and 2eV respectively) [23]. Also the energy threshold for the F^- formation from SF_6 on electron attachment is known to be 0.65eV (Bond dissociation energy of ($F\text{-}SF_5$) is 4.05eV and electron affinity of F is 3.4eV) [24]. Hence the additional energy required for forming the fragment ions like F^- and F_2^- has to come either from the donor or from internal energy of the acceptor. For identifying the source of this additional energy needed to form the different fragment ions it is important to have some control over the electron donor molecular states. For that purpose the contribution from the background gases needs to be suppressed.

The contribution from the background gases is eliminated by improving the quality of vacuum in the gas cell. This is achieved by pumping the interaction region to high vacuum using an oil free pumping system composed of a turbo molecular pump and scroll pump. After pumping the interaction region no negative ion signal is observed on focusing the XeCl laser beam on the gas cell of pure SF_6. This also clearly confirms the absence of any low energy stray secondary electrons and the role of background molecules acting as Rydberg electron donors to form negative ions from other molecules when sufficient care is not taken in the quality of the vacuum used in these experiments. After eliminating unknown Rydberg electron donors, we carried out experiments using specific molecules as electron donors. For this we chose organic compounds having relatively low ionization potential like aniline (I. P. 7.7eV) or cresol (I. P. 8.3eV) [21].

By focusing the laser beam on a mixture of SF_6 with aniline, a mass spectrum similar to that in Fig. 7.3 was obtained, including masses at 25 and 130 along with F^-, F_2^- as well as SF_6^-. However, it is found that the F^- and F_2^- are relatively weaker as compared to the previous observations. It is also found that all the previously observed features like pressure dependence and the effect of DC field are reproduced in the case of aniline SF_6 mixture when the partial pressure of SF_6 is increased while keeping the partial pressure of aniline constant. The measurements were repeated with a mixture of SF_6 and cresol. In this case, only SF_6^- and relatively weaker SF_5^- signal is observed.

The observed difference in the two experiments with aniline and cresol may be interpreted as due to the difference in their ionization potential. In the case of aniline

the Rydberg state that is accessed by two-photon excitation (8eV) lies 0.3eV above first ionization potential of the molecule. Hence in that case the Rydberg electron transfer takes place from the high-Rydberg state (HR state). In the case of cresol, the Rydberg state accessed lies 0.3 eV below the first ionization potential. Hence it would not have as large a principal quantum number as in the case of aniline. This makes the cross section for electron transfer from aniline Rydberg state accessed by two 308nm photons much larger than from that of cresol under the same photo-excitation condition. Moreover, the aniline Rydberg state will have relatively more excess energy. However, the excess energy present in the ionic core of the aniline is still insufficient to fragment SF_6^- and give rise to $F^-$and F_2^-. Hence in order to have the observed fragmentation, the acceptor SF_6 molecules must carry the extra energy. This is possible only if the SF_6 molecule is electronically excited due to the laser beam present in the interaction region. On examination of the electronic states of SF_6 we find that there exists an excited state at 8eV above the ground state [25]. This energy difference matches very well with two-photon absorption of the 308 nm laser used in the experiment. Thus we conclude that the formation of the fragment negative ion takes place through Rydberg electron transfer to electronically excited SF_6 molecules.

The cross section for the electron transfer from aniline Rydberg state is much larger than that for the cresol as the two Rydberg orbitals have different sizes. Hence although the cross section for two photon transition in the SF_6 under the experimental condition is smaller, the F^- signal is observable. The absence of F^- from laser irradiated cresol + SF_6 mixture could be explained as due to this difference. It also highlights the importance of HR states in the negative ion chemistry in plasmas.

7.2 Rydberg electron attachment to electronically excited CS_2

For CS_2 we followed the same procedure as in the case of SF_6. To begin with the XeCl excimer laser beam is focused in the CS_2 gas cell without using an oil free pump. The negative ions produced are mass analyzed using the same linear *ToFMS*. Typical mass spectrum obtained is shown in Figure 7.7. In this case only S^- fragment negative ion is observed.

The pressure dependence of the negative ion signal is studied for the pressure range from 0.02mTorr to 50mTorr. The pressure dependence is shown in Figure 7.8.

As can be seen from the figure, in the lower pressure regime i.e. unto 10mTorr the negative ion signal strength increases linearly with the pressure. This is similar to that observed in the case of SF_6. Hence it is concluded that in the case of CS_2 as well the background gases play role in the formation of negative ions.

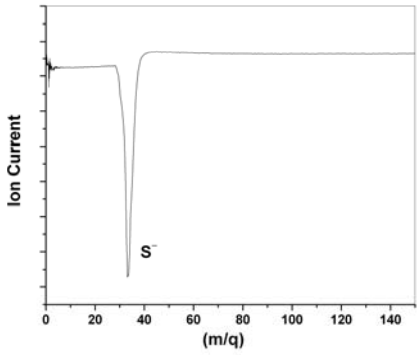

Figure 7.7: *Time of flight mass spectrum for negative ions obtained by focusing the XeCl excimer laser beam on CS_2 gas cell without pumping the interaction region with dry pump.*

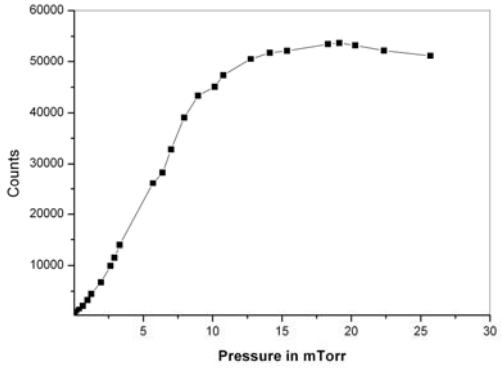

Figure 7.8: *Pressure dependence of S^- signal from CS_2 gas cell without using an oil-free pump*

The absence of any contribution from secondary electrons is confirmed by applying magnetic field in the interaction region as done earlier in the case of SF_6. Also the role of Rydberg states is confirmed by observing the reduction in the negative ion signal with the presence of small electric field in the interaction region. As can be seen in Figure 7.9, the suppression in the S^- signal is independent of the direction of the electric field present in the interaction region.

Unlike CH_3I, CCl_4, and SF_6, CS_2 does not attach electrons near zero energy. Hence, one does not expect to see Rydberg electron attachment to CS_2 molecules.

Thus in order to form negative ions from CS_2 by Rydberg electron attachment, it needs to be in an electronically excited state. CS_2 is known to have an absorption band that extends beyond 308nm, the wavelength of the laser used [25]. In the case of free electron attachment to ground state CS_2 three types of fragments are found to be formed, namely S^-, S_2^- and CS^-. The lowest resonance occurs at electron energy of 3.6 eV leading to the formation of S^- [26]. In order to form S^- from CS_2, the incoming electron needs at least 2.6 eV energy (based on electron affinity of S being 2.08 eV and bond dissociation energy of CS—S being 4.66 eV). Thus for obtaining S^- from CS_2, it should be in an electronically excited state. Experiments on electronically excited CS_2 using 308 nm laser followed by electron attachment have been found to yield S^- ions for electron energies starting from zero eV, with the peak cross section at 1.5eV [27]. Hence it is expected that the excited state CS_2 should show S^- formation through Rydberg electron attachment. This may explain the observed Rydberg attachment leading to S^- formation. However, since we do not have any idea about the nature of the Rydberg state, it may be difficult to say that Rydberg electron attachment to ground state CS_2 from a very highly excited Rydberg state with sufficient internal energy is not taking place.

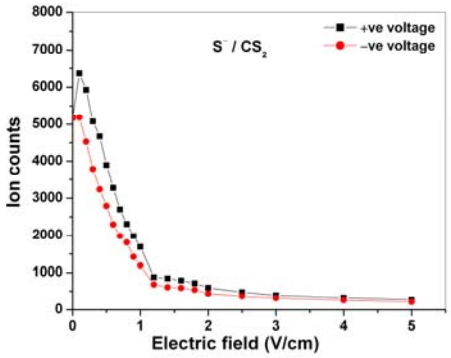

Figure 7.9: *Dependence of ion counts for S^- from CS_2 on DC electric field present in the interaction region.*

In order to identify the HR state, we conducted experiments using clean vacuum conditions and using known precursor Rydberg species. On focusing the 308 nm laser beam on pure CS_2 in the gas cell after it is pumped clean to high vacuum using oil free pumping system did not show the presence of any negative ions. This was followed by experiments on a mixture of CS_2 and aniline and CS_2 and cresol. The typical pulse energy used was about 40mJ with spot focused to 1mm x 2mm size. In

the case of CS_2 + cresol mixture no negative ion signal is observed where as the CS_2 + aniline mixture showed formation S^- ions on irradiation. The formation of S^- with aniline which has an excess energy of 0.3 eV clearly shows that the electron attachment is occurring to an electronically excited state of CS_2. This difference in the results from two mixtures can be attributed to the role of HR state in the Rydberg electron transfer mechanism.

To conclude, we have shown that the Rydberg electron transfer from HR states to the molecules in the electronically excited state is very efficient technique to produce fragment negative ions. The electronic excitation of the target molecule opens up new fragmentation channels not observed in the Rydberg electron transfer to ground state molecules.

Reference:

[1] L. Suess, R. Parthasarathy and F. B. Dunning, *Chem. Phys. Lett.*, **372**, 692 (2003).

[2] Y. Liu, L. Suess and F. B. Dunning, *J. Chem. Phys*., **122**, 214313 (2005) and references therein.

[3] W. D. Robertson, N. I. Hammer, J. E. Bartmess, R. N. Compton, K. Diri and K. D. Jordan, *J. Chem. Phys.* **122**, 204319 (2005) and references therein.

[4] L. Suess, Y. Liu, R. Parthasarathy and F. B. Dunning, *J. Chem. Phys*., **122**, 124315 (2005) and references therein.

[5] L. Suess, Y. Liu, R. Parthasarathy and F. B. Dunning , *J. Chem. Phys*., **121**, 7162 (2004) and references therein.

[6] L. Suess, R. Parthasarathy and F. B. Dunning, *J. Chem. Phys.*, **119**, 9532 (2003) and references therein.

[7] J. Huang, H. S. Carman Jr., and R. N. Compton, *J. Phys. Chem.* **99**, 1719 (1995).

[8] J. M. Weber, M. W. Ruf, and H. Hotop, *Z. Phys. D* **37** (1996) 351; *Chem. Phys. Lett.* **361**, 277 (2002).

[9] L. G. Christophorou, S. R. Hunter, L. A. Pinnaduwage, J. G. Carter, A. A. Christodoulides, and S. M. Spyrou, *Phys. Rev. Lett.* **58**, 1316 (1987).

[10] Lal A. Pinnaduwage and Loucas G. Christophorou, *Chem. Phys. Lett.*, **186**, 4 (1991).

[11] Lal A. Pinnaduwage and Loucas G. Christophorou, *Phys. Rev. Lett.* **70**, 754 (1993).

[12] Lal A. Pinnaduwage and Dennis L. McCorkle, *Chem. Phys. Lett.* **255**, 410 (1996).

[13] Panos G. Datskos, Lal A. Pinnaduwage and John F. Kielkopf, *Phys. Rev. Lett.* **55**, 4131 (1997).

[14] K. Nagesha and L. A. Pinnaduwage, *Chem. Phys. Lett.* **312**, 19 (1999).

[15] C. Tav, and L. A. Pinnaduwage, *J. Phys. D : Appl. Phys.* **33**, 2391 (2000).

[16] K. Nagesha and L. A. Pinnaduwage, *J. Chem. Phys.* **17**, 7124 (1998).

[17] J. A. D. Stockdale, F. J. Davis, R. N. Compton and C. E. Klot, *J. Chem. Phys*. **60**, 4279 (1974).

[18] D. Klar, M. –W. Ruff and H. Hotop, *Int. J. Mass Spectrom*., **205**, 93 (2001).

[19] X. Ling, K. A. Smith and F. B. Dunning, *Phys. Rev. A*, **47,** R1 (1993).

[20] M. T. Frey, S. B. Hill, K. A. Smith, F. B. Dunning and I. I. Fabrikant, *Phys. Rev. Lett*., **75**, 810 (1995).

[21] NIST chemistry webbook : http://webbook.nist.gov/chemistry

[22] G. W. Foltz, C. J. Latimer, G. F. Hildebrandt, F. G. Kellert, K. A. Smith, W. P. West, F. B. Dunning and R. F. Stebbings, *J. Chem. Phys*., **67**, 1352 (1977).

[23] L. G. Christophorou, Ed., *Electron-molecule Interactions and Their Applications - Vol I* (Academic Press, Orlando, Florida 1984).

[24] Ref. from NIST

[25] G. Herzberg *Molecular spectra and molecular structure part III, electronic spectra and electronic structure of polyatomic molecules* (D. Van Nostrand Company, Princeton, New Jersey 1966).

[26] E. Krishnakumar and K. Nagesha, *J. Phys. B: At. Mol. Opt. Phys.*, **25**, 1645 (1992).

[27] S. V. K. Kumar, E. Krishnakumar, S. A. Rangwala and V. S. Ashoka, *Phys. Rev. A*, **64**, 012707 (2001).

Chapter 8

Future Directions

One of the highlights of the results presented in this thesis is the discovery of functional group dependent site selective fragmentation of simple organic molecules through *DEA*. The molecules reported in this work are all of aliphatic compounds. The natural extension of the work reported here would be to look for the *DEA* induced site selective fragmentation in simple aromatic compounds. The site selectivity for the fragmentation by *DEA* in complex molecules of biological relevance, like DNA bases, has been shown in recent reports [1]. These studies on simple aromatic compounds will help in further understanding this process that is very important from the point of view of radiation damage and electron induced chemistry as well as astrobiology. These studies would include the absolute cross section measurements as well as the kinetic energy and angular distribution measurements in order to reveal the dynamics of this process in these molecules. The initial studies of *DEA* to molecules like benzene (C_6H_6), toluene ($C_6H_5CH_3$) and aniline ($C_6H_5NH_2$) carried out, but not included in this thesis, have shown promising results in this regard.

All the results that are reported in this thesis except those on the electron capture by C_{60} are obtained using the simple electron gun providing electron beam with energy resolution of 0.5 eV. As described in the 2nd chapter, in order to improve the resolution of the *VMI* data it is essential to perform the kinetic energy and angular distribution measurements using electron beam of better energy resolution. The trochoidal electron monochromator developed in the course of this thesis work should be used in the *VMI* experiment. Also better energy resolution of the electron beam will help to resolve the various closely spaced resonances.

The segmented *ToFMS* is probably the most efficient tool to measure the absolute cross section for the formation of the H^- ions in *DEA* to hydrogen containing molecules. Using the electron beam with high energy resolution along with segmented *ToFMS*, very accurate measurements of these absolute cross sections can be carried out for various hydrogen containing molecules. The probable list of these molecules includes simple species like H_2O, NH_3, CH_4, H_2S and many simple compounds for

which the accurate cross sections data do not exist. The data so generated will be important for understanding and modeling various electron induced processes such as interactions caused by the energetic hydride ions formed in *DEA*.

There have been several approaches that have been adopted to achieve the goal of controlling chemical reactions at the isolated molecule level as well as at the bulk scale. We believe that the discovery of functional group dependent site selective fragmentation of molecules has given a new possibility in achieving this goal. Use of electron induced processes to control chemical reactions appears to be the most feasible approach as far as the practical applications are concerned as generating electron beams and controlling their energy are quite reasonably achievable tasks. In order to realize full potential of the electron induced site selective fragmentation in this regards, it is essential to know the exact nature of the remaining neutral fragment formed in the *DEA* process. In this direction our efforts involving *VMI* technique to study the dynamics of the *DEA* process have shown a lot of promise. Another possible approach to study these neutral fragments can be through their spectroscopy on the surfaces using Scanning Tunneling Microscope (*STM*). In these experiments the electron beam of the *STM* will induce the *DEA* in the molecules adsorbed on the surface [2] and the same beam will do the spectroscopy of the fragments that are released on the surface.

As for practical applications using control of electron induced chemistry, it is necessary to study electron interactions with molecules in bulk. There are two ways one can approach this. The first approach is to use molecules condensed on surfaces. Some efforts have already been reported in this connection by others [3]. The second approach would be to carry out electron collisions at relatively higher pressures or in plasmas in which the electron temperature could be controlled.

All these studies that are reported or proposed so far are on the molecules in their ground state. Vibrational as well as electronic excitation of molecules will open up another dimension to the concept of the electron induced chemical control. One can tailor the fragmentation pattern in the *DEA* process by preparing the initial state of the molecule. In fact it has been demonstrated that a particular *DEA* channel can be enhanced or suppressed by electronic excitation of the target molecule [4]. Also the vibrational excitations of the target molecules are known to enhance the cross section for the DEA process [5]. This effect can be used for the enhancement of the cross section for the fragmentation at a particular site by exciting the target molecule to

high vibrational levels causing stretch in that particular bond. This concept is along the lines of much celebrated mode selective chemistry [6] but with addition of electron attachment. In fact the different life-times of the negative ion resonances along different dissociation pathways can possibly be used to tailor the outcome of a chemical reaction. It is also of interest from fundamental understanding as well as practical application point of view to study the dynamics of the *DEA* to excited state molecules. This can be done using *VMI* in the case of *DEA* to state selected excited molecules.

In order to prepare molecules in specific high lying vibrational levels at reasonable target densities it is necessary to employ sophisticated optical pumping techniques like stimulated emission pumping (*SEP*) [7] or stimulated Raman adiabatic passage (*STIRAP*) [8]. We are in the process of setting up an experiment employing SEP. For reasonable target densities in the excited state it is essential to start with vibrationally and rotationally cold target molecules in ground state. This can be achieved using supersonic expansion of the molecular beams [9]. For this purpose, we have developed a pulsed valve that gives a pulsed molecular beam. This pulsed valve uses a piezoelectric crystal to control the movement of a plunger that in turn controls the gas flow. We have also developed the necessary differential pumping stages and the entire set-up is ready to be assembled and tested.

An important finding that has come out of the work carried out towards this thesis is the orientation specific fragmentation of *O–H* bond in the compounds containing *OH* group. It would be interesting to look for such behavior in other functional groups like *NH*, *SH* etc. Also in order to prove the generality of this finding it will be important to measure the angular distribution of the H^-/D^- ions from molecules belonging to different symmetry groups. The most interesting case will be of the molecules belonging to C_1 symmetry group i.e. molecules having minimum symmetry. Such molecules are expected to give isotropic angular differential cross section, in general. However, with the orientation dependence of a given bond and not the molecule as a whole, we expect to see anisotropy in the angular distribution. We would also like to investigate the shadow seen in the angular distribution in the forward direction. As discussed in Chapter 5, this shadow could be seen when site specificity in the electron attachment process exists and when one part of the molecule casts its shadow on the site where selective electron capture occurs. This could have a direct significance to active screening of one part of a big molecule by

another part from an incoming electron. *VMI* measurements on *DEA* to big molecules with appropriate isotope substitution may show the significance of such a process.

The long standing controversy about the exact nature of the electron capture process near zero eV to C_{60} has been settled by the results obtained in the low energy electron attachment experiments. The observation of the long-lived C_{60}^- ions at electron energies above the first and the second ionization potential has brought up another issue. This is about the exact mechanism and nature of negative ion resonances at these energies. It would be interesting to know the dynamics of the capture process at these energies as these states are lying above the first and the second ionization of the neutral molecule. Some theoretical model addressing these issues and describing the dynamics of the capture process is warranted. Also as the parent negative ions are found to be long lived in the electron energy range from 0 to 12 eV, it is clear that several excited negative ion state of C_{60} are stable against dissociation and *autodetachment*. Hence it would be interesting to do the optical spectroscopy of this anion.

The work regarding the Rydberg electron transfer to excited molecule can be made more refined by performing such experiments with molecules excited to selected state. Here the Rydberg species, which can be rare gas atoms, excited to the specific Rydberg state can be prepared separately and made to collide with the selectively excited target molecules. Such experiments have already been carried out for ground state molecules [10]. However, there are no measurements on electron attachment from state selected Rydberg states to excited molecules. These measurements are crucial in modeling plasmas. With the currently available technology such measurements are feasible.

References:

[1] Sylwia Ptasinska, Stephan Denifl, Verena Grill, Tilmann D. Mark, Paul Scheier, Sascha Gohlke, Michael A. Huels and Eugen Illenberger, *Angew. Chem. Int. Ed.,* **44**, 1647 (2005); *Phys. Rev. Lett.*, **95**, 093201 (2005) and references therein.

[2] B. C. Stipe, M. A. Rezaei and W. Ho, *Science*, **280**, 1732 (1998).

[3] R. Balog and E. Illenberger, *Phys. Rev. Lett.* **91**, 213201 (2003).

[4] S. V. K. Kumar, E. Krishnakumar, S. A. Rangwala and V. S. Ashoka, *Phys. Rev. A*, **64**, 012707 (2001).

[5] L. G. Christophorou (ed.), *Electron-Molecule Interactions and Their Application, Vol. 1* (Academic Press INC., London, 1983).

[6] J. Jortner, R. D. Levine and B. Pullman (eds.), *Mode selective chemistry* (Kluwer academic, Dordrecht, 1991).

[7] Hai-Lung Dai and Robert W. Field, *Molecular spectroscopy and dynamics by stimulated emission pumping*, (World Scientific, Singapore, 1995).

[8] S. Schiemann, A. Kuhn, S. Steuerwald and K. Bergmann, *Phys. Rev. Lett.*, **71**, 3637 (1993).

[9] W. Demtroder, *Laser spectroscopy: basic concept and instrumentation*, (Springer-Verlag, Berlin, 2003).

[10] L. Suess, Y. Liu, R. Parthasarathy and F. B. Dunning, *J. Chem. Phys*., **122**, 124315 (2005) and references therein.